MECHANISMS OF TRANSGENERATIONAL CENTROMERE INHERITANCE

Evan Michael Smoak

A DISSERTATION

in

Biochemistry and Molecular Biophysics

Presented to the Faculties of the University of Pennsylvania

in

Partial Fulfillment of the Requirements for the

Degree of Doctor of Philosophy

2016

Supervisor of Dissertation

Michael A. Lampson, Ph.D.
Associate Professor of Biology

Supervisor of Dissertation

Ben E. Black, Ph.D.
Associate Professor of
Biochemistry and Biophysics

Graduate Group Chairperson

Kim A. Sharp, Ph.D.
Associate Professor of
Biochemistry and Biophysics

Dissertation Committee:

Marisa S. Bartolomei, Ph.D.	Professor of Cell and Developmental Biology
Joseph A. Baur, Ph.D.	Assistant Professor of Physiology
Shelley L. Berger, Ph.D.	Daniel S. Och University Professor
John Isaac Murray, Ph.D.	Assistant Professor of Genetics
Kim S. McKim, Ph.D.	Professor of Genetics, Rutgers University

MECHANISMS OF TRANSGENERATIONAL CENTROMERE INHERITANCE

DEDICATION

To my Grandparents, Marcella, Albino, Catherine, Henry:

For inspiring me with your lives.

To my Parents, Grace and John:

For encouraging my curiosity.

To my Sister, Meaghan:

For always finding the silver lining.

To my Husband, Zachary:

For moving to Philadelphia with me to have an adventure.

May our life together always be full of them.

ACKNOWLEDGMENT

So often in this journey I have thought of the beautiful painting “Sunday on La Grande Jatte” by the painter Georges Seurat. I love the work in an aesthetic sense, but what really captures me is its composition: so many individual, colorful dots that join together to build up the whole image. My journey towards completing this dissertation is much like a Pointillist work, it is made of up many individual people who have supported me. This work would not be possible without their support, and I would like to take a moment to thank them.

First, I would like to thank my mentors, Mike Lampson and Ben Black. Through your co-mentorship, I have learned to ask better questions, think more critically, and evolve as a scientist. Thank you both for the countless hours you spent in meetings with me, looking over my posters, abstracts, manuscripts, and presentations, and offering solid advice. Your patience and guidance during this stage of my scientific training has propelled me to become a better thinker and a better scientist, and I am so grateful that I got to be a part of your labs.

Thank you to the members of the Black Lab and Lampson Lab, both past and present. To the Black Lab: John Skinner, Tanya Panchenko, Kevan Salimian, Emily Bassett, Danielle Rogers, Jamie DeNizio, Lucie Guo, Glennis Logsdan, Jennine Dawicki-McKenna, Nikolina Sekulic, Samantha Falk—thank you for being awesome! Special thanks to Kevan, Tanya, Emily, and Nikolina for always offering such productive advice, both about life and about science; Jamie, for always having a smile ready with something positive to say; Lucie and Glennis, for making lab so fun and for the most memorable canoe ride I have ever had at a scientific meeting. I will always remember Glennis singing “Just Around the Riverbend” the entire time. Thank you also to my Black Lab lab spouse, Samantha Falk, who is a scientist of incomparable brilliance and a person with a huge heart. We started in the Black Lab around the same time and I will always treasure our discussions about science, CENP-A nucleosomes, Adobe Illustrator, Disney Songs, and,

perhaps most importantly, cake (especially of the birthday variety). In all seriousness, why would anyone ruin cheesecake by adding anise?

To the Lampson Lab: Dan Liu, Enxiu Wang, Dario Segura-Peña, Teresa Chiang, Maomao Zhang, Olga Davydenko, Ed Ballister, Michelle Riegman, Alyssa Mayo, Lukáš Chmátal, Takashi Akera, Aiko Iwata-Otsubo, Abram Calderon, Huaiying Zhang, Priyanka Kothari, Zach Feldman, Muyi Li, Karren Yang, Lam Tran, Jessica Schwartz, and Jonny Bell—you have all given me so much. Special thanks to: Teresa, for laying the groundwork for my project; Ed, for being the smartest person I've ever met and always providing me with motivation to become a better, more thorough scientist; Alyssa, for teaching me the importance of saying "Good morning, how are you?" every day and for sharing my love of idiomatic American English; Lukáš for great scientific conversations, pushing me out of my comfort zone in Puerto Rico after SSR, and for teaching me to take a vacation every once in a while; Olga, for demonstrating that radical candor is healthy and teaching me to use my voice more—I still miss our talks on the balcony; Takashi for smiling *always*, no matter the situation. I can always depend on him to make the day bright and to make the best coffee; Aiko, I will always treasure our conversations on science and challenging each other to be the best mentors we can be, as well as our conversations about birds, flowers, pandas, and whales! Special thanks to Jonny Bell for allowing me to cut my teeth on mentoring a young scientist. I am so proud of what we accomplished together. I will miss our time in lab together, but am so excited to see what your next chapters hold. Lastly, to the world's best baymate Maomao—you are the most tenacious, hardworking, and compassionate person I know. Thank you so much for your continued friendship and counsel, and for teaching me how to navigate when the water gets choppy.

Thank you to Richard Schultz and his lab for their willingness to spend so much time teaching me about the oocyte. Richard became my unofficial co-mentor and I so appreciate you waking up at dawn in California to Skype in to group meeting and give advice on my latest

experiments. You are a model of the kind of scientist I hope to be one day. In a category all her own, I thank Paula Stein. Paula, there are no words, in any language, great enough to explain your impact on me as a person and as a scientist. You changed my life when you introduced me to reproductive biology and took me under your wing as your apprentice. Everything I know about how to work with oocytes, I learned from you. Though you are too humble to ever admit it, you are a rock star and the most patient, giving, and kind teacher I've ever had. I look forward to a lifelong friendship and a return to Vieques to see more horses and to sit on the beach!

To the Grishchuk Lab: thank you for always giving me valuable feedback at Chromo Club.

To the Lynch Animal Facility: Thank you for your professionalism and friendliness—both the mice and I benefitted so much from your work. Michelle, JB, Rhonda, Druscilla, and Howard—it was my privilege to work with you all. Thank you also to the mice who gave their lives to support this work.

To my thesis committee: Marisa Bartolomei, Shelley Berger, John Isaac Murray, and Joe Baur, thank you for your counsel over the years, my science has grown stronger and I have developed professionally in large part due to your guidance. Marisa and Shelley, thank you for suggesting I try a project in the male germline. The experience broadened my horizons and gave me a challenge outside of my comfort zone for which I am most grateful.

To the Berger Lab: Lacey Luense, Angela Weller, Enrique Lin Shiao, and Jessica Bryant, thank you for taking me in as an honorary member of Team Testes and teaching me about sperm! Special thanks to Lacey and Enrique for a wonderful trip to NICHD—we need to grab another beer together soon.

To my Philly friends: Andy, Lauren, Richie, Walker, Jason, Carlos, Rob, Jeff, Brian, Sandya, Steph, Chris, Deirdre, Nicole, and Josh —thank you for making the journey through the last few years so fun and for providing necessary support and distractions! Moving to Philly from

NY was daunting because neither Zach nor I knew anyone, but you have all made the last 6 years the best possible way to spend our 20s!

To the DJs at 93.3 WMMR: you guys are “everything that rocks”. Thanks for always having the right soundtrack for my day—especially Pierre Robert, Jaxon, and Matt Cord for those late evenings in the collection room.

To my science teachers prior to graduate school: Diane Walsh, Jill Johanson Hartig, Christie Tursi Favata, Jim Coughlin, and my undergraduate mentor Dr. Ipsita Banerjee—thank you for seeing something a young scientist in me and encouraging me to nurture that spark.

Finally, I would like to thank my family, for taking me seriously when I was a child obsessed with dinosaurs who was convinced he would get a Ph.D. in paleontology (because secretly I was convinced I too would find the Great Valley from The Land Before Time, so I could study them for real). To my parents Grace and John, thank you for being my constant bedrock of support. You never stifled my curiosity, you bought me “The Big Book of Tell Me Why”, you let me grow crystals in the kitchen (even if it made the whole house smell of ammonia), and you drove me to Cold Spring Harbor to go to DNA camp at the DNA Learning Center. Historically you have both taken almost no credit for my success, but everything I am today is because of who you raised me to be. No words will ever be enough to thank you. To my sister, Meaghan, you have kept me so grounded in reality, and never let me turn a molehill into a mountain. Thank you for keeping it real and for keeping my feet firmly on the ground. You are phenomenal and I’m so lucky to be your brother.

Thank you also to my grandparents: Marcella (Nonna), Albino (Nonno), Catherine (Grandma), and Henry (Grandpa). Grandma and Grandpa believed I could do something with my life from the beginning. I will always remember going to the American Museum of Natural History and staring at the life-sized Blue Whale model (which was then in the cafeteria), totally captivated by the beauty of the natural world. They both passed away from cancer when I was a teenager,

but the care they received allowed me to internalize that greater scientific understanding held the key to disease prevention and cure. Nonno also passed away from cancer when I was two, but I think I wound up inheriting a lot of his stubbornness and drive to take calculated risks. Though the three of them are not here to see me complete this dissertation, I know they would be proud. Finally, I would like to thank Nonna, who came to America with Nonno and my mother from Croatia (then Jugoslavia) in 1961 looking for a better life. I live each day trying to make the most of the opportunity they wished for our family, and because of their sacrifice, I have an amazing life. Lastly, to my cousin Sandra Oplanich Levcovici, who took me to the lab with her when she was a research technician at Rockefeller and Memorial Sloan Kettering to see what real bench science was like, and for gifting me with my first copy of Albert's "Molecular Biology of the Cell" for my 13th birthday. It was an investment that paid off.

I would like to thank my in-laws, Bob, Cindy, my siblings-in-law, and all of my extended in-law family for being amazingly supportive during my Ph.D. and for always knowing exactly when to tell me that it was time to stop working for a bit and have some fun. I am honored to have the exceedingly ideal opportunity to be a part of a family of winners! Seriously, I couldn't have married into a better family, and I'm so grateful for all of your support.

Finally, I would like to thank my husband Zach Alexander Aguanno Smoak. You left your whole life behind in NY to move with me to Philadelphia and have an adventure. Along the way we got engaged, married when it was only possible in 6 states, picked up two cats, you earned a Masters from Drexel, and we made a lifetime of memories. Thank you for being my best friend, my confidant, my support system. You have picked me up from the lab at 3am, sacrificed weekends to let me work, and tolerated the fact that I smell like the mouse facility when I get home from work most days. I love you so much and the smartest decision I ever made was to go on that date to a handbell concert with you. On to the next adventure!

ABSTRACT

MECHANISMS OF TRANSGENERATIONAL CENTROMERE INHERITANCE

Evan Michael Smoak

Michael A. Lampson

Ben E. Black

Centromeres control genetic inheritance by directing chromosome segregation, but centromeres in most species are not genetically encoded. Instead, centromeres are specified epigenetically by the presence of Centromere Protein A (CENP-A), a histone H3 variant which replaces canonical histone H3 in centromeric nucleosomes. This dissertation describes underlying mechanisms governing CENP-A nucleosome transmission and epigenetic centromere inheritance during the cell cycle. In the first part of this dissertation, I discuss the role of the CENP-A nucleosome binding protein CENP-C in stabilizing CENP-A nucleosomes at the centromere. Our work demonstrates that CENP-C both reshapes the histone core of the nucleosome, and that CENP-C depletion leads to the rapid removal of CENP-A from centromeres. These data indicate that CENP-C is necessary for stable retention of CENP-A nucleosomes at the centromere, and highlight molecular requirements of maintaining and transmitting centromere identity. In the second part, I describe the mechanism by which centromeres are inherited through the mammalian female germline. In cycling somatic cells, CENP-A is maintained by a cell cycle-coupled pathway, and there is no known mechanism to assemble new CENP-A nucleosomes outside of the G1-phase of the cell cycle. This epigenetic mechanism raises the question of how centromere identity is maintained during the extended prophase I arrest in mammalian oocytes. Using mice I generated, in which the *Cenpa* locus is

conditionally inactivated in oocytes early in prophase I arrest, I tested whether centromere inheritance depends on a specialized meiotic loading pathway or on long-term retention of CENP-A nucleosomes loaded prior to prophase I arrest. We find that CENP-A nucleosomes are stably retained at centromeres for 12 months with no detectable contribution from meiotic loading. Our results show that CENP-A which is loaded before birth, prior to prophase I arrest, is fully functional 12 months later, indicating that stable retention of CENP-A nucleosomes underpins centromere inheritance through the female germline. Finally, I discuss my efforts to create a mouse model to study centromere inheritance in the mammalian male germline. Together, the data presented in this dissertation greatly enhance our understanding of the molecular mechanisms that contribute to transgenerational centromere inheritance.

TABLE OF CONTENTS

LIST OF TABLES

LIST OF FIGURES

List of Reproduced Publications

The following publications were used as the basis for the indicated chapters.

- Chapter 2 is based on:
  - Falk SJ*, Guo LY*, Sekulic N*, Smoak EM*, Mani T, Logsdon GA, Gupta K, Jansen LE, Van Duyne GD, Vinogradov SA, Lampson MA, Black BE. CENP-C reshapes and stabilizes CENP-A nucleosomes at the centromere. Science. 2015,328;699- 703.

- Chapter 3 is based on:
  - Smoak EM, Stein P, Schultz RM, Lampson MA, Black BE. Long-term retention of CENP-A nucleosomes underpins transgenerational centromere inheritance in the mammalian germline. Curr. Biol. 2016, http://dx.doi.org/10.1016/j.cub.2016.02.061.

*Authors contributed equally

CHAPTER 1:

Epigenetic Centromere Inheritance

1.1 Introduction

Inheriting the correct number of chromosomes is essential for genomic stability, and depends on accurate chromosome segregation during cell division. In eukaryotes, a chromatin locus known as the centromere directs faithful chromosome segregation. Centromeres fulfill this role by serving as the foundation for kinetochore assembly, which is responsible for making attachments between chromosomes and spindle microtubules (Black and Cleveland, 2011). Paradoxically, despite the fact that all centromeres are typically found within DNA comprised of highly repetitive sequences, in most eukaryotes these repeats are neither necessary nor sufficient to specify centromere location or for proper centromere function. Rather, centromere identity is defined epigenetically, by the inclusion of the histone H3 variant Centromere Protein A (CENP-A) into nucleosomes at centromeric chromatin.

Transmitting centromere identity to the next generation of cells is paramount. Without inheriting functional centromeres, chromosomes in dividing cells can no longer attach to spindle microtubules during mitosis or meiosis. The inability of chromosomes to bi-orient on the spindle, such that each daughter cell receives the correct number of chromosomes, leads to chromosome segregation defects such as aneuploidy. Aneuploidy, the loss or gain of one or more chromosomes, is typically found in cancer cells (Kops et al., 2005), and aneuploid gametes generated through meiotic chromosome mis-segregation give rise to chromosomally abnormal embryos, which either spontaneously abort or develop into offspring with severe physical and/or mental defects (Hassold and Hunt, 2001). For these reasons, transgenerational centromere inheritance is the keystone of faithful genome transmission to subsequent generations.

In this chapter, I provide an overview of the research that has informed the fundamental topic addressed by my dissertation work: transgenerational centromere inheritance. In a larger sense, a greater understanding of centromere inheritance mechanisms deepens our basic

knowledge of genetic inheritance. I begin by framing the centromere within this “big picture” context, and follow with a short history of the centromere and the discovery of CENP-A as the epigenetic mark that determines centromere location and function. I then discuss the known molecular mechanisms of centromere inheritance: both the proteins involved in maintaining centromere identity and the cellular programs that establish and maintain centromeres. Finally, I discuss the challenges the mammalian germline presents to transgenerational centromere inheritance. This motivates the two arms of my dissertation research: determining molecular factors that contribute to stable retention of CENP-A at the centromeres (Chapter 2) and understanding the mechanisms used by the mammalian germline to maintain and transmit centromere identity to offspring (Chapters 3 and 4).

1.2 Genetic Inheritance: Insight from Mendel’s Garden and Flemming’s Salamanders

To understand the importance of the centromere in the context of genetic inheritance, we must travel back to a time during which little was known about how traits were passed to the next generation. In 1865, Gregor Mendel published his work on trait inheritance in pea plants (Mendel, 1865) which led to his now well-known Laws of Inheritance, namely the Law of Segregation and the Law of Independent Assortment. What remained unknown at the time was *how* traits were inherited. The answer came in 1882, when Walther Flemming published his work on cell division (Flemming, 1882). Using cells from fire salamander embryos, Flemming described mitosis for the first time, after noticing that structures within the cell nucleus, which he called chromatin based on their ability to absorb aniline dyes, were distributed into daughter cells during cell division. The individual components of chromatin would be named chromosomes or “colored bodies” by Flemming’s colleague Heinrich Wilhelm Gottfried von Waldeyer-Hartz in 1888. Sadly, Mendel and Flemming remained unaware of each other’s work, and so it would be years before the discovery

of a connection between mitosis and genetic inheritance. In the early 1900s, Walter Sutton and Theodor Boveri independently concluded that chromosome segregation is the basis of genetic inheritance, now known as the Chromosome Theory of Inheritance (Boveri, 1902; Sutton, 1903). This theory was bolstered by Thomas Hunt Morgan in 1910, when he detected crossovers between homologous chromosomes during meiosis in Drosophila, which paved the way for understanding that genetic traits are transmitted to offspring through inherited chromosomes (Morgan, 1910).

Establishing that chromosomes were the vehicles of genetic inheritance, made it essential to understand the mechanisms by which chromosomes can be faithfully inherited by daughter cells. At the heart of this process lie centromeres, which were first described by Flemming in the late 1880s. When he stained cells with dye, he noticed a region within chromosomes which retained a greater amount of dye compared to other chromatin. He termed this region a “primary constriction” of the chromosome, and today we know them as centromeres. Even though centromeres were discovered over 130 years ago, it is only within the past ~30 years that the centromere field developed a more comprehensive understanding of centromere structure and function, as well as the mechanisms involved in inheriting the specialized nucleosomes that make it all possible.

1.3 Centromere Identity & CENP-A Nucleosomes

For cells to inherit centromeres, what components of the centromere must be transmitted? Today, nearly all models of centromere inheritance assert that propagation of chromatin-assembled CENP-A nucleosomes allows for epigenetic inheritance of centromere identity, independent of underlying DNA sequence (Black and Cleveland, 2011). However, this was not always the case. Initially, centromeres were thought to be genetically defined. The first centromere ever isolated came from budding yeast (*S. cerevisiae)*, where Louise Clark and John

Carbon showed that plasmids containing a centromeric DNA sequence, isolated from endogenous yeast centromeres, were able to persist for several cell-cycles (Clarke and Carbon, 1980). Extensions of this work showed that in budding yeast, the centromere is defined by a 125bp DNA sequence (Bloom and Carbon, 1982; Fitzgerald-Hayes et al., 1982; Panzeri and Philippsen, 1982; Saunders et al., 1988). In addition to yeast, it was discovered that repetitive DNA at the human centromere was made of tandemly arranged 171bp DNA monomers (termed α-satellite DNA) (Manuelidis, 1976; Manuelidis, 1978; Waye and Willard, 1987; Willard and Waye, 1987). Mouse centromeres also contain two classes of repetitive DNA termed major and minor satellite repeats, which are 234bp and 120bp respectively (Horz and Altenburger, 1981; Manuelidis, 1981; Pietras et al, 1983). Evidence of a defined, repetitive DNA element at centromeres, across many species from yeast to mammals, suggested that centromere identity was genetically defined.

While centromeres are still thought to be defined genetically in budding yeast, in all other eukaryotes studied centromere identity is now thought to be epigenetic, and dependent on the presence of chromatin-assembled CENP-A nucleosomes. As the naming convention might suggest, CENP-A, along with CENP-B and CENP-C, was among the first centromere proteins to be identified. A full historical perspective of CENP-A's discovery was recently published (Earnshaw, 2015). Shortly after CENP-A's discovery, it was found to co-purify with core histones and nucleosome core particles isolated from HeLa cell extract—leading to the hypothesis that CENP-A was probably a histone-like protein (Palmer et al., 1987). Indeed, human CENP-A and histone H3.1 share ~62% homology in their histone fold domains, but have completely divergent N-terminal tails (Sullivan et al., 1994), providing evidence that CENP-A is a histone H3 variant. CENP-A loss at the centromere is catastrophic for cells, leading to severe deficiencies in chromosome segregation and mitotic checkpoint functions (Buchwitz et al., 1999; Chen et al., 2000; Howman et al., 2000; Lermontova et al., 2011; Maehara et al., 2010; Oegema et al., 2001;

Régnier et al., 2005; Sanyal and Carbon, 2002; Stoler et al., 1995), highlighting CENP-A's fundamental role in chromosome inheritance.

The strongest evidence for the epigenetic nature of centromere identity came from the discovery of human neocentromeres. Neocentromeres are ectopic centromeres that arise when CENP-A nucleosomes migrate from their original location in α-satellite DNA to a new location on the chromosome that does not contain α-satellite repeats, which supports a fully functional centromere (Barry et al., 1999; Choo, 1997; Depinet et al., 1997; Scott and Sullivan, 2014). No requirement exists that DNA at neocentromeres must change to become more like α-satellite DNA in order to maintain centromeres (Barry et al., 1999), suggesting that sequence was neither necessary, nor sufficient for centromere specification. In 2004, researchers at the Royal Children's Hospital in Australia made an exciting discovery during routine karyotyping on a patient sample (Amor et al., 2004). They found that the centromere on one copy of Chromosome 4 had translocated to another region on the same chromosome and the original centromere had been silenced, meaning it no longer recruited kinetochore proteins. Instead, centromere-specific proteins such as CENP-C, and CENP-E were recruited to the neocentromere (Amor et al., 2004). Incredibly, the same neocentromere was observed in multiple generations of the family, meaning that the neocentromere was meiotically stable and could be passed through the germline (Amor et al., 2004).

Further evidence for the epigenetic nature of the centromere came from experiments in fruit flies (*Drosophila),* which showed that CENP-A (called CID in the referenced papers) incorporation into non-centromeric chromatin causes neocentromere formation (Blower and Karpen, 2001; Maggert and Karpen, 2001; Sullivan et al., 2001). Similarly, targeting CENP-A-LacI to non-centromeric chromatin containing a LacO array is sufficient for the formation of functional centromeres in flies and human, and can recruit other kinetochore proteins such as CENP-C and

HEC1 (Barnhart et al., 2011; Mendiburo et al., 2011). When taken together, these studies provide strong evidence that centromere identity is conferred by the presence of CENP-A nucleosomes at the centromere, rather than an underlying genetic sequence. Thus, to inherit a centromere a chromosome must inherit and stably retain CENP-A nucleosomes.

1.4 Transgenerational Centromere Inheritance

In order to understand centromere inheritance, we must understand how CENP-A nucleosomes are maintained through the cell cycle and ultimately passed on to daughter cells. The cell cycle dependent maintenance of CENP-A nucleosomes is well defined in somatic cell culture models, and depends on three key steps: distributing CENP-A nucleosomes to sister centromeres during DNA replication, maintenance of CENP-A nucleosomes through cell division, and replenishing CENP-A nucleosomes at the centromere in the subsequent cell cycle (Fig. 1.1). While much is known about this centromere inheritance mechanism in cycling somatic cells, very little is known about centromere inheritance in the germline. Though the basic features of CENP-A maintenance: distribute, maintain, replenish, likely remain similar, gametogenesis in males and females presents unique challenges to CENP-A nucleosome inheritance, which may require alterations to the mechanisms used by cycling somatic cells. Some mechanisms by which mammalian gametes transmit centromere identity to offspring are explored in this dissertation. In order to frame the questions addressed by my dissertation work, it is helpful to look at an overview of what is known about each of the three steps required for centromere maintenance, as well as discuss questions about centromere inheritance that are still unanswered in somatic cells and gametes.

1.4.1 Partitioning CENP-A Nucleosomes in S-phase

The mechanisms involved in CENP-A nucleosome inheritance are cyclic in nature, so discussion of known inheritance pathways can begin at any point in the cell cycle. Here, it seems

natural to begin in S-phase, when chromosomes, and thus centromeres, are duplicated for the purpose of transmission to daughter cells. In fruit flies and humans, centromeric DNA is replicated in mid-to-late S-phase (Shelby et al., 1997; Shelby et al., 2000; Sullivan and Karpen, 2001), and fluorescence pulse-chase labeling has demonstrated that CENP-A nucleosomes are equally distributed between centromeres on daughter strands (Jansen et al., 2007). Only CENP-A nucleosomes already at the parental centromere are distributed during S-phase, and there is no contribution from nascent CENP-A chromatin assembly at this point in the cell cycle (Jansen et al., 2007). This reduction effectively dilutes the amount of CENP-A at each centromere to ~50% of the amount present prior to replication (Jansen et al., 2007), but allows CENP-A nucleosomes to be inherited by both sister centromeres. Since centromere replication cuts the number of CENP-A nucleosomes per centromere by half, newly replicated centromeric chromatin would theoretically have nucleosome gaps which prior to S-phase hosted CENP-A nucleosomes. Experiments done in Drosophila utilizing stretched chromatin fibers and labeled histone H3.3, indicate that H3.3 is deposited in the gaps left by CENP-A dilution, serving as a placeholder molecule until nascent CENP-A is assembled at the centromere (Dunleavy et al., 2011).

The mechanisms underlying CENP-A nucleosome partitioning to sister centromeres during S-phase are likely the same in somatic cells and germ cells. In humans, new CENP-A protein is made in late-G2 phase (Shelby et al., 2000), but is not deposited at centromeres until after mitotic (and presumably after meiotic) exit (Jansen et al., 2007). As such, chromatin-assembled CENP-A nucleosomes must persist at the centromere between S-phase and G1-phase, in the absence of any nascent CENP-A chromatin assembly. Data showing that CENP-A exhibits virtually no turnover and is only lost through dilution over successive cell cycles (Bodor et al., 2013; Hemmerich et al., 2008; Jansen et al., 2007), suggest that CENP-A nucleosomes are exceedingly stable. In constrast, histones H3.1 and H4 have a half-life of ~8 hours, with the exception of centromeric H4 (presumably in complex with CENP-A), which is as stable as CENP-

A itself (Bodor et al., 2013). This extraordinary stability is likely a lynchpin in transmitting centromere identity to the next generation. In the next section, I discuss both extrinsic and intrinsic features of CENP-A nucleosomes that may contribute to their stabile retention at the centromere, as well as the challenges gametogenesis presents to CENP-A retention and centromere inheritance.

1.4.2 CENP-A Nucleosome Retention: Extrinsic and Intrinsic Basis of Stability

CENP-A nucleosome retention at the centromere serves two important functions: first, it ensures kinetochore assembly during mitosis and meiosis; second, it guarantees that new CENP-A deposition, which is dependent on chromatin-assembled CENP-A nucleosomes, is targeted to the centromere. What mechanisms allow CENP-A to remain stably chromatin bound throughout the cell cycle? The answer to this question is multifactorial (McKinley and Cheeseman, 2016), likely depending on contributions from both intrinsic features of CENP-A nucleosomes, relative to their H3.1 containing counterparts, as well as extrinsic protein factors that stabilize CENP-A nucleosomes. Like all histones, CENP-A is structurally comprised of a long, largely unstructured N-terminal tail and four α-helices (αN and α1-3) connected by two loops (Sullivan et al., 1994). These α-helices form the histone fold domain. Differences in the sequence of the CENP-A histone fold domain make it distinct from canonical histone H3.1 and preferentially guide CENP-A incorporation into centromeric chromatin (Black et al., 2007). Chief among these differences in human CENP-A are residues 75-114 known as the CENP-A Targeting Domain (CATD). The CATD is vital in facilitating the interactions at the interface of CENP-A and histone H4 in CENP-A/H4 heterodimers (Barnhart et al., 2011).

The CATD is not only essential for targeting CENP-A to the centromere, but may play a crucial role in CENP-A retention by conferring conformational rigidity to regions within the $(CENP\text{-}A/H4)_2$ heterotetramer. Hydrogen/deuterium exchange experiments coupled with mass

spectrometry, which were carried out on recombinant $(H3.1/H4)_2$ and $(CENP\text{-}A/H4)_2$ heterotetramers, revealed differential rates of deuterium exchange along the peptide backbone between the two heterotetramers (Black et al., 2004; Black et al., 2007). In particular, the region of the CATD that contacts histone H4 displayed slower deuterium exchange when compared to the same region of H3.1/H4 interaction. This result suggests that this region of the $(CENP\text{-}A/H4)_2$ heterotetramer is more rigid than that found within $(H3.1/H4)_2$ heterotetramers. A high-resolution crystal structure of the $(CENP\text{-}A/H4)_2$ heterotetramer revealed that this stabilized region contains 6 amino acid residues which are more hydrophobic than their $(H3.1/H4)_2$ counterparts (Sekulic et al., 2010). These residues reduced conformational flexibility by 10-fold at the CENP-A/H4 interface (Bassett et al., 2012; Black et al., 2004). Further, mutation of all 6 residues back to their H3.1 counterparts reduced the level of CENP-A accumulation at the centromere by 20-fold (Bassett et al., 2012). These data suggest that information encoded directly into the CENP-A protein sequence and structure may influence CENP-A nucleosome retention.

In addition to stability conferred by intrinsic features of CENP-A nucleosomes, a bevy of centromere specific proteins may also contribute to CENP-A retention extrinsically. CENP-A nucleosomes recruit the constitutive centromere associated network (CCAN), a collection of ~16 proteins that localize to the centromere throughout the cell-cycle and are imperative for directing assembly of the kinetochore during cell division (Cheeseman and Desai, 2008; Perpelescu and Fukagawa, 2011). Among these, are a subset which have been termed the CENP-A Nucleosome Associated Complex ($CENP\text{-}A^{NAC}$), which is comprised of CENP-H, CENP-C, CENP-M, CENP-N, CENP-U/50 and CENP-T (Foltz et al, 2006; Okada et al., 2006). Two of these proteins, CENP-C and CENP-N, contact CENP-A nucleosomes directly (Carroll et al., 2009; Guse et al., 2011; Kato et al., 2013) and data presented in Chapter 2 of this dissertation demonstrate that CENP-C binding to CENP-A can actually reshape CENP-A nucleosomes and plays an important role in retaining them at the centromere (Falk et al., 2015; Falk et al., 2016). Though other $CENP\text{-}A^{NAC}$

proteins have not been shown to bind directly to CENP-A nucleosomes, it is possible they also contribute to CENP-A nucleosome stability through as-yet-unknown indirect pathways.

What we know about CENP-A retention and centromere inheritance is based largely on work done with recombinant proteins and somatic cell culture models. CENP-A retention and transmission to the next generation, is likely as important in gametes, though much less is known about how centromere identity is maintained and inherited through the germline. Gametogenesis presents unique challenges, with regard to regulating CENP-A retention and centromere inheritance, that are not typically present in cycling somatic cells. In the case of female gametes, oocytes are arrested in prophase I during early development (Von Stetina and Orr-Weaver, 2011) (Fig. 1.1). These oocytes remain in prophase I arrest for a period of a few days to decades depending on species. Eventually, select oocytes from this arrested pool are cyclically recruited for maturation and prepare for fertilization. The process by which centromere identity is maintained during this prolonged arrest remains poorly understood in many species, although a meiotic loading pathway for CENP-A has been observed in Drosophila (Dunleavy et al., 2012), and in holocentric worms centromere inheritance through the female germline is completely CENP-A independent (Gassmann et al., 2012; Monen et al., 2005) (though this may represent a specialized case due to the holocentric nature of *C. elegans*: CENP-A localizes to the entire chromosome arm and the whole length of the chromosome acts as the centromere). The data presented in Chapter 3 begin to uncover the mechanism by which centromeres identity is maintained in mammalian oocytes and ultimately passed to offspring.

While oocytes must contend with the elongated prophase I arrest, the male germline faces its own radically different hurdle to CENP-A retention (Fig. 1.1). During spermatogenesis, nearly all histones are ultimately replaced by basic proteins called protamines during the chromatin-to-nucleoprotamine transition (Rathke et al., 2014). During this transition, chromatin

assumes a highly compacted conformation, first through replacement of nearly all histones with transition proteins, and then replacement of these transition proteins with arginine-rich proteins called protamines (Hud et al., 1993; Balhorn, 2007). The inclusion of protamines into chromatin allows sperm chromatin to assume a highly compacted toroid architecture, and by the end of this transition, the chromatin is completely transcriptionally inactive. Some nucleosomes have been shown to survive the transition and remain chromatin bound, but the function of these remaining histones is the subject of lively debate (Brykczynska et al., 2010; Erkek et al., 2013; Hammoud et al., 2009; Meyer-Ficca et al., 2013; Samans et al., 2014; van de Werken et al., 2014).

Though nearly all histones are removed from sperm chromatin, CENP-A nucleosomes survive the chromatin-to-nucleoprotamine transition. This fact has been known since near the beginning of CENP-A's discovery, because CENP-A protein was first isolated from calf thymus and bull sperm (Palmer et al., 1990; Palmer et al., 1991). Immunoblot data comparing total CENP-A protein isolated from calf thymus and bull sperm show that the amount of CENP-A protein present in thymus cells is totally retained in sperm. However, the mechanism by which CENP-A nucleosomes evade the replacement machinery and are retained is unknown. CENP-A stabilizing proteins like CENP-C are absent in mature sperm from Xenopus and Drosophila (Milks et al., 2009; Raychaudhuri et al, 2012), though it is unknown at what point CENP-C is lost in these species, or if mammalian sperm lack CENP-C.

How CENP-A nucleosomes are preferentially retained in sperm chromatin while most other histones are lost is but one example of the many questions that remain unanswered. How does nuclear compaction in sperm deal with chromatin which contains CENP-A nucleosomes compared to protamine-wrapped chromatin? Do CENP-A nucleosomes play additional roles in chromatin organization during spermatogenesis? Is it important for offspring that sperm retain all

of the CENP-A? Chapter 4 of this dissertation details my efforts to generate a mouse model capable of answering some of these important questions in centromere biology.

In most cases, stable retention of CENP-A nucleosomes is essential in dividing cell types for successful genetic inheritance. The last of the three key steps in centromere inheritance is to replenish CENP-A nucleosomes at the centromere, prior to dilution during the subsequent S-phase.

1.4.3 Nascent CENP-A Chromatin Assembly

Since 50% of CENP-A nucleosomes are lost by dilution during S-phase, more CENP-A nucleosome must be placed at the centromere during every cell cycle to restore pre-S-phase CENP-A levels and avert the risk of chromosome segregation errors. A common feature of CENP-A chromatin assembly among species is its restriction to only one part of the cell-cycle, and the initial trigger for each of these events may be the same. However, the timing of CENP-A nucleosome assembly is not the same in all organisms: in humans nascent CENP-A chromatin assembly is restricted to G1-phase (Jansen et al., 2007; Black et al., 2007), whereas in S. pombe it is restricted to S-phase/G2-phase (Takayama et al., 2008), and G2/prophase in plants (Lermontova et al., 2006). These data suggest that where CENP-A is loaded (i.e. at the centromere) is more important than when it is loaded during each cell-cycle.

Recent evidence suggests that CENP-C-mediated recruitment of a Mis18 complex protein Mis18 Binding Protein 1 (Mis18BP1) to centromeres as early as metaphase is the first step in nascent CENP-A chromatin assembly, and CENP-C has been implicated in playing a role in CENP-A loading through direct interactions with the Mis18 complex (Moree et al., 2011). CENP-A chromatin assembly at the centromere in humans and C. elegans, continues with localization of the Mis18 complex to centromeres (Fujita et al., 2007; Kim et al., 2012; Hayashi et

al., 2004; Maddox et al., 2007). The Mis18 complex is comprised of three proteins: Mis18α, Mis18β, and Mis18BP1 (Fujita et al., 2007). In human cell lines, knockdown of Mis18α and Mis18β prevents loading of nascent CENP-A onto chromatin and in C. elegans, RNAi knockdown of the Mis18BP1 orthologue KNL-2 similarly prevents new CENP-A chromatin assembly (Maddox et al., 2007). In humans, Mis18BP1 localizes to centromeres only from late anaphase through early G1-phase (Fujita et al., 2007), concomitant with CENP-A deposition. Recent work shows that cell cycle dependent phosphorylation of Mis18 subunits, regulated by polo-like kinase 1 (Plk1), ensure that CENP-A chromatin assembly is restricted to the appropriate cell cycle phase (McKinley and Cheeseman, 2014). Additionally, levels of cyclin-dependent kinase 1 and 2 (Cdk1/2) are essential to regulating appropriate temporal Mis18 localization (Silva et al., 2012). Throughout S-phase/G2-Phase/M-phase, Mis18 complex assembly is precluded by phosphorylation on specific residues of Mis18BP1 by Cdk1/2, and aberrant CENP-A loading can be triggered outside of G1-phase with a knockdown of Cdk1/2 in human cells (Silva et al., 2012). Cyclin degradation also seems to be required for CENP-A loading in Drosophila (Dunleavy et al., 2012). The targeting of the Mis18 complex to centromeres allows the CENP-A-specific histone chaperone HJURP to target CENP-A/H4 dimers to the centromere (Bassett et al., 2012; Dunleavy et al., 2009; Foltz et al., 2009), though the exact mechanism by which CENP-A/H4 dimers are assembled into chromatin remains unknown.

1.5 Summary

Centromere inheritance in most eukaryotic species is dependent on successful transmission of CENP-A nucleosomes from one generation to the next. While much is known about the molecular pathways that govern CENP-A nucleosome distribution, retention, and assembly, many questions remain unanswered. What role do CENP-A nucleosome binding proteins play in CENP-A nucleosome stability? How are centromeres inherited through the

mammalian germline, and how does CENP-A deal with the distinctive challenges inherent to gametogenesis? In Chapter 2, I will focus on the protein CENP-C, which binds directly to CENP-A nucleosomes, and its role in stabilizing CENP-A nucleosomes at the centromere. In Chapters 3 and 4, I will discuss my work in understanding centromere inheritance in the mammalian germline, both in uncovering the mechanism by which centromeres are inherited through the female mammalian germline (Chapter 3) as well as my efforts to build a mouse model to ask several important questions about CENP-A nucleosomes in the male germline (Chapter 4). Finally, in Chapter 5, I offer my thoughts on future experiments that will build off of the work I present in this dissertation, and some concluding remarks.

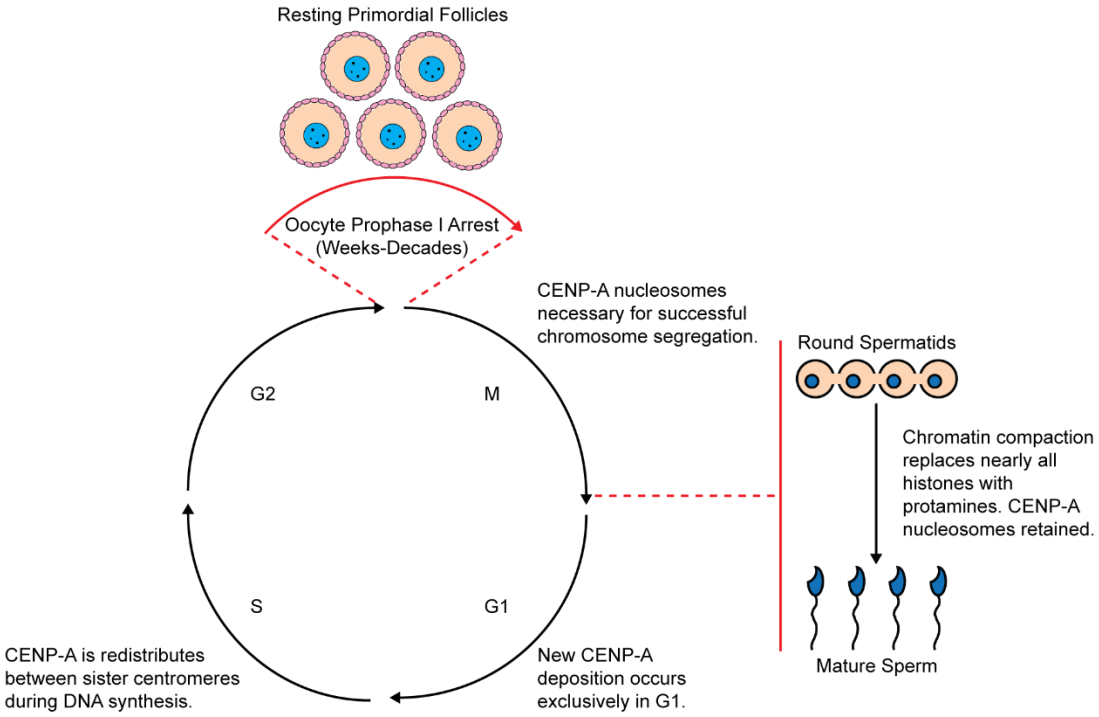

Figure 1.1 CENP-A Nucleosome Inheritance and the challenges of gametogenesis

Centromere inheritance pathways are tightly coupled to the cell cycle and have been well described in cycling somatic cells. However, both female and male gametogenesis present unique challenges to centromere inheritance pathways. Oocytes are arrested in prophase I for weeks to decades in many species, and it is unclear how CENP-A nucleosomes persist at the centromere during this time. In sperm, successful meiosis yields four round spermatids which then undergo further development to become mature sperm. During this time, chromatin becomes highly compacted through the removal of nearly all histones, in exchange for protamines. However, CENP-A nucleosomes are completely retained, raising questions as to how they avoid eviction. In both somatic cells and gametes, CENP-A nucleosome stability plays

an important role in centromere inheritance, though the basis of that stability is a topic of intense investigation.

CHAPTER 2:

CENP-C Reshapes and Stabilizes CENP-A Nucleosomes at the Centromere

2.1 Abstract

Inheritance of each chromosome depends upon its centromere. A histone H3 variant, CENP-A, is essential for epigenetically marking centromere location. We find that CENP-A is quantitatively retained at the centromere upon which it is initially assembled. CENP-C binds to CENP-A nucleosomes and is a prime candidate to stabilize centromeric chromatin. Using purified components, we find that CENP-C reshapes the octameric histone core of CENP-A nucleosomes, rigidifies both surface and internal nucleosome structure, and modulates terminal DNA to match the loose wrap that is found on native CENP-A nucleosomes at functional human centromeres. Thus, CENP-C affects nucleosome shape and dynamics in a manner analogous to allosteric regulation of enzymes. CENP-C depletion leads to rapid removal of CENP-A from centromeres, indicating their collaboration in maintaining centromere identity.

2.2 Introduction

Centromeres direct chromosome inheritance at cell division, and nucleosomes containing a histone H3 variant, CENP-A, are central to current models of an epigenetic program for specifying centromere location (Black and Cleveland, 2011). The centromere inheritance model in metazoans suggests that the high local concentration of pre-existing CENP-A nucleosomes at the centromere guides the assembly of nascent CENP-A which occurs once per cell cycle following mitotic exit. This model predicts that after initial assembly into centromeric chromatin, CENP-A must be stably retained at that centromere; otherwise centromere identity would be lost before the next opportunity for new loading in the following cell cycle. Here, we use biochemical reconstitution to measure the shape and physical properties of CENP-A nucleosomes with and without its close binding partner, CENP-C, and combine these studies with functional tests that reveal the mechanisms underlying the high stability of centromeric chromatin.

2.3 Results:

2.3.1 CENP-C physically alters the shape and rigidity of CENP-A Nucleosomes

CENP-C recognizes CENP-A nucleosomes via a region termed its central domain (a.a. 426-537; CENP-C^{CD}) (Carroll et al., 2010; Kato et al., 2013). We first considered how CENP-C^{CD} may affect the overall shape of the CENP-A-containing nucleosome using an intranucleosomal fluorescence resonance energy transfer (FRET)-based approach. We designed an experiment to measure FRET efficiency, Φ_{FRET}, between two fluorophores on defined positions on the H2B subunits of CENP-A nucleosomes in the absence or presence of CENP-C^{CD}, and then used these measurements to calculate intranucleosomal distances (Figs. 2.1). The H2B distances for CENP-A nucleosomes in the absence of CENP-C^{CD} are ~5 Å further apart than expected from their crystal structure (PDB ID 3AN2) (Tachiwana et al., 2011), indicating that CENP-A-containing nucleosomes in solution prefer a histone octamer configuration not captured in the crystal structure. It is likely that CENP-A nucleosomes sample both conformations in solution, with crystal contacts stabilizing the form that was reported (Tachiwana et al., 2011). In contrast to CENP-A nucleosomes, conventional nucleosomes have smaller H2B distances in solution (Fig. 2.1) that are consistent with their crystal structure (Luger et al., 1997). Separation of H2A/H2B dimers from each other is consistent with a nucleosome model based on rotation of the CENP-A/CENP-A' interface in $(CENP\text{-}A/H4)_2$ heterotetramers (Sekulic et al., 2010). Upon binding of CENP-C^{CD}, with the known stoichiometry of two CENP-C^{CD} molecules per nucleosome (Kato et al., 2013), the H2A/H2B distances shorten to ones that are nearly identical to conventional nucleosomes (Fig. 1). The differences we observed between H3 nucleosomes, CENP-A nucleosomes, and CENP-A nucleosomes in a complex with CENP-C^{CD} are found using either the human α-satellite DNA sequence that corresponds to the most heavily occupied site at centromeres (Hasson et al., 2013) or the completely synthetic '601' nucleosome positioning sequence (Lowary and Widom, 1998) (Fig. 1).

The shape change we measure within the nucleosome upon CENP-C^{CD} binding most likely occurs through rotation at the four-helix bundles between histone dimer pairs within the octameric core with inter-histone contacts being stabilized or destabilized depending on the preference for rotational state. We tested this prediction using hydrogen/deuterium exchange-mass spectrometry (HXMS). Strong protection of CENP-A nucleosomes (Figs. 2.2A) is conferred by CENP-C^{CD} binding on peptides spanning helices that are predicted (Kato et al., 2013) to contact it (i.e. the α3 helix and C-terminal residues of CENP-A, the α2 helices of both H4 and H2A, and regions of H2A encompassing its acidic patch residues). In addition to the surface changes induced by CENP-C^{CD}, there are internal changes to the nucleosome that we measure by HX (Figs. 2.2A,B) that are consistent with the change in nucleosome shape that we observed by FRET (Fig. 2.1). The separation of H2A/H2B dimers in CENP-A nucleosomes lacking CENP-C^{CD} (Fig. 2.1) is predicted to weaken an internal, intermolecular β-sheet that serves as the physical connection between the H2A subunit on one face of the nucleosome and the H4 subunit on the opposite face. When CENP-C^{CD} binds to the CENP-A nucleosome, peptides spanning the corresponding b-sheet residues of both H2A and H4 exhibit extra protection from HX by 1-2 deuterons, where the same level of HX takes 5-10 times longer to occur than in CENP-A nucleosomes lacking CENP-C^{CD} (Figs. 2.2).

Since CENP-C might also affect the extent that DNA wraps the nucleosomes, we reconstituted CENP-A nucleosomes using an 195 bp DNA sequence from α-satellite DNA (Harp et al., 1996) that contains a contiguous sequence spanning the major binding site it occupies on human centromeres (Hasson et al., 2013) (Fig. 2.3A). We first over-digested CENP-A nucleosomes and found very strong protection of 100 bp. Using a subsequent restriction digest of the 100 bp digestion product, we found that they were uniquely positioned with their dyad precisely where the same sized fragment previously mapped with native centromeric particles (Hasson et al., 2013). CENP-A-containing nucleosomes have many discrete intermediate

digestion products before the strongly protected 100 bp fragment is generated (Figs. 2.3A,B). When CENP-C^{CD} is bound, digestion products larger than a nucleosome core particle (e.g. >145 bp where DNA strands could cross at ~165 bp for conventional nucleosomes (Kornberg, 1977) are missing at early timepoints (Fig. 2.3B). This suggests that when CENP-C^{CD} binds to the nucleosome the DNA above the dyad rarely crosses, as it would normally cross for conventional nucleosomes. Second, digestion to the 100 bp final fragment proceeds more quickly (Fig. 2.3B). Thus, transient unwrapping of two helical turns (i.e. ~20 bp) from each terminus of the nucleosome is enhanced when CENP-C^{CD} is bound.

To determine if CENP-C^{CD} binding leads to a steady-state structural change of nucleosomal DNA, we used small-angle neutron scattering (SANS) with contrast variation. When CENP-C^{CD} binds to CENP-A nucleosome core particles, the distance distribution profiles reflecting the shape in solution substantially redistribute for both the protein- and DNA-dominated measurements (Figs. 2.3C). The increase in larger interatomic vectors for the protein component is expected to accompany an additional component (CENP-C^{CD}). The pronounced redistribution of vectors to both smaller and larger distances in DNA dominated scattering when CENP-C^{CD} is bound is attributed to compaction of the nucleosome core (smaller vectors), and opening of the nucleosome terminal DNA when CENP-C^{CD} is bound (larger vectors).

2.3.2 CENP-A nucleosomes remain assembled at their centromere of origin

The centromeric pool of CENP-A and its partner, histone H4, are not degraded in human cells over long timeframes (Bodor et al., 2013; Jansen et al., 2007) independently of nascent CENP-A chromatin assembly (Bodor et al., 2013). These findings were based on pulse labeling using the SNAP-tag and monitoring the entire population at all centromeres (Bodor et al., 2013; Jansen et al., 2007), but monitoring the fate at individual centromeres has not been reported. Does CENP-A exchange between centromeres during the cell cycle, or does it essentially never

vacate the particular centromere upon which it was initially assembled? The answer to this question is key to understanding the mechanisms underlying the maintenance of centromere identity, so we sought to answer it before addressing a potential role of CENP-C in stabilizing CENP-A nucleosomes.

We took two complementary approaches in cells to determine whether CENP-A is stably retained at the centromere upon which it is initially deposited. First, we used cell cycle-synchronized fluorescence pulse labeling of CENP-A in 'donor' cells and subsequent cell fusion with an 'acceptor' cell line. The donor cells express SNAP-tagged CENP-A that has been pulse labeled with TMR-Star (TMR*) to irreversibly label CENP-A (Jansen et al., 2007) prior to cell fusion. The acceptor cells express YFP-tagged CENP-A that is loaded at all centromeres, continuing even after fusion. If substantial exchange occurs between centromeres after the nucleoplasm is shared, then the pulse labeled CENP-A will be distributed among all the centromeres of the fused cell. However, if negligible exchange occurs, then the pulse labeled CENP-A will be restricted to the donor centromeres. At time points through the subsequent cell cycle until the second mitosis (Fig. 2.4A), we observed no detectable exchange of the TMR* labeled donor CENP-A to the acceptor centromeres in a shared nucleoplasm. The ultimate time point in this experiment is key because the appearance of sister centromeres provides unequivocal evidence that the underlying centromere DNA duplicated in the previous S-phase, but the TMR* signal remained with donor centromeres. Quantification of the fluorescence at each centromere in these heterokaryons yields a bimodal distribution. The donor centromere group with high TMR* and low YFP (Fig. 2.4B, 'x' symbols) has an average TMR* signal of 0.538 +/- 0.005 (normalized arbitrary units where the maximal measured TMR* signal in each heterokaryon equals 1; Fig. 2.4C), whereas the acceptor centromere group with high YFP and low TMR* (Fig. 2.4B, triangle symbols) has an average TMR* signal of 0.055 +/- 0.005 (Fig. 2.4C). These data indicate that once assembled at a centromere, an individual CENP-A molecule is stably

maintained at that particular centromere. Further, our findings extend earlier reports which concluded that CENP-A exhibits no turnover at centromeres based on FRAP experiments which demonstrated failure of fluorescently tagged CENP-A to recover over a 3-4 hour period after photobleaching at various cell-cycle phases outside of early G1 (Hemmerich et al., 2008).

As a complementary approach to test CENP-A stability at individual centromeres, we used a photoactivatable version of CENP-A (CENP-A-PAGFP). CENP-A-PAGFP expression levels are doxycycline dependent (Fig. 2.5). We induced expression of CENP-A to the extent that it is present at locations throughout the nucleus, but with clear enrichment at centromeres, and then activated a defined region of each cell nucleus (Fig. 2.4D [0 hr post-photoactivation]). CENP-A-PAGFP signal is quantitatively retained at the activated centromeres and does not accumulate at unactivated centromeres (Fig. 2.4D,E), indicating that there is negligible exchange between centromeres, consistent with our cell fusion results. In contrast, CENP-A-PAGFP signal in bulk chromatin decays with ~50% of the protein removed by 8 hr following photoactivation. To compare CENP-A-PAGFP retention to canonical histone H3.1, we generated a line of HeLa cells which expressed histone H3.1-PAGFP. We found that the half-life of H3.1-PAGFP was similar to ectopically localized CENP-A (Fig. 2.6). To determine if H3.1 retention was increased at the centromere, we transfected histone H3.1-PAGFP expressing cells with a plasmid encoding CENP-B-mCherry, in order to analyze H3.1-PAGFP signal at centromeres (Fig. 2.7). Our results show that H3.1-PAGFP is not strongly retained at centromeres.

2.3.3 CENP-C stabilizes CENP-A nucleosomes at the centromere

To determine if CENP-C stabilizes CENP-A at centromeres, we combined SNAP labeling of CENP-A with CENP-C depletion (Fig. 4) for which we generated a cell line with a chromosomally integrated, doxycycline-inducible CENP-C shRNA cassette. In this system, inducible CENP-C depletion requires several days before cell death occurs (Fig. 2.8A) following

mitotic kinetochore failure (Fukagawa and Brown, 1997), so there is an experimental window of time in which we can test if CENP-A nucleosome retention persists after the majority of CENP-C protein has been depleted (Figs. 2.8B,C). SNAP labeling of the existing pool of CENP-A (Fig. 2.8B [Day 2]) combined with monitoring cell number allows one to account for the entire pool of CENP-A in the dividing cell population during the course of the experiment (Jansen et al., 2007). This approach also overcomes the limitation of the CENP-A-PAGFP approach (Fig. 2.4D) where measurements beyond ~8 hr become problematic due to cell divisions. In our SNAP system, CENP-C depletion leads to a dramatic decrease in the retention over 24 hr of the existing pool of CENP-A at centromeres (Fig. 2.8B,C). Without CENP-C depletion, the average retention of CENP-A is slightly >100% (112% +/- 63% s.d.), an increase that is explained by having a small pool of pre-nucleosomal CENP-A in the cell population that is labeled by the TMR* pulse and subsequently incorporated into centromeres. To test whether nascent CENP-A deposition is also decreased when CENP-C is depleted, we synchronized cells at S-phase using a double-thymidine block, then labeled all CENP-A-SNAP with a non-flourescent SNAP-ligand. We then labeled the nascent pool of CENP-A-SNAP with TMR* ~6.5 hours after releasing the cells from the second thymidine block, when nearly all of the cells should be in G2-phase, just prior to nascent CENP-A chromatin assembly in the subsequent G1-phase (Fig. 2.9). We found that nascent CENP-A deposition is decreased when CENP-C is depleted, which is consistent with CENP-C's proposed role in the CENP-A assembly reaction (Erhardt et al., 2008; Moree et al., 2011). However, the decrease in loading would only impact incorporation of the small pre-nucleosomal pool in the CENP-A retention measurements (Fig. 2.8B,C). Thus, our findings implicate CENP-C in stabilizing CENP-A nucleosomes at centromeres. Since CENP-C may recruit or stabilize other members of the CCAN which may in turn contribute to stable retention of CENP-A nucleosomes, we cannot exclude the possibility that removing CENP-C destabilizes CENP-A nucleosomes through loss of additional centromere proteins. However, we favor a model

in which CENP-C is the key molecule responsible for stable retention of CENP-A nucleosomes, based on the fact that it binds directly to CENP-A containing nucleosomes.

2.4 Discussion

CENP-A nucleosomes are highly stable at the centromeres upon which they are initially assembled. This stability is possible through collaboration with CENP-C. Along with the intranucleosomal rigidity of CENP-A and histone H4, where the key interfacial amino acids are important for accumulation at centromeres (Bassett et al., 2012; Black et al., 2004; Sekulic et al., 2010), the physical changes imposed by CENP-C combine to make CENP-A nucleosomes at centromeres very long-lived (Fig. 2.10). Our data support a model of a steady-state octameric histone core where H2A/H2B dimers can exchange from either terminus of the CENP-A nucleosome. At the center, there is an essentially immobile $(CENP\text{-}A/H4)_2$ heterotetramer (Bodor et al., 2013) (Fig. 2.4 and 2.8). Thus, the physical properties related to CENP-A nucleosome stability at centromeres are tied to the intrinsic properties of the $(CENP\text{-}A/H4)_2$ heterotetramer (Bassett et al., 2012; Black et al., 2004; Sekulic et al., 2010) and the extrinsic properties imposed by CENP-C (Figs. 2.1-2.3).

At the centromere, there is a high local concentration of CENP-A, which results in a high local concentration of CENP-C (Fig. 2.10). Together, CENP-A and CENP-C collaborate to form a stable complex that maintains the epigenetic mark of the centromere. In the chromatin arms, CENP-A levels do not reach a sufficient threshold to recruit CENP-C and CENP-A is quickly turned over (Fig 2.10). Our experiments support the idea that CENP-A-containing nucleosomes prefer an atypical shape in the absence of CENP-C, but adopt a conventional overall histone octamer shape when CENP-C binds. In addition, our reconstitutions on native centromere DNA of octameric CENP-A nucleosomes very closely match the DNA wrapping properties of CENP-A nucleosomes isolated from functional human centromeres (Hasson et al., 2013), especially when

CENP-C is bound (Fig. 2.3B). This is in stark contrast to half-nucleosomes (termed hemisomes; i.e. one copy each of CENP-A, H4, H2A, and H2B) that wrap 65 bp of DNA (Furuyama et al., 2013) and have been proposed by others to be the major form at centromeres (Bui et al., 2012; Henikoff et al., 2014). Importantly, until now CENP-C has been considered primarily as a protein that recognizes CENP-A and bridges centromeric chromatin to other proteins important for centromere and kinetochore function (Carroll et al., 2010; Erhardt et al., 2008; Guse et al., 2011;Kato et al., 2013; Przewloka et al, 2011; Screpanti et al., 2011; Tomkiel et al., 1994) and helping target new CENP-A chromatin assembly at the centromere each cell cycle (Erhardt et al., 2008; Moree et al., 2011), but our findings that its binding directs changes to the shape and dynamics of the nucleosome suggest that it could also play a role in the special stability of CENP-A at centromeres in a manner analogous to allosteric regulation of enzymes. This has potential implications for chromatin regulation at diverse chromosome locations, as such a feature has not been reported for some other non-catalytic nucleosome binding proteins studied to date, like RCC1 and Sir3 (Armache et al., 2011; Makde et al., 2010), but now is worth considering for these and other nucleosome binding proteins. Directing a structural change upon binding of one component to a macromolecular complex to alter its behavior is a general strategy in biology, and our work with CENP-C importantly illustrates that a nucleosome—in this case, the special type at the centromere—is no exception.

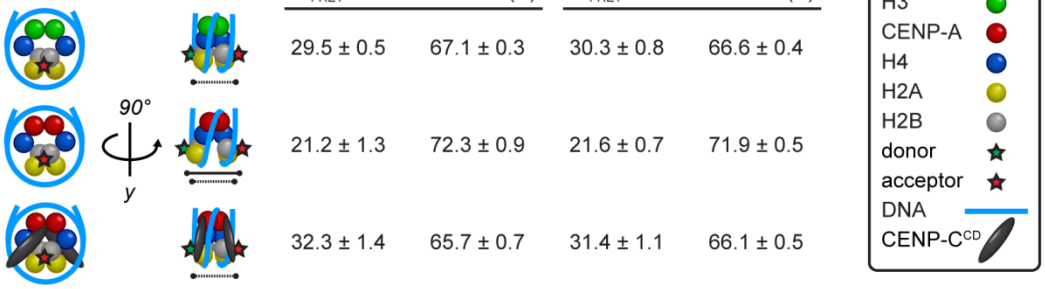

	α-satellite DNA		Widom 601 DNA	
	Φ_{FRET} (%)	Distance (Å)	Φ_{FRET} (%)	Distance (Å)
	29.5 ± 0.5	67.1 ± 0.3	30.3 ± 0.8	66.6 ± 0.4
	21.2 ± 1.3	72.3 ± 0.9	21.6 ± 0.7	71.9 ± 0.5
	32.3 ± 1.4	65.7 ± 0.7	31.4 ± 1.1	66.1 ± 0.5

Figure 2.1 CENP-A nucleosomes have a conventional shape only upon CENP-C^{CD} binding

Calculated FRET efficiencies (Φ_{FRET}) and distances between donor and acceptor fluorophores on H2B S123C for the indicated nucleosomes on either α-satellite or Widom 601 DNA. Data are shown as the mean ± s.e.m of three independent nucleosome reconstitutions.

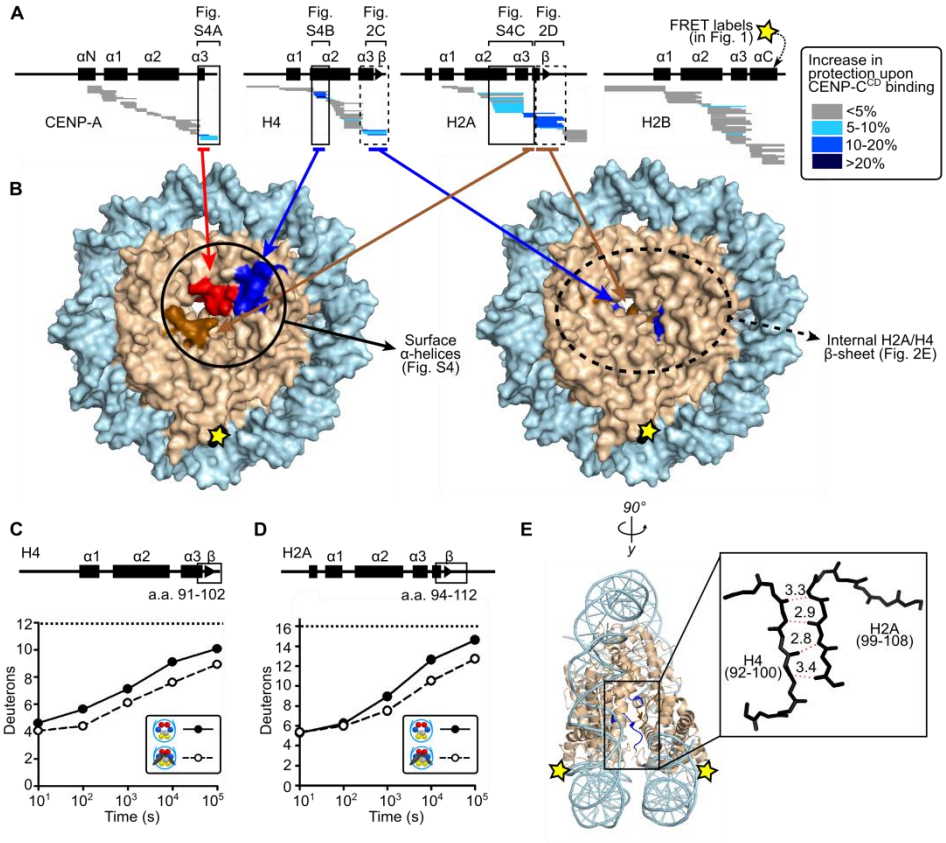

Figure 2.2 CENP-C^{CD} rigidifies CENP-A nucleosomes

(**A**) HXMS of all histone subunits of the CENP-A nucleosome from a single time point (10^4 s). Each horizontal bar represents an individual peptide, and peptides are placed beneath schematics of secondary structural elements. (**B**) Regions showing substantial protection from HX mapped onto the structure of the CENP-A nucleosome (PDB 3AN2). (**C** and **D**) Comparison of representative peptides spanning the β-sheet region in histone H4 and histone H2A over the time course. The maximum number of deuterons possible to measure by HXMS for each peptide is shown by the dotted line. (**E**) The internal H4/H2A interface mapped onto the canonical nucleosome crystal structure (PDB 1KX5).

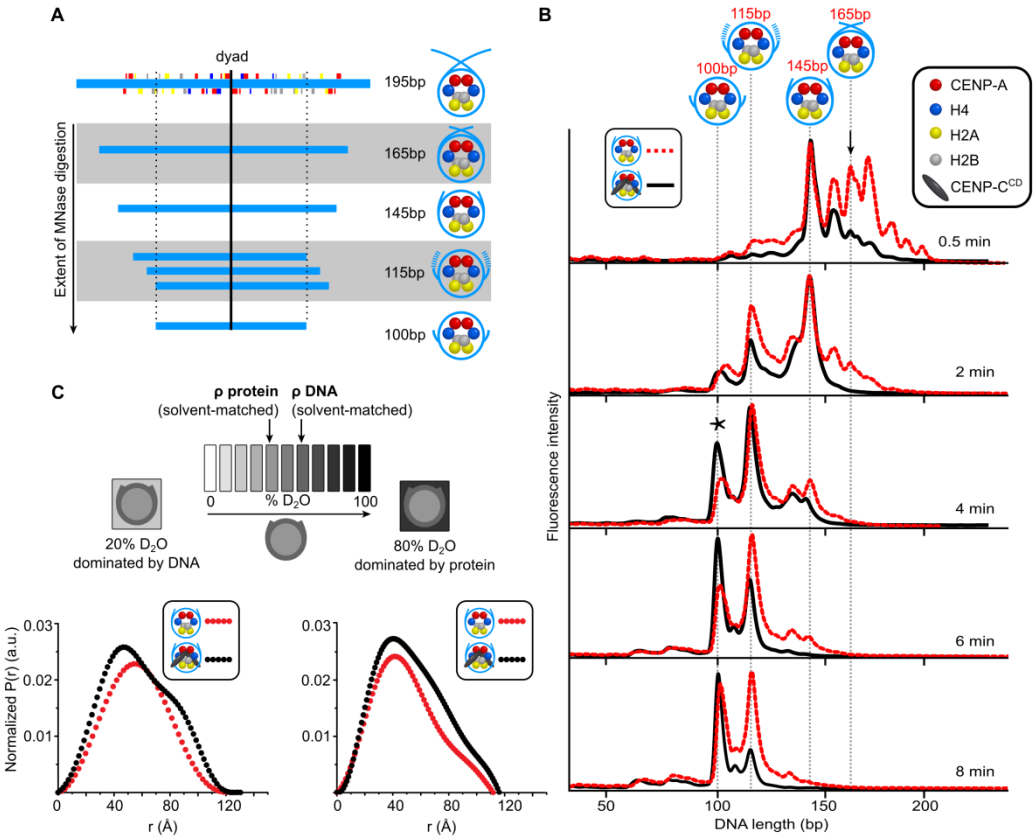

Figure 2.3 Alterations in the nucleosome terminal DNA upon CENP-C^{CD} binding

(**A**) Major MNase-digested DNA fragments observed for CENP-A nucleosomes assembled on its native centromere sequence. (**B**) MNase digestion profiles of CENP-A nucleosomes in the absence (red) and presence (black) of CENP-C^{CD}. The black arrow (0.5 min) points to the 165 bp peak (DNA crossed at the dyad). The asterisk (4 min) denotes the final 100 bp peak. (**C**) Scheme of SANS contrast variation experiment together with paired distance distribution curves for CENP-A nucleosomes alone (red) and bound by CENP-C^{CD} (black) in the indicated SANS contrast variation conditions.

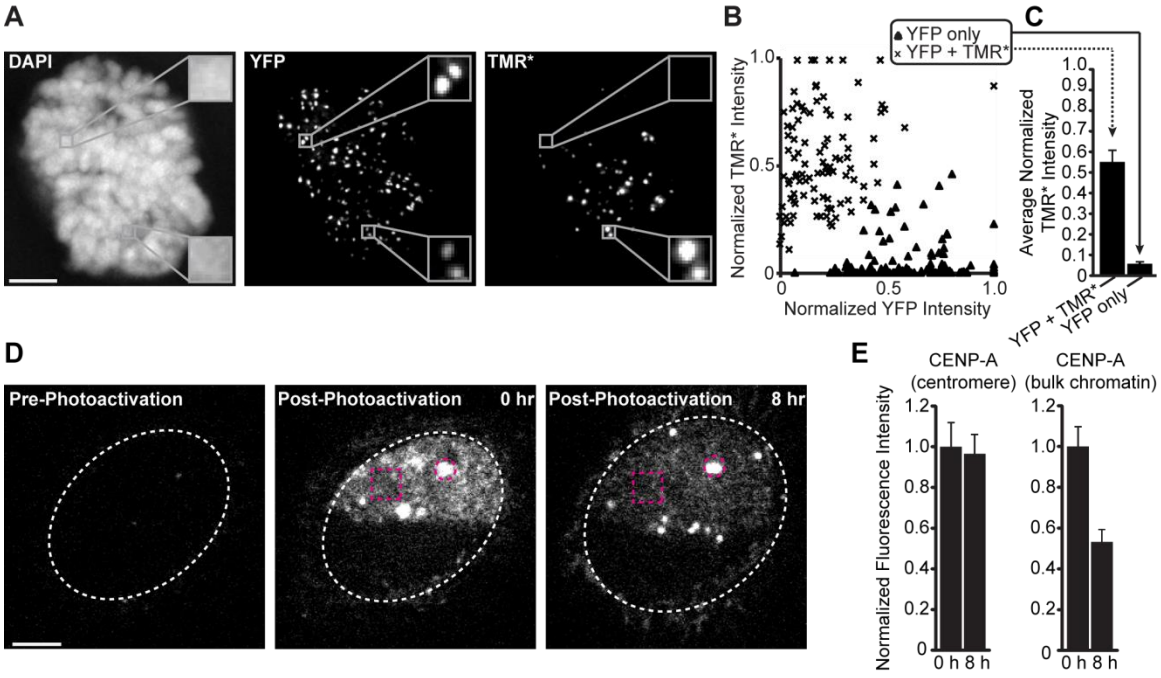

Figure 2.4 CENP-A is stably retained at its centromere of origin

(**A-C**) Cells expressing SNAP-tagged CENP-A were pulse labeled with TMR-Star (TMR*), then fused with cells expressing YFP-tagged CENP-A. Representative images (A) show a cell in the second mitosis after fusion; insets 3x magnification. X-means clustering was used to classify YFP only (triangles) or YFP and TMR* ('x' marks) centromeres (B), and mean (± s.e.m) TMR* intensity was calculated for each group (C). (**D, E**) Cells expressing high levels of CENP-A-PAGFP were photoactivated in bulk (box) and centromeric (circle) chromatin. Representative images (D) show a subset of centromeres in a single z-section. Fluorescence intensity was quantified at 0 and 8 hrs after photoactivation (E, mean ± s.e.m).

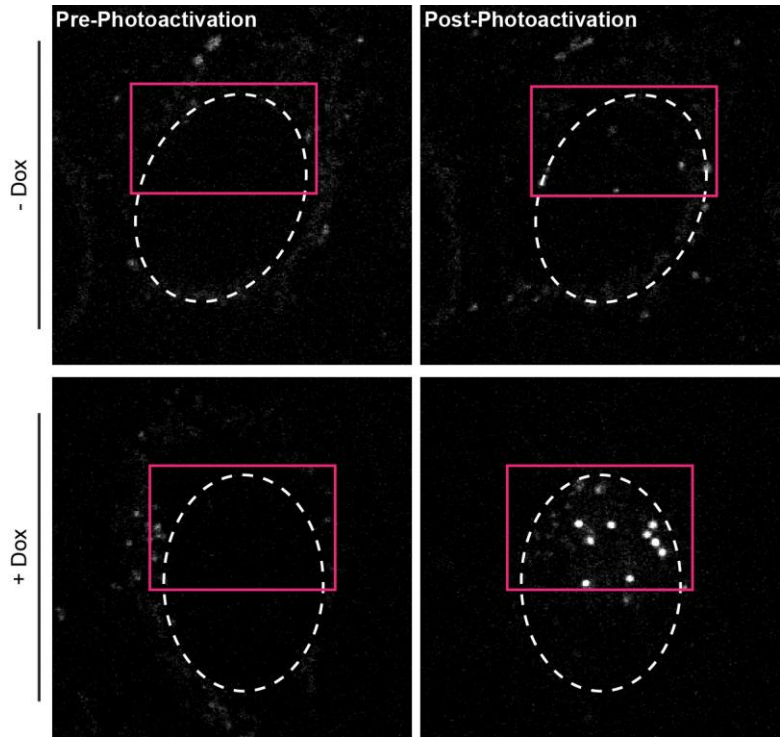

Figure 2.5 Levels of CENP-A-PAGFP overexpression are doxycycline-dependent

Representative images of cells treated with or without 50 ng/mL of dox for 48 hr and then immediately photoactivated. Pink boxes denote the photoactivated region and white dotted lines denote the nucleus. Note that at 50 ng/mL of dox does not result in the same level of CENP-A expression as seen in Fig. 4D where 20x [Dox] is used.

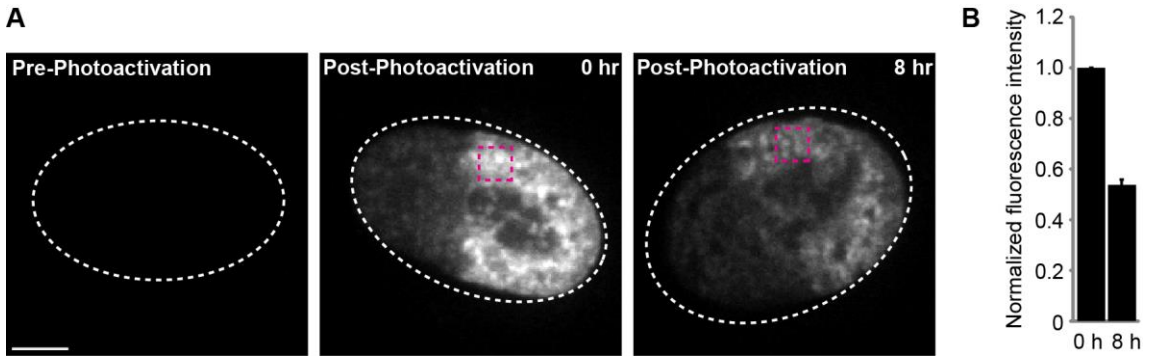

Figure 2.6 Measuring the turnover of H3.1.

(**A**) Representative image of experiment with H3.1-PAGFP photoactivation in a section of the nucleus. Pink box defines a representative ROI selected for quantification. Note that the images show a single z-section through the nucleus. Scale bar = 5 μm. (**B**) Quantification of experiment in (**A**). Data shown as mean ± s.e.m.

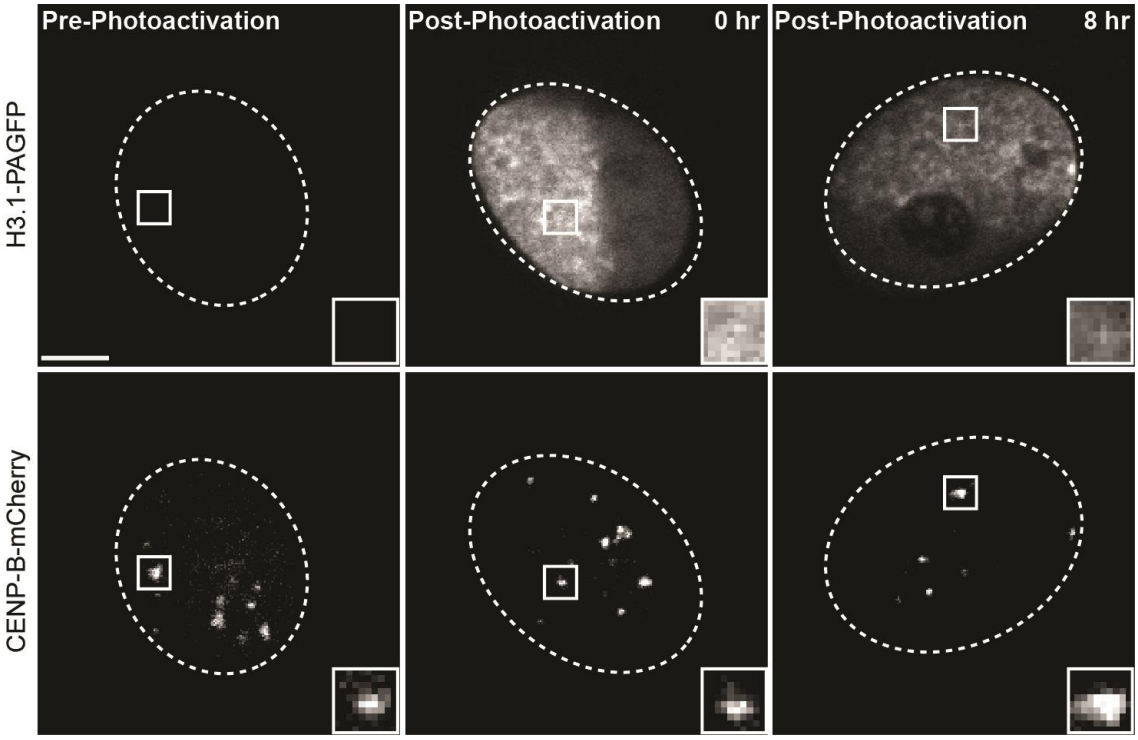

Figure 2.7 H3.1 is not strongly retained at centromeres.

HeLa cells constitutively expressing H3.1-PAGFP and transfected with a plasmid encoding CENP-B-mCherry (Liu et al., 2010). H3.1-PAGFP near the centromere is slightly more intense both before and after an 8 hr incubation following photoactivation. Insets are 2x magnification. Scale bar = 5 μm.

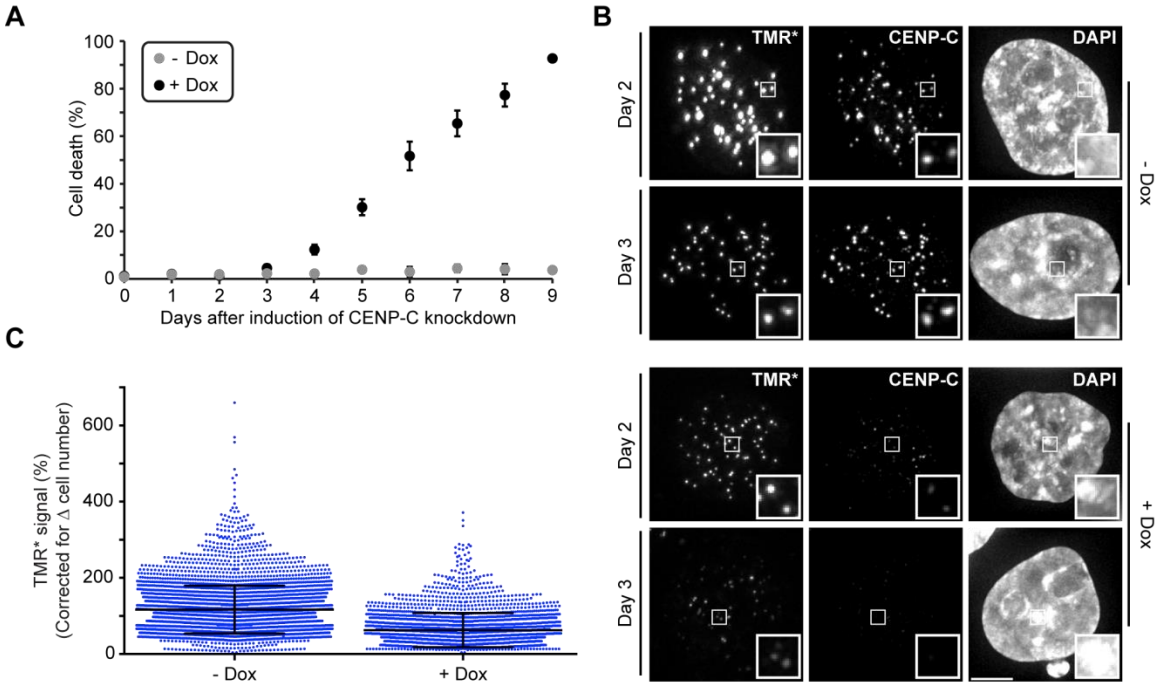

Figure 2.8 Depletion of CENP-C reduces the high stability of CENP-A at centromeres.

(**A**) CENP-C knockdown begins causing cell death 4 days post-induction (mean ± s.d.) (**B, C**) Cells with (+ Dox) and without (- Dox) CENP-C depletion were pulse labeled with TMR* (Day 2), and the relative CENP-A-SNAP signals were analyzed (Day 3). Quantification shows CENP-A-SNAP signal retained at day 3 (>2500 centromeres plotted with mean ± s.d.). Scale bars, 5 μm.

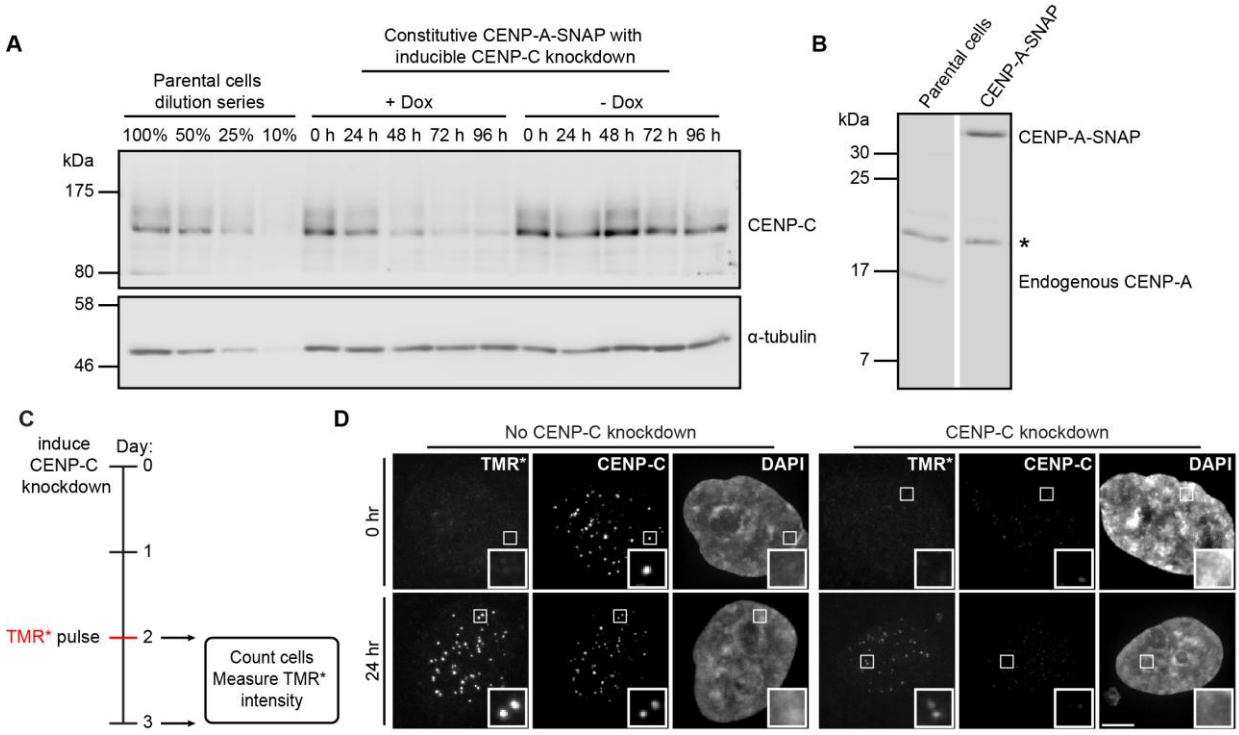

Figure 2.9 CENP-C knockdown effects on retention and assembly of CENP-A at the centromere.

(**A**) Immunoblot of CENP-C levels in inducible CENP-C knockdown cells at indicated timepoints after Dox addition, compared to the cells without Dox. Whole cell lysate dilutions from parental cells were used to measure the extent of CENP-C knockdown. α-tubulin levels were used as a loading control. (**B**) Immunoblot of CENP-A levels in parental and CENP-A-SNAP cell lines. Asterisk denotes non-specific band. (**C**) Schematic for tracking CENP-A levels upon CENP-C knockdown (see Fig. 2.8B,C). (**D**) Cells were synchronized using a double-thymidine block and pulse-labeled with TMR* 6.5 hours post-release to label the nascent pool of CENP-A just prior to loading. Left, representative maximum projected immunofluorescence images of CENP-A-SNAP cells. Right, representative images of CENP-A-SNAP + CENP-C knockdown cells. Insets are a 3x magnification of selected representative centromeres. Scale bar = 5 μm.

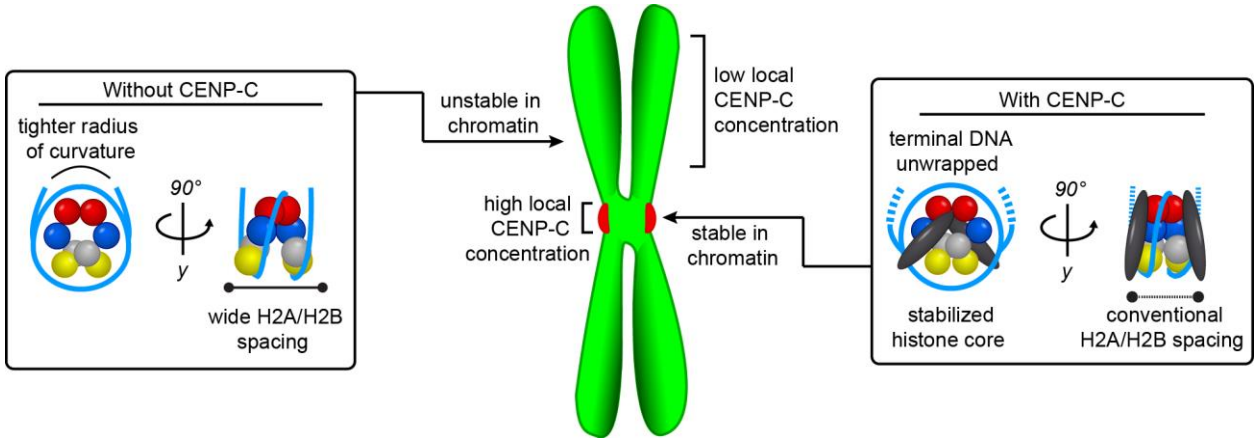

Figure 2.10 Summary model for collaboration of CENP-C with CENP-A nucleosomes in specifying centromere location.

2.5 Methods

2.5.1 *FRET* experiments

Recombinant human H2B was mutated using QuikChange (Stratagene) to contain a single cysteine (K120C or S123C) and then purified as described for the wildtype H2B (Sekulic et al., 2010). Lyophilized protein was dissolved in unfolding buffer (6 M Gnd-HCl, 10 mM Tris-HCl pH 7.5 at 20ºC, 0.4 mM TCEP) for 1 hr at RT and a 30-molar excess of either maleimido coumarin 343 (C343) or maleimido rhodamine B (RhB) dissolved in DMF was added dropwise to the protein. The reaction proceeded overnight shielded from light and was quenched with 10 mM DTT and run over a PD-10 column (GE Healthcare) to separate out free dye. Labeled H2B was then mixed with equimolar amounts of H2A for dimer reconstitution and purification using previously established methods (Dyer et al., 2004; Sekulic et al., 2010). Labeling efficiencies, E, ranged from 45-90% and were calculated by spectroscopy using the Beer-Lambert law using the following equation (Lackowicz, 2007):

$$\mathbf{E = [(A_{280} - (CF\ A_{max})/\varepsilon_{protein} l]/(A_{max}/\varepsilon_{fluorophore} l)\ (1)}$$

where A_{280} is the absorbance of protein at 280 nm, A_{max} is the absorbance of fluorophore at its maximum wavelength, $\varepsilon_{protein}$ and $\varepsilon_{fluorophore}$ are the molar extinction coefficients for protein and fluorophore, respectively, l is the pathlength, and CF is the correction factor for contribution to the protein A_{280} from the fluorophore. Labeling efficiency was further confirmed by SDS-PAGE (coomassie blue staining) and mass spectrometry. α-satellite DNA derived from a sequence described by Harp, *et al.* (Harp et al., 1996) or the 601 DNA sequence described by Lowary and Widom (Lowary and Widom, 1998) were used in nucleosome assembly reactions. Briefly, a 145 bp region derived from a human α-satellite sequence with 25 bp of flanking DNA on each side was cloned into the pUC19 plasmid using EcoRI and XbaI restriction sites. The α-satellite DNA monomer was then amplified from the plasmid by PCR using primers specific to the flanking DNA

regions. The complete α-satellite sequence is: 5'-CGTATCGCCTCCCTCGCGCCATCAG ATCAATATCCACCTGCAGATTCTACCAAAAGTGTATTTGGAAACTGCTCCATCAAAAGGCATG TTCAGCTCTGTGAGTGAAACTCCATCATCACAAAGAATATTCTGAGAATGCTTCCGTTTGCCT TTTATATGAACTTCCTGATCTGAGCGGGCTGGCAAGGCGCATAG-3', with the 145 bp α-satellite region underlined. Typically, DNA from multiple 96-well PCR reactions were pooled, ethanol precipitated, resuspended in TE buffer and purified by anion-exchange chromatography. Widom 601 DNA was purified as described (Hasson et al., 2013). Nucleosomes were assembled on either DNA sequence and uniquely positioned using the gradual salt dialysis method followed by thermal shifting for 2 hr at 55ºC (Dyer et al., 2004). Assembly was assessed by native PAGE (ethidium bromide and coomassie blue staining) and by SDS-PAGE (coomassie blue staining). As mentioned above, the fluorophores for FRET measurements were C343, serving as an energy donor (D), and RhB, serving as an acceptor (A). C343 and RhB were selected because their calculated R_0 (Förster radius; distance at which energy transfer efficiency is 50%) is 58 Å, which is within the range of predicted dimer distances where energy transfer would be most sensitive to changes in FRET efficiency. For synthesis of fluorophores, all solvents and reagents were obtained from standard commercial sources and used as received. Selecto silica gel (Fisher Scientific, particle size 32-63 μm) was used for column chromatography. ^{1}H NMR spectra were recorded on a Varian Unity 400 MHz spectrometer. Mass spectra were obtained on a MALDI-TOF MS Microflex LRF instrument (Bruker Daltonics), using α-cyano-4-hydroxycinnamic acid as a matrix. The compound maleimido C343 was synthesized by a CDMT-assisted peptide coupling of C343 and 1-(2-Aminoethyl)pyrrol-2,5-dione. 1-(2-Aminoethyl)pyrrol-2,5-dione was synthesized as described (Richter et al., 2012). C343 was dissolved in DMF at 0°C, 2-chloro-4,6-dimethoxy-1,3,5-triazine and N-methylmorpholine (NMM) were added, and the mixture was stirred for 1 hr. 1-(2-Aminoethyl)pyrrol-2,5-dione and NMM were dissolved separately in DMF and added dropwise to the C343 mixture. The reaction was stirred at 0°C for 2 hr and then warmed to room

temperature and stirred for 12 hr. The solvent was removed under vacuum and the residue was purified by column chromatography (silica gel, DCM). The fraction containing maleimido C343 was collected, the solvent was evaporated, and the product was dried under vacuum. ^{1}H NMR ($CDCl_3$, δ): 8.94 (s, 1H), 8.57 (s, 1H), 6.99 (d, 2H, ^{3}J = 3.5 Hz), 6.70 (s, 2H), 3.80 (t, 1H, ^{3}J = 5.8 Hz), 3.65 (m, 2H), 3.34 (m, 4H), 2.88 (t, 2H, ^{3}J = 6.3 Hz), 2.77 (t, 2H, ^{3}J = 6.1 Hz), 1.97 (m, 4H). For MALDI-TOF, the m/z (mass-to-charge ratio) calculated for $C_{22}H_{21}N_3O_5$ was 407.15; the following species were found; 407.102 [M]+ and 429.767 [M+Na]+. Maleimido RhB was synthesized by a HBTU-assisted peptide coupling of RhB piperazine amide (Nguyen et al., 2003) and N-maleimidoglycine (Kassianidis et al., 2006). ^{1}H NMR ($CDCl_3$, δ): 7.78-7.72 (m, 3H), 7.53-7.51 (m, 1H), 7.29 (m, 2H), 7.10-7.05 (br s, 2H), 6.72 (s, 2H), 6.70 (s, 2H), 4.38 (s, 2H), 3.66-3.55 (m, 8H), 3.49-3.41 (m, 8H) 1.33 (t, 12H, ^{3}J = 7 Hz). For MALDI-TOF, the m/z calculated for $C_{38}H_{42}N_5O_5^+$ was 648.32; the following species were found; 648.358. Steady-state emission measurements were performed on a FS900 spectrofluorometer (Edinburgh Instruments), equipped with a photon-counting R2658P PMT (Hamamatsu). Samples were excited at 450 nm, the wavelength at which the absorbance of an equimolar mixture of C343 and RhB is dominated by C343 (>99%), and measurements were performed using dilute solutions (OD_{max}< 0.1) in a Spectrosil quartz cuvette (1 cm optical path length, Starna Cells). As a result, only negligible RhB emission is observed under these conditions in the absence of FRET. Emission spectra were corrected by the detector quantum yield and normalized by the incident light intensity at the excitation wavelength. The final emission spectra used in quantum yield calculations (see below) are expressed in counts (photons) per second (CPS). Absorbance measurements were performed using a LAMBDA 35 UV/Vis spectrophotometer (PerkinElmer). FRET efficiency was calculated based on donor quenching in the presence of an acceptor fluorophore (Forster, 1946; Lorenz et al., 1999; Stryer and Haugland, 1967). The quantum yield of fluorescence was calculated using the following equation (Crosby and Demas, 1971):

$$\Phi_S = \Phi_R[(A_R(\lambda_R)/A_S(\lambda_S)][n_S^2/n_R^2][D_S/D_R] \quad (2)$$

where Φ is quantum yield, A(λ) is the absorbance value at the designated excitation wavelength, n is the refractive index of the solution (n_S = 1.333 and n_R = 1.361), and D is the integrated emission spectrum. The subscripts S and R refer to the sample and reference solutions, respectively. Rhodamine 6G in 100% ethanol was used as a reference actinometer (Φ_R= 0.95) (Kubin and Fletcher, 1982).

Because of the nature of nucleosome reconstitutions, nucleosomes reconstituted with both C343- and RhB-labeled dimers (i.e. our FRET samples) contain some percentage of C343-only nucleosomes. Both C343- and RhB-labeled dimers exhibited ~90% labeling efficiency, meaning that ~10% of the dimers used in a reconstitution reaction are unlabeled. This leads to a mixture of nucleosomes characterized by the following equation:

$$UU + DU + DD + DA + AA + AU = 1 \quad (3)$$

where UU represents the subset of nucleosomes that contain two unlabeled dimers, DU represents the subset of nucleosomes that contain one C343-labeled dimer and one unlabeled dimer, DD represents the subset of nucleosomes with two C343-labeled dimers, DA represents the subset of nucleosomes with one C343-labeled dimer and one RhB-labeled dimer, AA represents the subset of nucleosomes with two RhB-labeled dimers, and AU represents the subset of nucleosomes with one RhB-labeled dimer and one unlabeled dimer. Because we are using donor quenching to calculate FRET efficiency, we only consider C343-containing species, so equation 3 is simplified to the following equation:

$$a + b = 1 \quad (4)$$

where a represents the normalized population of DU and DD nucleosomes and b represents the normalized population of DA nucleosomes in the FRET sample. Both a and b can be calculated using the known labeling efficiencies of both donor-labeled and acceptor-labeled dimers determined from spectroscopy and mass spectrometry analysis.

In order to account for the subset of DU and DD nucleosomes present in our FRET samples when measuring donor quenching, a separate control sample of C343-only nucleosomes are reconstituted and measured alongside every experimental sample. The following equation is then used to calculate the quantum yield of C343 in nucleosomes containing both C343 and RhB dimers:

$$\Phi_{DA} = [\Phi_T - a(\Phi_{DD})]/b \quad (5)$$

where Φ_{DA} is the quantum yield of C343-RhB nucleosomes (DA), Φ_T is the total quantum yield of all C343-containing nucleosomes (DU + DD + DA), Φ_{DD} is the quantum yield of C343-only nucleosomes (DU + DD), and a and b represent the fraction of C343-only nucleosomes and C343-Rhb nucleosomes in a sample, respectively, determined as described above. Φ_T and Φ_{DD} are calculated from the FRET sample and the C343-only sample, respectively, using equation 2 above.

FRET efficiency, Φ_{FRET}, is then determined based on the following equation (Lakowicz, 2007):

$$\Phi_{FRET} = 1-(\Phi_{DA}/\Phi_{DD}) \quad (6)$$

The distance, r, between the two fluorophores is then calculated using the following equation (Lakowicz, 2007):

$$r = R_0[(1/\Phi_{FRET})-1]^{1/6} \quad (7)$$

where R_0 is the Förster radius. For the C343/RhB pair, the R_0 was calculated to be 58 Å, using the following equation (Lakowicz, 2007):

$$R_0 = 9790(J\kappa^2\Phi_{DD}n^{-4})^{1/6} \text{ Å} \quad (8)$$

where J is the spectral overlap integral for C343/RhB pair, Φ_{DD} is the quantum yield of C343, n is the refractive index of the solvent (n=1.333), and κ^2=2/3 is the orientation factor for freely rotating fluorophores (Lakowicz, 2007). Our assumption of orientational averaging as in the case of freely rotating transition dipole moments was confirmed by our anisotropy measurements (see below). The measured anisotropy for the fluorophore pair was found to be less than 0.2, confirming that usage of formula (7) was appropriate for estimation of interchromophoric distances. Steady-state fluorescence anisotropy measurements were performed on a QuantaMaster Spectrophotometer (PTI). Samples were diluted to 0.5-1.0 μM in 150 mM NaCl, 20 mM Tris-HCl pH 7.5 at 4°C, 1 mM EDTA, 1 mM DTT and excited at 450 nm for C343 and 567 nm for RhB. Anisotropy, r, was calculated in FeliX32 software using the following equation (Lakowicz, 2007):

$$r = (I_{VV} - G\, I_{VH})/(I_{VV} + 2G\, I_{VH}) \quad (9)$$

where I_{VV} is the parallel polarized fluorescence intensity, I_{VH} is the perpendicular polarized fluorescence intensity, and G is the correction factor for the setup. Lifetime measurements, τ, were performed using a FluoroLog fluorometer (Horiba Scientific). The excitation source was an LED (NanoLED), λ_{max}=441 nm with an average repetition rate of 1 MHz. Samples were in 150 mM NaCl, 20 mM Tris-HCl pH 7.5 at 4°C, 1 mM EDTA, 1 mM DTT at 0.5-1.0 μM. Emission was measured at 491 nm using a bandpass filter (5 nm). Lifetimes were fitted exponentially using DAS6 software (Horiba Scientific).

2.5.2 HXMS

CENP-A mononucleosomes were reconstituted with the same 195 bp α-satellite DNA described above in the FRET studies and concentrated to 0.9 mg/ml with Centricon concentrators (Millipore, Billerica, MA). Recombinant human CENP-C^{CD} consisting of the central domain only (a.a. 426-537, the plasmid for recombinant human CENP-C^{CD} expression was a generous gift from A. Straight, Stanford, USA) was GST-tagged and purified over a GST column followed by PreScission protease cleavage (GE Healthcare) and ion-exchange chromatography and prepared in a buffer containing 20 mM Tris pH 7.5, 200 mM NaCl, 0.5 mM EDTA, 1 mM DTT. To form complexes with CENP-C^{CD}, 2.2 moles of recombinant CENP-C^{CD} were added per mole of CENP-A nucleosomes. To the nucleosome-only sample the buffer used for CENP-C^{CD} preparation was added so that the chemical composition of the buffers were identical in all cases. Deuterium on-exchange was carried out by adding 5 µL of each sample (containing approximately 4 µg of nucleosomes or complex) to 15 µL of deuterium on-exchange buffer (10 mM Tris, pD 7.5, 0.5 mM EDTA, in D_2O) so that the final D_2O content was 75%. Reactions were quenched at the indicated time points by withdrawing 20 µL of the reaction volume, mixing in 30 µL ice cold quench buffer (2.5 M GdHCl, 0.8% formic acid, 10% glycerol), and rapidly freezing in liquid nitrogen prior to proteolysis and LC-MS steps. HX samples were individually melted at 0°C then injected (50 µl) and pumped through an immobilized pepsin (Sigma) column at initial flow rate of 50 µl/min for 2 min followed by 150 µl/min for another 2 min. Pepsin was immobilized by coupling to Poros 20 AL support (Applied Biosystems) and packed into column housings of 2 mm x 2 cm (64 µL) (Upchurch). Protease-generated fragments were collected onto a C18 HPLC trap column (800 µm x 2 mm, Dionex) and eluted through an analytical C18 HPLC column (0.3 x 75 mm, Agilent) by a linear 12-55% buffer B gradient at 6 µl/min (Buffer A: 0.1% formic acid; Buffer B: 0.1% formic acid, 99.9% acetonitrile). The effluent was electrosprayed into the mass spectrometer (LTQ Orbitrap XL, Thermo Fisher Scientific). The SEQUEST (Bioworks) software program was used to

identify the likely sequence of parent peptides using nondeuterated samples via tandem MS. MATLAB based MS data analysis tool, ExMS, was used for data processing (Kan et al., 2011).

2.5.3 MNase digestions

Nucleosomes were assembled using the same 195 bp α-satellite DNA sequence used in FRET studies using the same assembly approach described above. Nucleosomes were digested for various times with 2 U/μg of MNase (Roche) at room temperature (22°C). Reactions were terminated with the addition of guanidine thiocyanate and EGTA. The DNA was isolated using a MinElute PCR purification kit (Qiagen) and analyzed on an Agilent 2100 Bioanalyzer.

2.5.4 SANS

Nucleosome core particles were assembled on the α-satellite 145 bp sequence described above. The sequence was cloned in tandem copies separated by EcoRV sites in pUC57. The 145 bp fragments were released by EcoRV digestion and purified away from the backbone by anion exchange chromatography. Following nucleosome reconstitutions, performed as described above, the nucleosomes were purified by preparative electrophoresis (Prep Cell, BioRad) using a 5% native gel to separate free DNA and any other non-nucleosomal species (Dyer et al., 2004). SANS experiments were performed at the National Institutes of Standards and Technology Center for Neutron Research NG-3. Samples were prepared by dialysis at 4ºC against matching buffers containing 20% or 80% D_2O for a minimum of 3 hr using a 6-8 kDa cutoff D-tube dialyzer (Novagen). Samples were centrifuged at 10,000 X g for 5 min at 4ºC and then loaded into Hellma quartz cylindrical cells (outside diameter of 22 mm) with 1 mm path lengths and maintained at 6ºC during the experiment. Sample concentrations were determined by Bradford analysis and optical absorbance at 260 nm. Scattered neutrons were detected with a 64 cm × 64 cm two-dimensional position-sensitive detector with 128 × 128 pixels at a resolution of 0.5 cm/pixel. Data reduction was performed using the NCNR Igor Pro macro package (Kline, 2006). Raw counts

were normalized to a common monitor count and corrected for empty cell counts, ambient room background counts and non-uniform detector response. Data were placed on an absolute scale by normalizing the scattered intensity to the incident beam flux. Finally, the data were radially-averaged to produce scattered intensity, I(q), versus q curves. The scattered intensities from the samples were further corrected for buffer scattering and incoherent scattering from hydrogen in the samples. Data collection times varied from 0.5-2 hr, depending on the instrument configuration, sample concentration and buffer conditions. Sample-to-detector distances of 11 m (q-range 0.006-0.043 $Å^{-1}$, where $q = 4\pi\sin(\theta)/\lambda$, where λ is the neutron wavelength and 2θ is the scattering angle), 5 m (q-range 0.011–0.094 $Å^{-1}$), and 1.5 m (detector offset by 20.00 cm, q-range 0.03–0.4 $Å^{-1}$) at a wavelength of 6 Å and a wavelength spread of 0.15 were collected for each contrast point. We observed good agreement between Rg and I(0) values determined from either inverse Fourier analysis using GNOM or from Guinier analysis. The program MULCh (Whitten et al., 2008) was used to calculate theoretical contrast and to analyze contrast variation data. Distance distribution curves were normalized for total molecular mass for the complex.

2.5.5 SNAP labeling experiments and cell fusions

CENP-A-SNAP HeLa cells for fusion experiments were labeled with TMR* (NEB) as described previously and subjected to a double thymidine block with a final thymidine concentration of 2 mM (Bodor et al., 2013; Jansen et al., 2007). YFP-CENP-A HeLa cells (Black et al., 2007), CENP-A-SNAP Hela cells (Jansen et al., 2007), and SNAP-tagged core histone (H3.1, H3.3, H4, and H2B)-expressing HeLa cells (Boder et al., 2013; Ray-Gallet et al., 2011) are all established lines. After labeling with TMR*, CENP-A-SNAP HeLa cells were trypsinized, counted, and co-seeded onto poly-D-lysine (Sigma-Aldrich) treated coverslips along with an equivalent number of HeLa cells constitutively expressing YFP-CENP-A. Cells were arrested in growth medium (DMEM supplemented with 10% fetal bovine serum (FBS), 100 U/mL penicillin,

and 100 mg/mL streptomycin) containing 2 mM thymidine for 17 hr. Cells were then washed 3x with PBS, fused with 50% PEG-1500 (Roche) for 30 s and subsequently washed in PBS and placed in media containing 24 μM deoxycytidine to release from thymidine block. After 9 hr, cells were blocked again with media containing thymidine for 17 hr. Cells were released from thymidine with DMEM media containing 24 μM deoxycytidine and nocodazole was added 7 hr post-release at a final concentration of 400 ng/mL. Coverslips were fixed and processed for immunofluorescence at the timepoints outlined in Fig. S12A. HeLa-based cell lines for inducible CENP-A-SNAP with and without shRNAs, and constitutive CENP-A-SNAP with inducible shRNAs directed against CENP-C were generated by recombinase-mediated cassette exchange (RMCE) using the HILO RMCE system (a generous gift from E.V. Makeyev, Nanyang Technological University, Singapore (Khandelia et al., 2011)). pEM784 was used to express nuclear-localized Cre recombinase. pEM791 was modified for inducible expression of CENP-A-SNAP-HA3, CENP-A-SNAP-HA3 plus 2 shRNAs against CENP-C (5'-tgctgttgactttctaccttgaaggagttttggccgctgactgactccttcaatagaaagtcaa-3' and 5'-tgctgacaagtttgttcttggactcagttttggccactgactgactgagtccaaacaaacttgt-3'), constitutive CENP-A-SNAP-HA3 driven by the EF1α promoter plus 2 shRNAs against CENP-C, and CENP-A-PAGFP respectively. CENP-C knockdown was induced in constitutive CENP-A-SNAP cell lines by treating for 48 hr with 2 μg/mL doxycycline prior to TMR* labeling for pulse-chase experiments to measure the retention of CENP-A protein at centromeres. Cells were fixed either immediately after labeling or again 24 hr later. Cell number was also determined at these time points, so that the total level of CENP-A turnover could be calculated, as described (Bodor et al., 2013). For experiments to measure the amount of new CENP-A assembly with or without CENP-C knockdown, cells were treated with 50 ng/mL of doxycycline during a double thymidine block procedure that spanned 48 hr. Following release from the double thymidine block, CENP-A-SNAP was quenched with SNAP-Cell Block (NEB) then released for 6.5 hr to allow for new

synthesis of CENP-A-SNAP protein. The nascent pool of CENP-A-SNAP protein was then pulse-labeled with TMR*, and the cells were cultured for an additional 17.5 hr prior to fixation and processing for immunofluorescence. A separate sample was labeled with TMR* immediately after the quench step to confirm successful quenching of 'old' CENP-A. For immunofluorescence, cells were fixed in 4% formaldehyde for 10 min at room temperature followed by permeabilization using PBS + 0.5% Triton X-100. Samples were stained with DAPI before mounting with Vectashield medium (Vector laboratories). The following primary antibodies were used: mouse mAb anti-CENP-A (1:1000 Enzo), rabbit pAb anti-CENP-C (1:2000) (Bassett et al., 2010), and mouse mAb anti-HA.II antibody (1:1000, Covance). AlexaFluor488- and AlexaFluor647-conjugated secondary antibodies were obtained from Invitrogen and were used at 1:1000. Images were captured at 23°C using software (LAF; Leica) by a charge-coupled device camera (ORCA AG; Hamamatsu Photonics) mounted on an inverted microscope (DMI6000B; Leica) with a 100x 1.4 NA objective. For each sample, images were collected at either 0.2 µm z-sections (Figs. 4A, S12-15,17) or 0.49 µm z-sections (Figs. 2.4A, 2.8B, and 2.9D) that were subsequently deconvolved using identical parameters. The z-stacks were projected as single two-dimensional images and assembled using PhotoShop (version 13.0; Adobe), ImageJ (1.48v) (Schneider et al., 2012), and Illustrator (version 16.0; Adobe). To quantify fluorescence intensity in cell fusions, individual centromeres from non-deconvolved maximum projections were selected and the intensity of both TMR* and YFP signal were determined after subtracting the background fluorescence measured from adjacent regions of the cell using ImageJ. For each unique fusion, the levels of fluorescence for both channels were normalized to the highest measured value in that channel, leading to normalized values for YFP intensity and TMR* intensity for each centromere in the fused cell. Thus, each centromere is a data point that has an associated TMR* and YFP value assigned to it, which were then run through the machine learning x-means clustering algorithm of Weka (Hall et al., 2009; Pelleg and Moore, 2000), which partitions the data

points into n clusters based on their closeness to an assigned mean value. This generated the two groups of data points (YFP only and YFP + TMR*) in the plot seen in Fig. 4B. To quantify fluorescence intensity in experiments with CENP-C knockdown, the Centromere Recognition and Quantification (CRaQ) macro (Bodor et al., 2012) was run in ImageJ with standard settings using a reference channel and DAPI. Total CENP-A staining was used as the reference channel to define ROIs for quantification of TMR* intensity. CENP-A fluorescence intensity values at the final time point were normalized to reflect the total pool of labeled CENP-A by accounting for the increase in cell number in the dividing cell populations following TMR* pulse. 2800-4200 centromeres from >70 cells were analyzed for each time point.

2.5.6 PAGFP experiments

CENP-A-PAGFP cells were generated with the RMCE system (Khandelia et al., 2011), as described above, and expression was induced with 1 mg/mL doxycycline 2 days prior to photoactivation and continued for the duration of the experiment. H3.1-PAGFP cells were created by viral integration of an H3.1-PAGFP transgene via the pBabe retroviral system. Cells were cultured in growth medium at 37°C in a humidified atmosphere with 5% CO_2. For live imaging, cells were plated on 22 x 22 mm glass coverslips (#1.5; Thermo Fisher Scientific) coated with poly-D-lysine (Sigma-Aldrich). Coverslips were mounted in magnetic chambers (Chamlide CM-S22-1, LCI) using growth medium without phenol red (Invitrogen). Temperature was maintained at 37°C with 5% CO_2 using an environmental chamber (Incubator BL; PeCon GmbH). Evaporation of media was prevented by applying a thin layer of mineral oil over the media within the magnetic chamber. Prior to photoactivation, a single plane image of the unactivated nucleus was acquired to be used for background subtraction. Cells were subsequently photoactivated by defining an ROI surrounding ~half of the nucleus and then activated using a pointable 405 nm laser (CrystaLaser) set to 10% power and one repetition using iLAS^2 software run through

MetaMorph, followed by acquisition of an image of a single z-plane. Cells were then followed by DIC for 8 hr, at which point a final single plane image was acquired. Images were acquired with a confocal microscope (DM4000; Leica) with a 100x 1.4 NA objective lens, an XY Piezo-Z stage (Applied Scientific Instrumentation), a spinning disk (Yokogawa Corporation of America), an electron multiplier charge-coupled device camera (ImageEM; Hamamatsu Photonics), and a laser merge module equipped with 488 nm and 593 nm lasers (LMM5; Spectral Applied Research) controlled by MetaMorph software (Molecular Devices). To quantify the retention of CENP-A-PAGFP in bulk chromatin, a 25 x 25 pixel region-of-interest (ROI) was drawn in ImageJ on a region of photoactivated bulk chromatin and the average fluorescence was recorded. Recorded fluorescence measurements were corrected for background by subtracting the fluorescence value of the pre-photoactivated ROI. This corrected average fluorescence of the ROI was then multiplied by the area of the ROI in order to calculate the average fluorescence of the area. These area fluorescence measurements of the bulk chromatin ROI for each cell were averaged to generate the final numbers for comparison. Upon overexpression, CENP-A initially assembles into nucleosomes at centromeres and at locations throughout the genome (Heun et al., 2006; Lacoste et al., 2014). Functional centromeres do not spread throughout chromosomes under these conditions. We note that there is a small soluble pool of CENP-A in bulk chromatin that is mobile throughout the nucleus, but this does not significantly contribute to quantification and does not diffuse to the unactivated portion of the nucleus in earlier time points. To quantify the retention of CENP-A-PAGFP in centromeric chromatin, single planes were thresholded to create ROIs around all visibly photoactivated centromeres and the average fluorescence as well as the total centromeric area were both recorded. Fluorescence measurements were corrected for background by subtracting the fluorescence value of the pre-photoactivated ROIs. This corrected average fluorescence of the ROI was then multiplied by the area of the ROIs in order to calculate

the average fluorescence of the area. These area fluorescence measurements of the centromeric chromatin ROIs for each cell were averaged to generate the final numbers for comparison.

2.5.7 Cell lethality assay

Constitutive CENP-A-SNAP HeLa cells with doxycycline-inducible shRNAs directed against CENP-C were seeded in 6-well plates in triplicate at 8.4 x 10^4 cells per well and with daily introduction of 2 µg/mL dox. Cells were collected and stained with 0.4% Trypan Blue (CellGro) and counted on a hemocytometer to calculate the percentage of cell death based on trypan blue uptake.

2.5.8 Immunoblotting

Samples derived from whole cell lysates were separated by SDS-PAGE and transferred to a nitrocellulose membrane for immunoblotting. Blots were probed using the following antibodies: human ACA (2 µg/mL, Antibodies Incorporated), rabbit anti-CENP-C (1.7 µg/mL) and mouse mAb anti-α-tubulin (1:4000, Sigma-Aldrich). Antibodies were detected using a horseradish peroxidase-conjugated secondary antibody at 1:10,000 (human) and 1:2000 (rabbit or mouse) (Jackson ImmunoResearch Laboratories) and enhanced chemiluminescence (Thermo Scientific).

CHAPTER 3:

Long-term retention of CENP-A nucleosomes in mammalian oocytes underpins transgenerational inheritance of centromere identity

3.1 Abstract

Centromeres control genetic inheritance by directing chromosome segregation but are not genetically encoded themselves. Rather, centromeres are defined by nucleosomes containing CENP-A, a histone H3 variant (Black and Cleveland, 2011). In cycling somatic cells, centromere identity is maintained by an established cell cycle-coupled CENP-A chromatin assembly pathway, but how centromeres are inherited through the mammalian female germline is unclear because of the long (months to decades) prophase I arrest. We show that mouse oocytes retain the pool of CENP-A nucleosomes assembled before birth, and this pool is sufficient for centromere function, fertility, and genome transmission to embryos. Indeed, oocytes lack any measurable CENP-A nucleosome assembly through the entire fertile lifespan of the female (>1 year). Thus, the remarkable stability of CENP-A nucleosomes confers transgenerational centromere identity in mammals.

3.2 Introduction

A pathway for centromere inheritance between somatic cell cycles is well established (Black and Cleveland, 2011). CENP-A nucleosomes redistribute equally between sister centromeres during DNA replication, and newly synthesized CENP-A is assembled at human centromeres exclusively in early G1-phase of the cell cycle (Falk et al., 2015; Jansen et al., 2007). Therefore, centromere inheritance depends on retention of CENP-A nucleosomes from incorporation into chromatin in S-phase until new loading in the subsequent G1-phase. This cell cycle-coupled mechanism of centromere maintenance raises the question of how centromeres are inherited between generations in the mammalian female germline. Between pre-meiotic S-phase in the oocyte and the subsequent G1-phase in the zygote, mammalian oocytes arrest in an extended prophase I that may last from a few months to decades depending on species (Von Stetina and Orr-Weaver, 2011). Three attractive models could explain how centromere identity is

maintained during this meiotic arrest: **1)** CENP-A is not retained at centromeres during female meiosis, and centromere identity in the germline is independent of CENP-A, **2)** CENP-A is maintained through the action of a meiotic chromatin assembly pathway, which is distinct from the timing of the established cell cycle-coupled pathway in cycling somatic cells, or **3)** CENP-A nucleosomes assembled at oocyte centromeres are extremely stable and maintain centromere identity in the absence of any nascent CENP-A chromatin assembly during the prolonged arrest. The first two models have strong precedent in holocentric worms (Gassmann et al., 2012; Monen et al., 2005) and flies (Dunleavy et al, 2012), respectively. The third model is supported by the notable stability of CENP-A nucleosomes in chromatin: they do not measurably redistribute between centromeres during an entire cell cycle, and their turnover in rapidly dividing somatic mammalian cells is so slow that it can be explained by dilution through segregation on daughter strands of replicating centromere DNA (Bodor et al., 2013; Falk et al., 2015; Jansen et al., 2007). We use mouse as a model system to distinguish between these models for centromere inheritance in the mammalian female germline.

3.3 Results

3.3.1 CENP-A loading does not occur on short timescales during prophase I arrest

We first tested for a meiotic CENP-A chromatin assembly pathway on a short timescale in full grown germinal vesicle intact (GV) oocytes by injecting cRNAs encoding fluorescently tagged proteins: CENP-A, the histone H3 variant H3.3, or CENP-C, which binds CENP-A nucleosomes at centromeres (Falk et al., 2015; Kato et al., 2013) (Fig. 3.1A). We find that H3.3-mCherry assembles into chromatin, as previously shown in oocytes (Akiyama et al., 2011; Nashun et al, 2015), and GFP-CENP-C targets to centromeres, but no CENP-A-GFP is detected at centromeres either in prophase of meiosis I (GV) or after maturation to metaphase II (MII; Fig. 1B,C), though we do detect a measureable increase in GFP fluorescence in oocytes injected with

CENP-A-GFP cRNA (Fig. 3.2A). The CENP-A-GFP cRNA produced functional protein capable of assembly at centromeres, as shown by co-localization of CENP-A-GFP and mCherry-CENP-C in 4-cell embryos (Fig. 3.1D,E). We obtained similar results using CENP-A tagged with Flag and HA epitopes instead of GFP (Fig. 3.2B,C). These data show that a meiosis-specific loading pathway does not assemble measurable CENP-A in full grown oocytes on a timescale of ~40 h.

3.3.2 Generating *Cenpa* conditional knockout mice

To test for CENP-A nucleosome assembly on timescales of many months during the prophase I arrest, we designed a genetic experiment in which we knocked out *Cenpa* in oocytes in resting primordial follicles (Fig. 3.3A). Oocytes in these animals would rely on CENP-A nucleosomes that were assembled at centromeres prior to the knockout. Therefore, if CENP-A is simply lost at oocyte centromeres, as in the worm (Fig. 3.3B, model 1) (Gassmann et al., 2012; Monen et al., 2005), then CENP-A should become undetectable in both knockout and control oocytes. Alternatively, if centromere inheritance depends on meiotic assembly of nascent CENP-A nucleosomes, then centromeric CENP-A levels should decrease in the knockout oocytes over time (Fig. 3.3B, model 2). Finally, if centromere inheritance relies on the stable retention of preassembled CENP-A nucleosomes, then we expect little change in centromeric CENP-A protein levels over time (Fig. 3.3B, model 3). Because a pool of long-lived CENP-A protein in the oocyte would confound interpretation of our gene deletion experiment, we measured total CENP-A protein in oocytes as compared to cycling NIH 3T3 cells. We found that 500 oocytes (4n) have approximately the same amount of CENP-A protein as ~1000 NIH 3T3 cells (with each cell between 3-6n, because they are near-tetraploid and from an asynchronous cycling population) (Fig. 3.4A). These data exclude the possibility that a large pool of excess CENP-A protein exists in oocytes to replenish CENP-A at centromeres in the absence of new synthesis.

To conditionally knock out *Cenpa*, we generated a mouse carrying a *Cenpa* allele in which exons 2-5 are flanked by *loxP* sites (Fig. 3.3C) and used cre-recombinase driven by the *Gdf9* promoter to inactivate *Cenpa* in oocytes in resting primordial follicles (Lan et al., 2004). Multiple lines of evidence indicate that the *Gdf9* promoter is active in these oocytes at an early stage. First, our microarray data show a high level of *Gdf9* mRNA in isolated oocytes from resting primordial follicles collected two days after birth (day 2) (Pan et al., 2005). Second, in an experimental system in which β-gal expression depends on *Gdf9-Cre* expression, primordial follicles stain positive at day 12 (Lan et al., 2004). Because the first wave of follicle development begins at day 5, the β-gal positive oocytes in these primordial follicles must be in the resting state. Third, *Gdf9-Cre* mediated deletion of the *Tsc1* or *Pten* genes, which are essential to maintain quiescence of primordial follicles, leads to activation of the entire pool of primordial follicles by day 23 (Adhikari et al., 2010; Reddy et al., 2008). Finally, *Gdf9-Cre* mediated expression of Diptheria toxin leads to complete loss of oocytes by 8 weeks of age (Uhlenhaut et al., 2009). We derived $Cenpa^{fl/fl}$;*Gdf9-Cre*- (WT) or $Cenpa^{fl/fl}$;*Gdf9-Cre*+ (KO) females in a C57BL/6J background (Fig. 3.4B, Table 3.1). To confirm that the *Cenpa* gene locus is deleted in KO oocytes, we measured *Cenpa* mRNA levels by analyzing cDNA libraries created by reverse transcription of pooled mRNA from KO or WT oocytes (Fig. 3.5A). We found that KO oocytes from young animals (14-19 weeks) contain only trace amounts of *Cenpa* mRNA (0.7% ± 0.3%) relative to that present in WT oocytes (Fig. 3.5B,C). Additionally, we detected measurable differences in *Cenpa* mRNA when cDNA from KO and WT oocytes was mixed in the following ratios: 100% KO, 90% KO/10% WT, and 95% KO/5% WT (Fig. 3.5D,E). These data demonstrate that the *Cenpa* locus is efficiently excised in all KO oocytes and exclude the possibility of a stored pool of long-lived *Cenpa* mRNA.

3.3.3 Stable retention of CENP-A nucleosomes underlies centromere inheritance in the oocyte

Now positioned to test models for how centromere identity is maintained in mammalian oocytes, we measured centromeric CENP-A levels in the oocytes of WT and KO mice after aging them for 11-14.5 months (Fig. 3.3D-F). Centromeres are highly clustered in young oocytes and become even more clustered with age (Fig. 3.3G). We measured total centromeric CENP-A fluorescence in each oocyte (Fig. 3.3F-H) and normalized the signal to that in oocytes obtained from young C57BL/6J controls, to compare biologically replicated experiments (Fig. 3.3F). We find that aged KO and WT oocytes are indistinguishable, inconsistent with nascent CENP-A nucleosome assembly during the prolonged prophase I arrest (Fig. 3.3B, model 2). Similarly, cohesion is established in pre-meiotic S-phase without detectable cohesin turnover during prophase I (Burkhardt et al., 2016). Further, both the WT and KO groups retain ~70% of the CENP-A protein seen in the young C57BL/6J group, showing that the majority of CENP-A present since early prophase I arrest in the primordial follicle is retained at the centromere for ~1 year. This retention is also inconsistent with a model where CENP-A is removed from centromeres in oocytes and then centromere identity is reestablished in the early embryo, as in worms (Fig. 3.3B, model 1) (Gassmann et al., 2012; Monen et al., 2005). These findings are, however, entirely consistent with a model (Fig. 3.3B, model 3) where CENP-A nucleosomes assembled at the centromere before the prophase I arrest maintain centromere identity and function for the fertile lifespan of the female.

3.3.4 CENP-A nucleosomes assembled prior to prophase I arrest provide full fertility

A broadly conserved feature of eukaryotic centromeres is the essential role of CENP-A nucleosomes in building a functional kinetochore (Black et al., 2007; Goshima et al., 2003; Howman et al, 2000; Ravi et al., 2010; Régnier et al., 2005; Stoler et al., 1995). To test whether

the persistence of CENP-A nucleosomes at the centromere, rather than persistent expression, suffices for its essential function in the oocyte, we measured progression to metaphase II (MII) and chromosome alignment on MII spindles (Fig. 3.6A). Oocytes collected from 12 month old KO and WT mice were similar in both assays, consistent with our finding that centromeric CENP-A levels are equivalent between the two groups (Fig. 3.6B,C). Fewer oocytes from the 12 month groups matured to MII eggs compared to young C57BL/6J controls, consistent with age-related meiotic defects (Chiang et al., 2010; Lister et al., 2010; Subramanian and Bickel, 2008).

As the ultimate test of centromere function after *Cenpa* deletion in oocytes, we measured fertility of WT and KO females. We used 5-9 month old females, as older animals (WT or KO) have prohibitively low fecundity and thus yield too few data points. We find that fertility is indistinguishable between WT and KO females, indicating that CENP-A nucleosomes assembled at centromeres in oocytes before the prophase I arrest provide full fertility months later (Fig. 3.7A). Prior to receiving CENP-A protein, message, and/or gene from the WT sperm, meiotic divisions in the oocyte would be completed with the CENP-A nucleosomes assembled 5-9 months earlier.

Our findings demonstrate that *Cenpa* deletion early in the prophase I arrest has no effect on oocyte maturation or female fertility. To independently verify that the *Cenpa* locus was deleted, we designed a cross in which survival of half of the offspring would depend on the presence of an intact maternal *Cenpa* allele in the egg (Fig. 3.7B). We used the *Ddx4* promoter, which turns on in primordial germ cells, to excise a floxed *Cenpa* allele in spermatogonial stem cells (Gallardo et al., 2007). Thus, $Cenpa^{fl/+}$*;Ddx4-Cre/*+ males produce mature sperm that are either $Cenpa^{-}$ or $Cenpa^{+}$. If *Cenpa* is deleted in oocytes from KO females, all eggs produced will be $Cenpa^{-}$. Crossing a KO female with a $Cenpa^{fl/+}$*;Ddx4-Cre/*+ male should produce embryos that are either $Cenpa^{-/+}$ or $Cenpa^{-/-}$, depending on the sperm genotype. $Cenpa^{-/+}$ animals are viable and fertile,

but *Cenpa*$^{-/-}$ is an embryonic lethal phenotype (Howman et al., 2000), so the surviving offspring from the cross should all be *Cenpa*$^{-/+}$ and the litter sizes should be small. If *Cenpa* is not deleted in all oocytes, some offspring will be *Cenpa*$^{fl/+}$or *Cenpa*$^{fl/-}$. We find that pups generated from this cross are exclusively *Cenpa*$^{-/+}$ (Fig. 3.7B), confirming that the *Cenpa* locus is excised in all KO female oocytes. The viability of the *Cenpa*$^{-/+}$ pups provides additional evidence that the CENP-A nucleosomes present at centromeres in KO oocytes are sufficient to produce a viable MII egg and support early embryogenesis.

3.3.5 Transgenerational centromere inheritance depends on retention of CENP-A nucleosomes present during early prophase I arrest

To determine whether CENP-A nucleosomes present early in the prophase I arrest are sufficient for transgenerational inheritance of centromere identity, we examined the offspring of KO females crossed to normal C57BL/6J males. Defects in centromere inheritance between the maternally and paternally inherited chromosomes would be most apparent in metaphase I of the offspring, when the homologous chromosomes are paired. We crossed WT or KO females with C57BL/6J males, collected oocytes from F1 pups that were either *Cenpa*$^{fl/+}$ or *Cenpa*$^{-/+}$ (Fig. 3.7C), and matured them to metaphase I *in vitro*. On each bivalent, we measured CENP-A levels on each side (i.e., at the centromeres of the homologous chromosomes) by immunofluorescence. If centromere inheritance were partially impaired, we would expect asymmetric CENP-A staining on each bivalent, which would imply that the maternal centromeres inherited less CENP-A. We find that it is symmetric, however, and the ratio of CENP-A staining within each bivalent is close to one for both genotypes (Fig. 3.7D,E). Thus, faithful transgenerational centromere inheritance is maintained by the stable retention of CENP-A nucleosomes through the extended prophase I arrest of the oocyte.

3.4 Discussion:

Taken together, our results provide clear genetic evidence that stable retention of CENP-A nucleosomes underlies centromere inheritance through the mammalian female germline. CENP-A protein incorporated into centromeric chromatin before the prophase I arrest, most likely in the G1-phase preceding meiotic entry, displays spectacular longevity and is sufficient to provide essential centromere function for >1 year. This mechanism of centromere inheritance represents a new paradigm when compared to what has been described in other organisms (Dunleavy et al., 2012; Gassmann et al., 2012; Monen et al., 2005). Our results stand in stark contrast to recent reports in which deposition of another histone H3 variant, H3.3, during prophase I is required for normal chromatin structure and gene expression and oocyte survival (Nashun et al., 2015; Tang et al., 2015). Thus, centromeric chromatin remains extremely stable while nucleosome assembly in bulk chromatin is ongoing and essential during the extended prophase I arrest. Pericentromeric heterochromatin (e.g. immunostaining for HP1β and H3K9me3; Fig. 3.8A,B) is similar between oocytes and NIH 3T3 cells, so we prefer the notion that the stability we observe in the oocyte is a property conferred by CENP-A nucleosomes (Black et al, 2004), themselves, and/or other components of the centromere (Falk et al., 2015; Falk et al., 2016). In addition to the important implications for understanding how centromere identity is transmitted transgenerationally in mammals, our findings also advance what we know about the functions of long-lived proteins. Many of the most remarkable examples are from metabolically inactive environments (e.g., crystallin and collagen (Masters et al., 1977; Verzijl et al., 2000)) or of some nuclear components of non-dividing neurons (Commerford et al., 1982; Savas et al., 2012; Toyama et al, 2013). Our findings extend the role of long-lived proteins to one that plays a central and essential role in the orchestration of chromosome segregation in the quintessential pluripotent cell type. At the centromere, the remarkable stability of CENP-A nucleosomes through

the fertile lifespan of the female cements the epigenetic information required to faithfully guide chromosome inheritance and transmit the chromosomal location of the centromere to offspring.

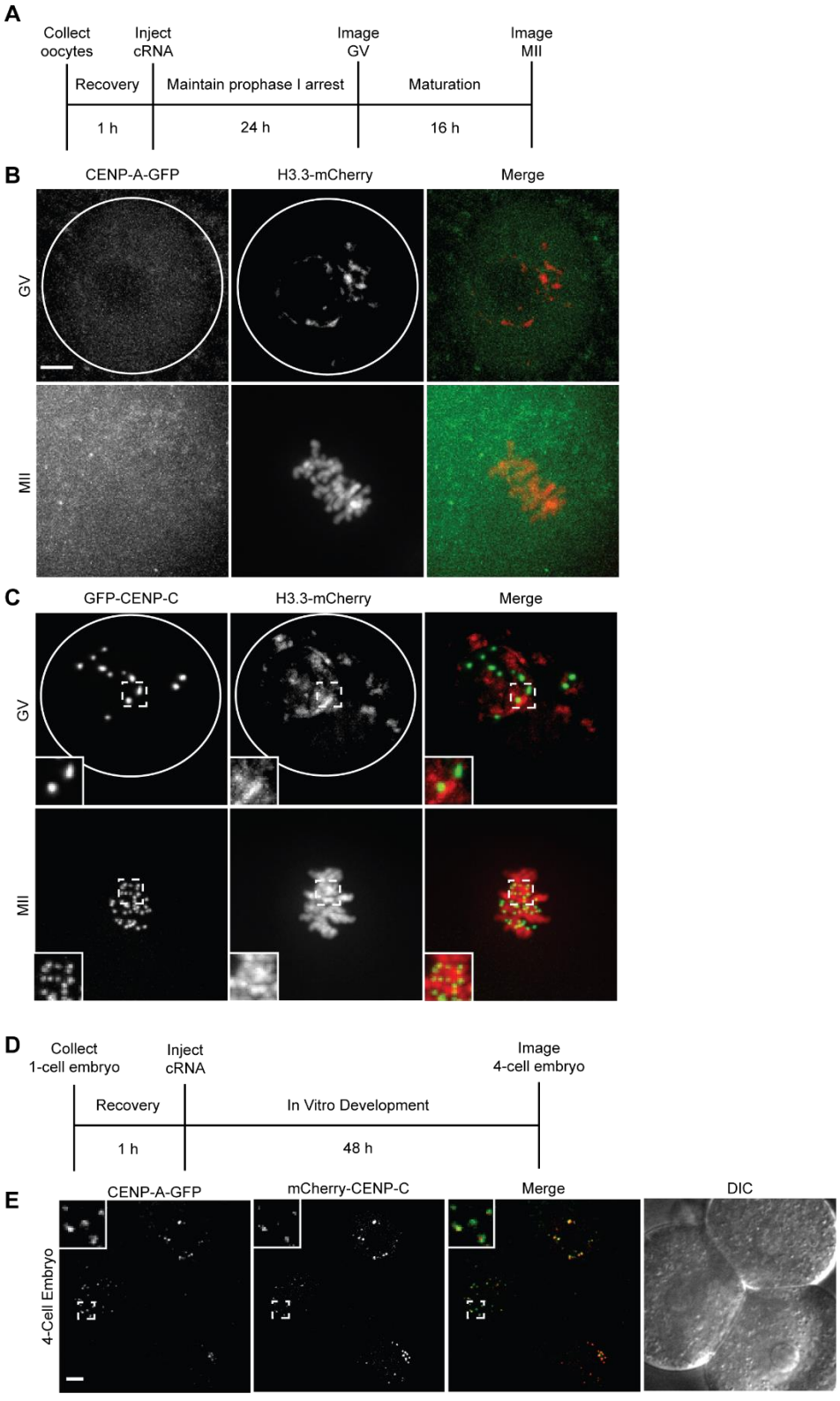
A
Collect oocytes
Inject cRNA
Image GV
Image MII
Recovery
Maintain prophase I arrest
Maturation
1 h
24 h
16 h
B
CENP-A-GFP
H3.3-mCherry
Merge
GV
MII
C
GFP-CENP-C
H3.3-mCherry
Merge
GV
MII
D
Collect 1-cell embryo
Inject cRNA
Image 4-cell embryo
Recovery
In Vitro Development
1 h
48 h
E
CENP-A-GFP
mCherry-CENP-C
Merge
DIC
4-Cell Embryo

Figure 3.1 Absence of CENP-A chromatin assembly in full grown oocytes or MII eggs

(**A-C**) Oocytes were injected with cRNA for CENP-A-GFP and H3.3-mCherry or GFP-CENP-C and H3.3-mCherry, and imaged live in germinal vesicle-intact (GV) or metaphase II (MII) stages as shown in the schematic (A). Representative images show CENP-A-GFP and H3.3-mCherry (B) or GFP-CENP-C and H3.3-mCherry (C) at GV or MII stages (n≥10 in each case). Images are maximal intensity projections of confocal z-series; insets show 1.6x magnification of centromeres labeled with GFP-CENP-C. White circle represents nuclear envelope. (**D, E**) 1-cell stage embryos were injected with cRNA for mCherry-CENP-C and CENP-A-GFP and imaged live at the 4-cell stage, as shown in the schematic (D). Representative images show an optical section of 3 blastomeres (n=27); insets show 3x magnification of CENP-A-GFP and mCherry-CENP-C localized at centromeres. Scale bars 5 μm.

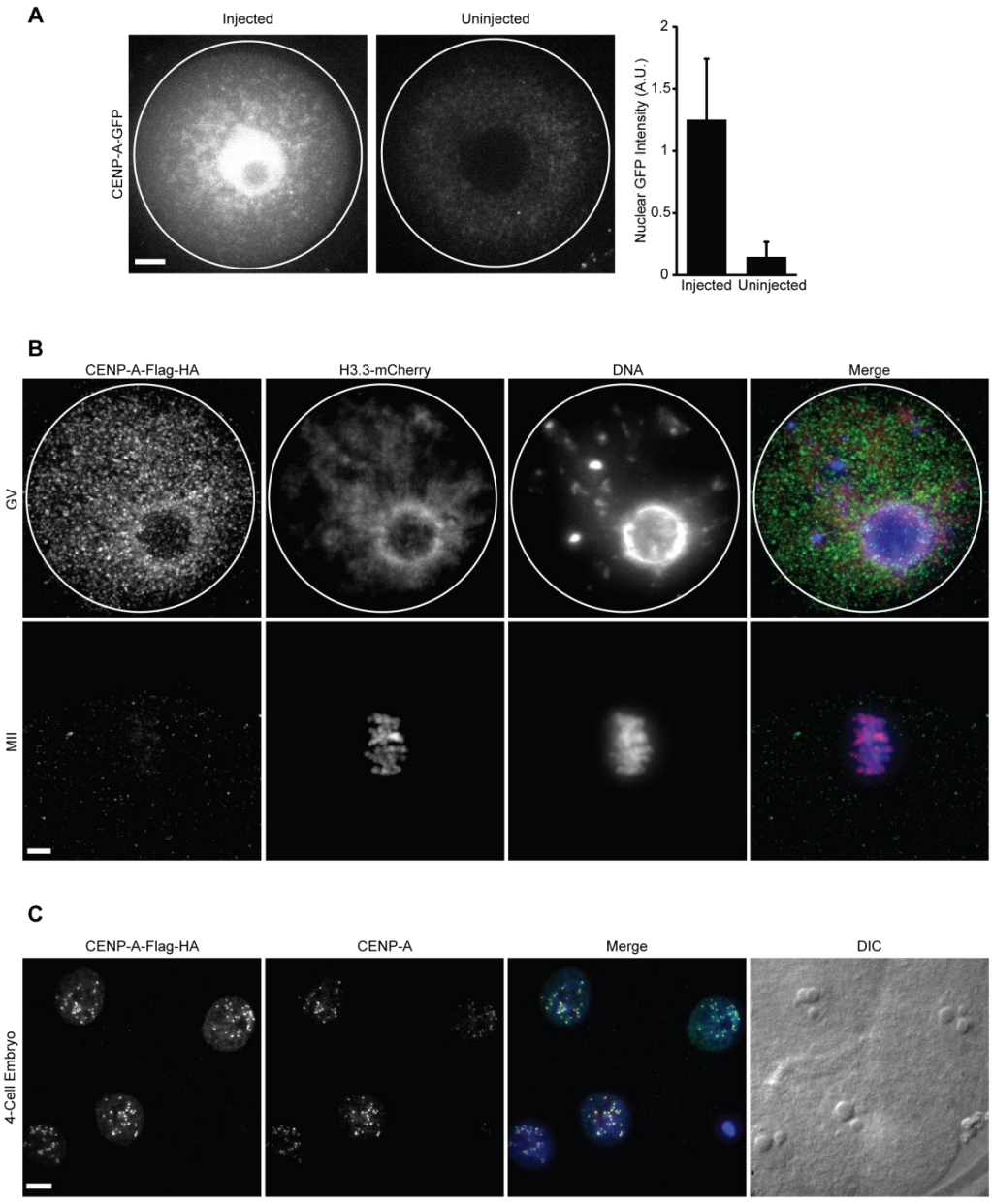

Figure 3.2 Oocytes injected with CENP-A-GFP cRNA have increased GFP fluorescence; absence of CENP-A loading in oocytes injected with CENP-A-Flag-HA cRNA.

(**A**) GV oocytes injected with cRNA encoding CENP-A-GFP display an increased GFP fluorescence compared to uninjected controls, though no CENP-A-GFP localizes to centromeres (n=20 for both injected and uninjected oocytes). White circle represents zona pellucida. Error bars s.d. (**B**) Oocytes were injected with cRNA for CENP-A-Flag-HA and H3.3-mCherry and fixed and stained with HA antibodies at either the germinal vesicle-intact (GV) or metaphase II (MII) stages. Representative images show CENP-A-Flag-HA and H3.3-mCherry. Images are maximal intensity projections of confocal z-series. White circle represents nuclear envelope. In merged images: CENP-A-Flag-HA is in green, H3.3-mCherry is in red, and DNA is in blue. (**C**) 1-cell stage embryos were injected with CENP-A-Flag-HA and fixed and stained with CENP-A and HA antibodies at the 4-cell stage. In merged image: CENP-A-Flag-HA is in green, CENP-A is in red, and DNA is in blue. Scale bars 10 μm.

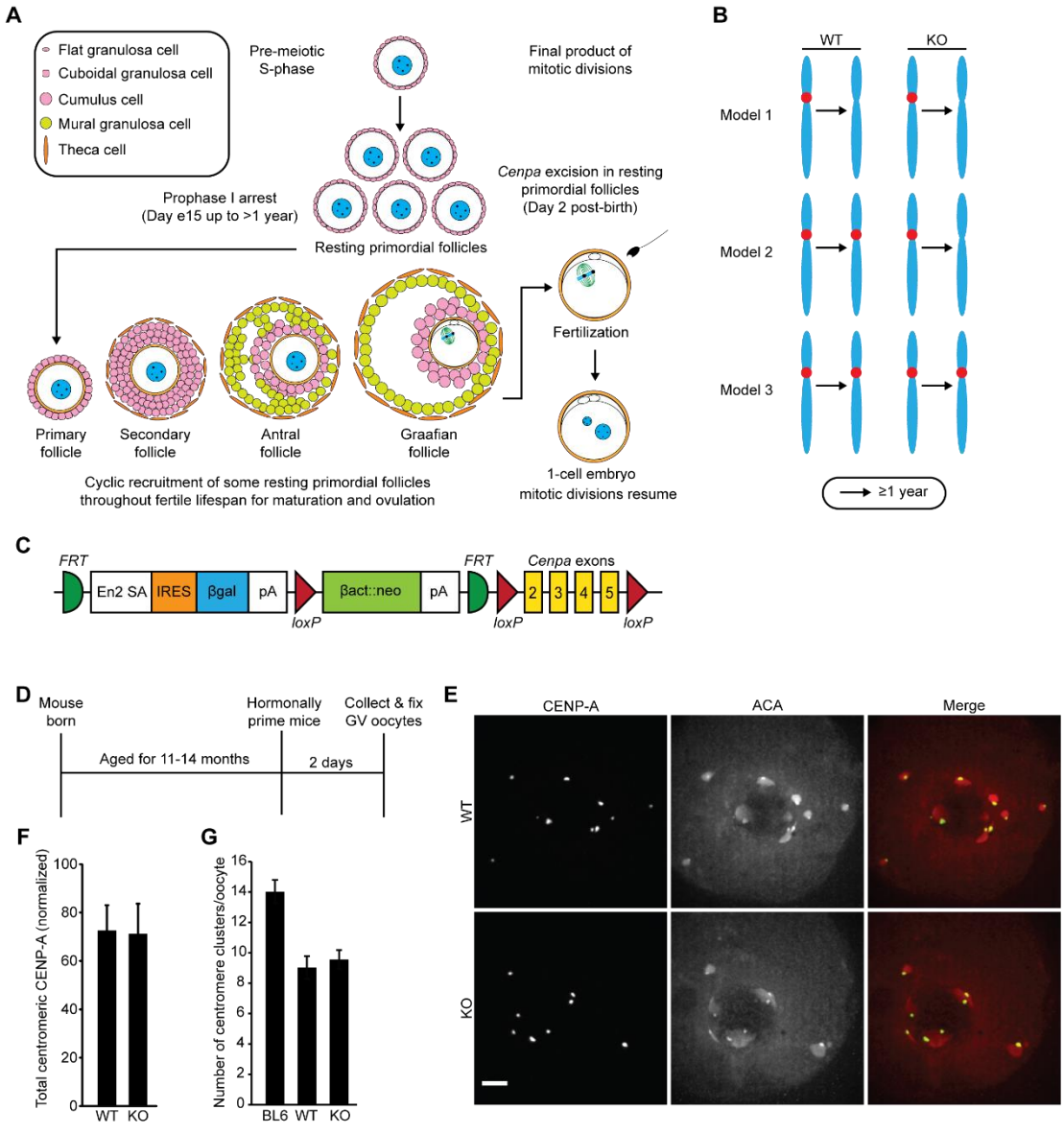

Figure 3.3 CENP-A nucleosomes are stably retained at oocyte centromeres for >1 year.

(**A)** Oocytes arrest in prophase I in resting primordial follicles, which are cyclically recruited starting five days after birth to begin growth towards a Graafian follicle, the final stage

before ovulation. Primordial follicles can remain in the resting phase for a period lasting >1 year before they are recruited for maturation and ovulation. After fertilization, the maternal and paternal pronuclei enter G1-phase and begin mitotic cell cycles. Cre expression driven by the *Gdf9* promoter excises *Cenpa* in resting primordial follicles two days after birth. (**B**) Three models for centromere inheritance in the mammalian oocyte. See Results & Discussion for details. (**C**) Schematic of *Cenpa* conditional knockout gene locus. The neomycin selection cassette used for selection of ES cells is flanked by *FRT* sites. *Cenpa* protein coding exons 2-5 are flanked by *loxP* sites. (**D-F**) Oocytes were collected from 11-14.5 month old WT and KO mice, or from young C57BL/6J (BL6) controls, and CENP-A levels were analyzed by immunofluorescence, with ACA to co-label centromeres (schematic, D). Images (E) of oocytes with intact germinal vesicles (GV) are maximal intensity projections of confocal z-series; scale bar 5 μm. Total centromeric CENP-A staining was quantified for each oocyte (n=64 oocytes from 4 WT mice; n=85 oocytes from 5 KO mice) and normalized to young C57BL/6J controls (n=155 oocytes, 8 mice) for each experiment. Normalized values were averaged over multiple experiments (F; error bars, s.d.). (**G**) The number of centromere clusters was counted in each oocyte and averaged over each group (error bars, s.d.).

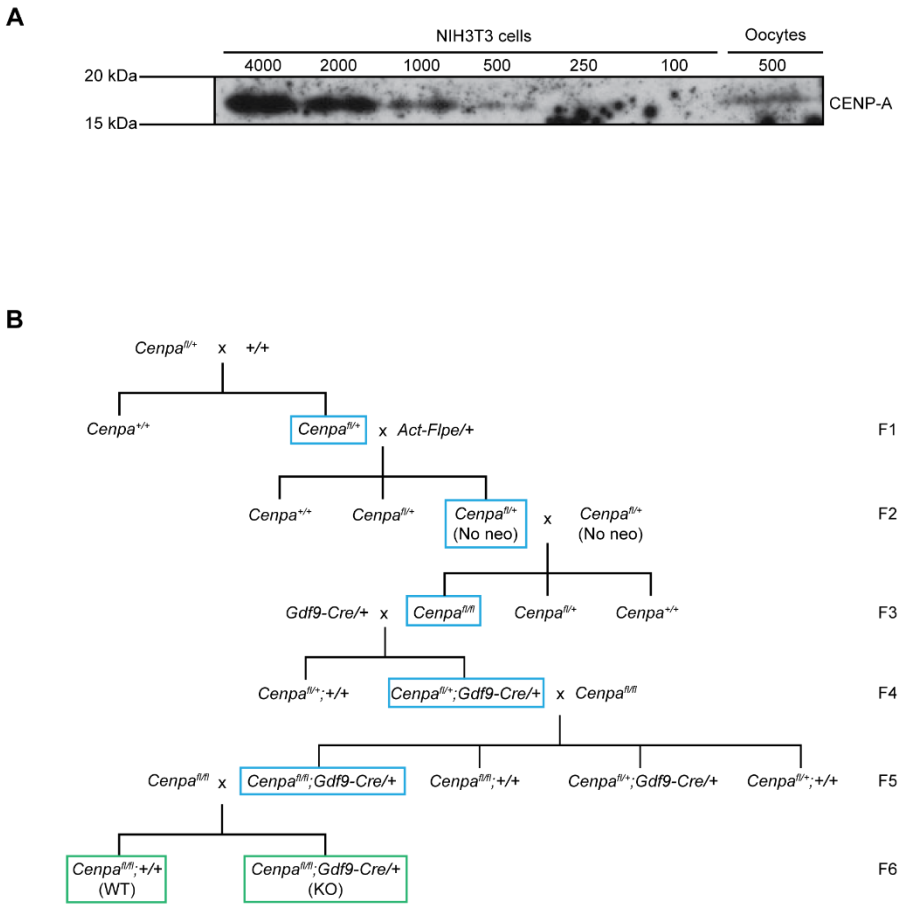

Figure 3.4 Oocytes do not contain a pool of excess CENP-A protein; Cenpa Conditional KO Breeding Scheme.

(**A**) Immunoblot of total CENP-A protein from whole cell lysates from an unsynchronized population of cycling NIH 3T3 cells or from CF-1 oocytes. Lysates from the indicated numbers of NIH 3T3 cells, from 100 to 4,000, are compared to 500 oocytes. (**B**) Breeding scheme for generation of WT and KO animals used in experiments (green boxes). The neomycin cassette was removed in the F1 cross with mice homozygous for Flp-recombinase under the control of the

human β-actin promoter. Blue boxes indicate mice kept at each stage and used in further crosses.

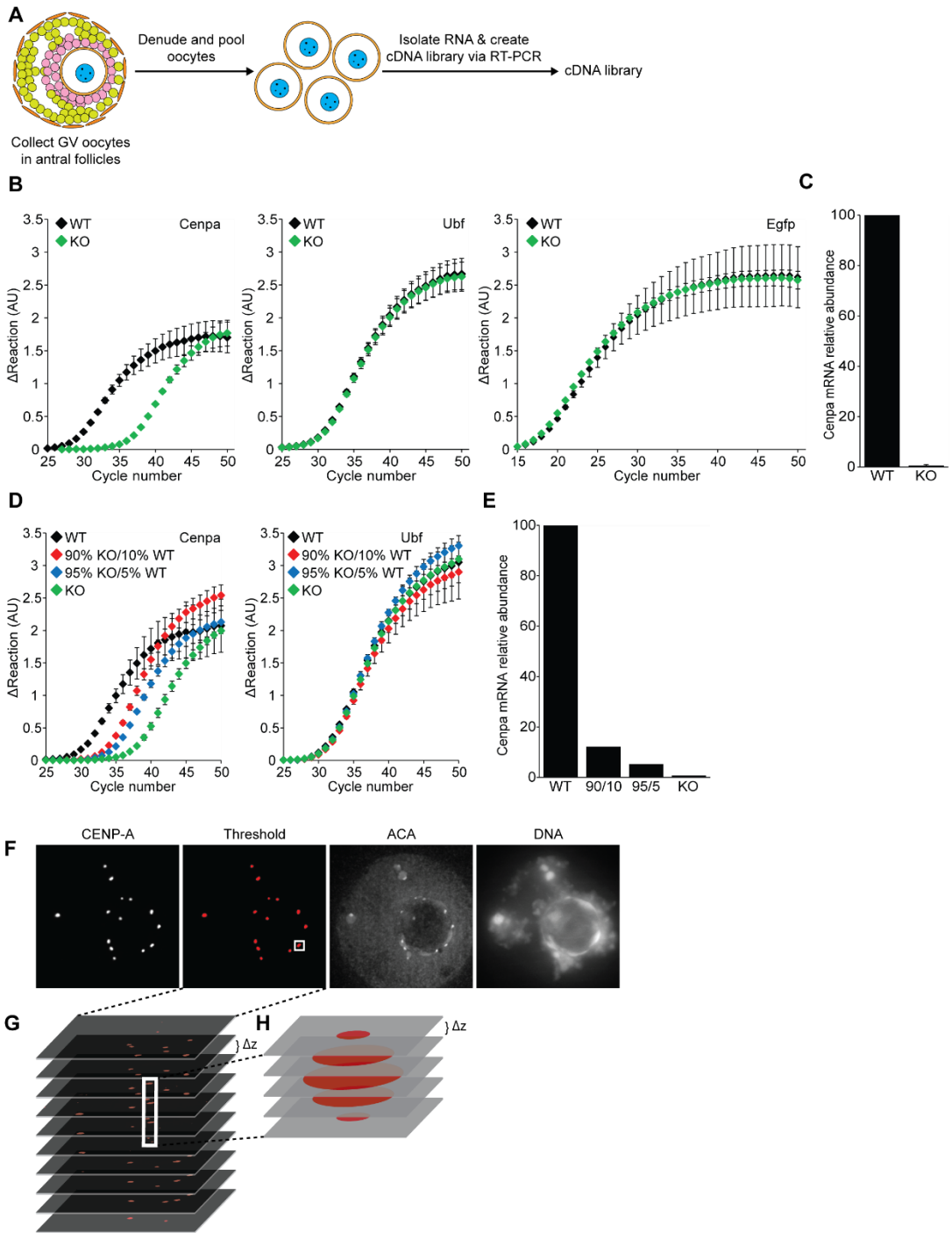

Figure 3.5 Cenpa KO oocytes contain only trace amounts of Cenpa mRNA; CENP-A immunofluorescence quantification.

(**A**) Experimental schematic of cDNA library preparation. (**B**) Representative Real-Time qPCR data comparing relative abundance of *Cenpa* mRNA between WT and KO oocytes. 1 oocyte equivalent was loaded per well. *Ubf* was used as an endogenous control to normalize the total amount of cDNA recovered from WT and KO oocytes. *Egfp* was used as an exogenous control to normalize the total amount of cDNA recovered by reverse transcription of mRNA isolated from WT and KO oocytes. Error bars, s.d. (**C**) *Cenpa* mRNA relative abundance between WT and KO oocytes, using the comparative Ct method; error bars, s.d. (**D**) Representative real-time qPCR data comparing relative abundance of *Cenpa* mRNA between cDNA mixes prepared from 100% WT cDNA (WT), 90% KO cDNA mixed with 10% WT cDNA (90/10), 95% KO cDNA mixed with 5% WT cDNA (95/5), or 100% KO cDNA (KO). *Ubf* was used as an endogenous control. Error bars represent s.d. (**E**) *Cenpa* mRNA relative abundance between WT, 90/10, 95/5, and KO cDNA libraries, using the comparative Ct method; error bars, s.d. (**F**) Maximal intensity projections of confocal z-series showing CENP-A staining, CENP-A thresholding, ACA, and DAPI staining from a representative GV oocyte used in the quantification shown in Fig. 2F (**G**) Individual z-planes showing centromeres in the white box in (A) in three dimensions. Total centromeric CENP-A intensity is quantified within the thresholded areas, integrated in three dimensions for each particle. (**H**) Schematic of a single CENP-A particle. Integrated intensity is determined by multiplying the thresholded volume by the mean pixel intensity.

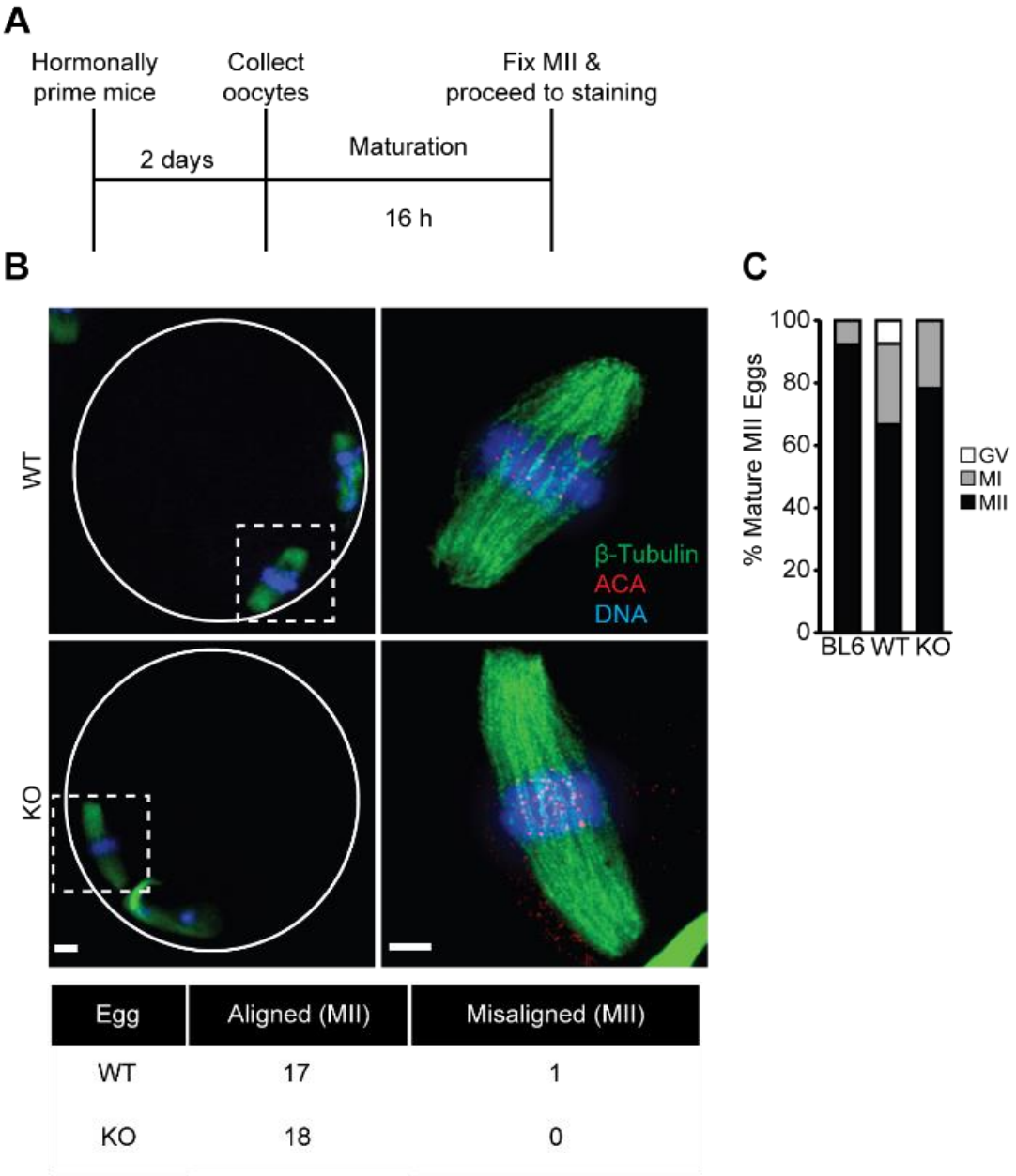

Egg	Aligned (MII)	Misaligned (MII)
WT	17	1
KO	18	0

Figure 3.6 CENP-A nucleosomes assembled early in prophase I support normal meiotic centromere function.

(**A-C**) Oocytes were collected from 12 month old WT and KO females, or young

C57BL/6J controls, matured in vitro to MII, and stained for β-tubulin, ACA to label centromeres, and DNA (schematic, A). Representative images (B) show MII eggs at 20X magnification (scale bar 10 μm), white circle represents zona pellucida; dashed squares are regions imaged at 100x (scale bar 5 μm). The percent in each group that remained arrested with an intact germinal vesicle (GV), arrested at metaphase I, or progressed normally to MII was quantified (C, n=27 oocytes from 3 WT mice, 23 oocytes from 3 KO mice, or 26 oocytes from 2 C57BL/6J (BL6) mice). The table summarizes how many MII eggs from WT and KO females had chromosomes aligned at metaphase.

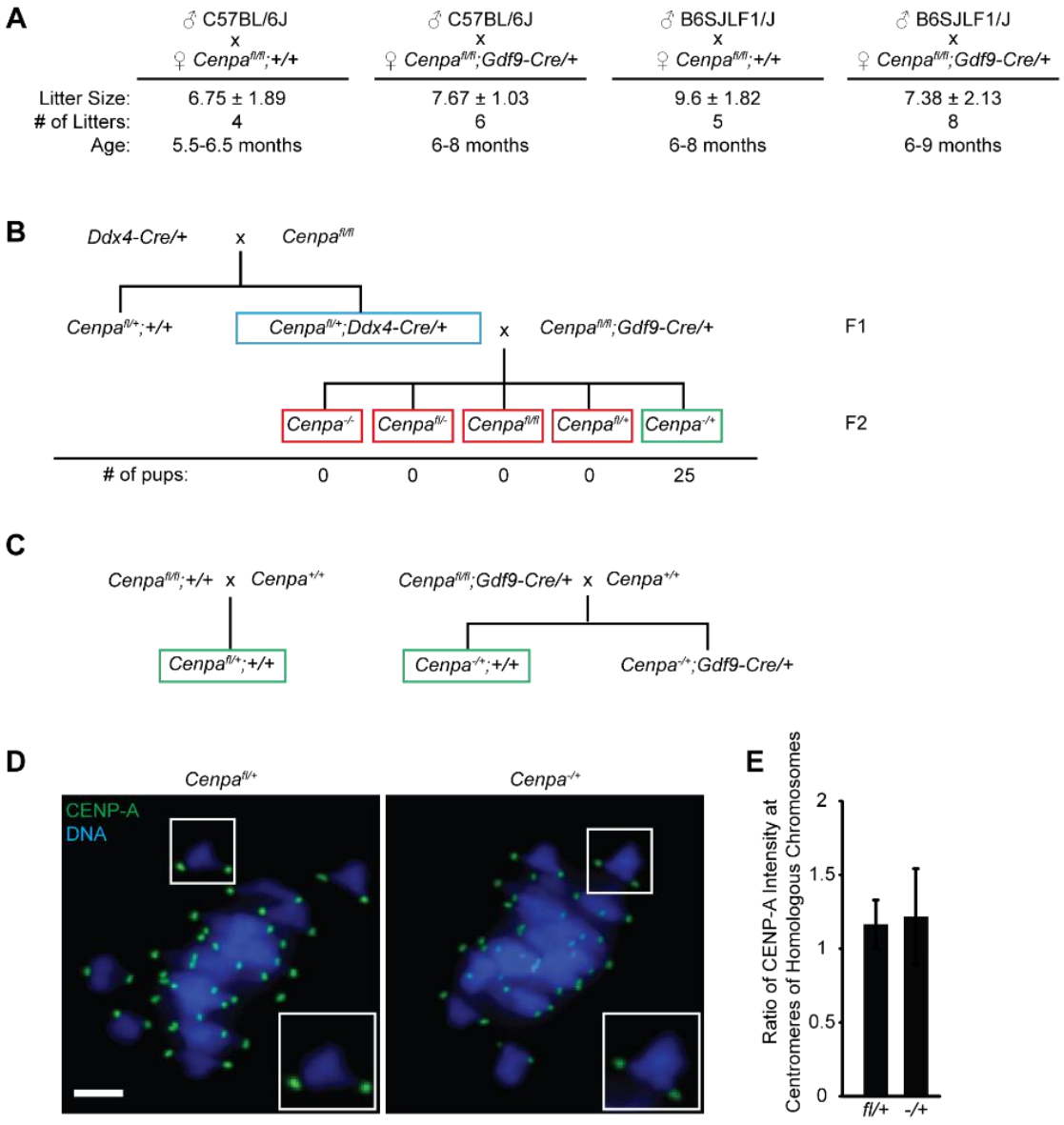

Figure 3.7 CENP-A nucleosomes assembled in early prophase I support normal fertility and transgenerational centromere inheritance.

(**A**) WT (n=5) and KO (n=6) females were mated with either C57BL/6J or B6SJLF1/J

males to determine fertility. Average litter size (± s.d.), number of litters, and age of the females are reported. (**B**) *Cenpa*$^{fl/+}$*;Ddx4-Cre/+* males (blue box) were mated to *Cenpa*$^{fl/fl}$*;Gdf9-Cre/+* females (n=2 females, 3-6 months old). The red box represents offspring that are either predicted to die in utero (all *Cenpa*$^{-/-}$*)* or are predicted to be impossible to produce if there is full excision of the *Cenpa*^{fl} allele. The green box represents animals that are predicted to survive (all *Cenpa*$^{-/+}$) if all oocytes are indeed *Cenpa*$^{-/-}$. Surviving pups were genotyped and found to be exclusively *Cenpa*$^{-/+}$ with no intact *Cenpa*^{fl} allele. (**C**) Breeding scheme to generate F1 pups that are *Cenpa*$^{fl/+}$ or *Cenpa*$^{-/+}$. Green boxes indicate mice used in experiment. (**D,E**) Oocytes from F1 pups were fixed in metaphase I and stained for CENP-A and DNA. CENP-A intensity was measured at each centromere, and the ratio of brighter/dimmer intensity was calculated (E) for each bivalent (n≥238 bivalents for WT and KO). Error bars s.d. Scale bar 5 μm.

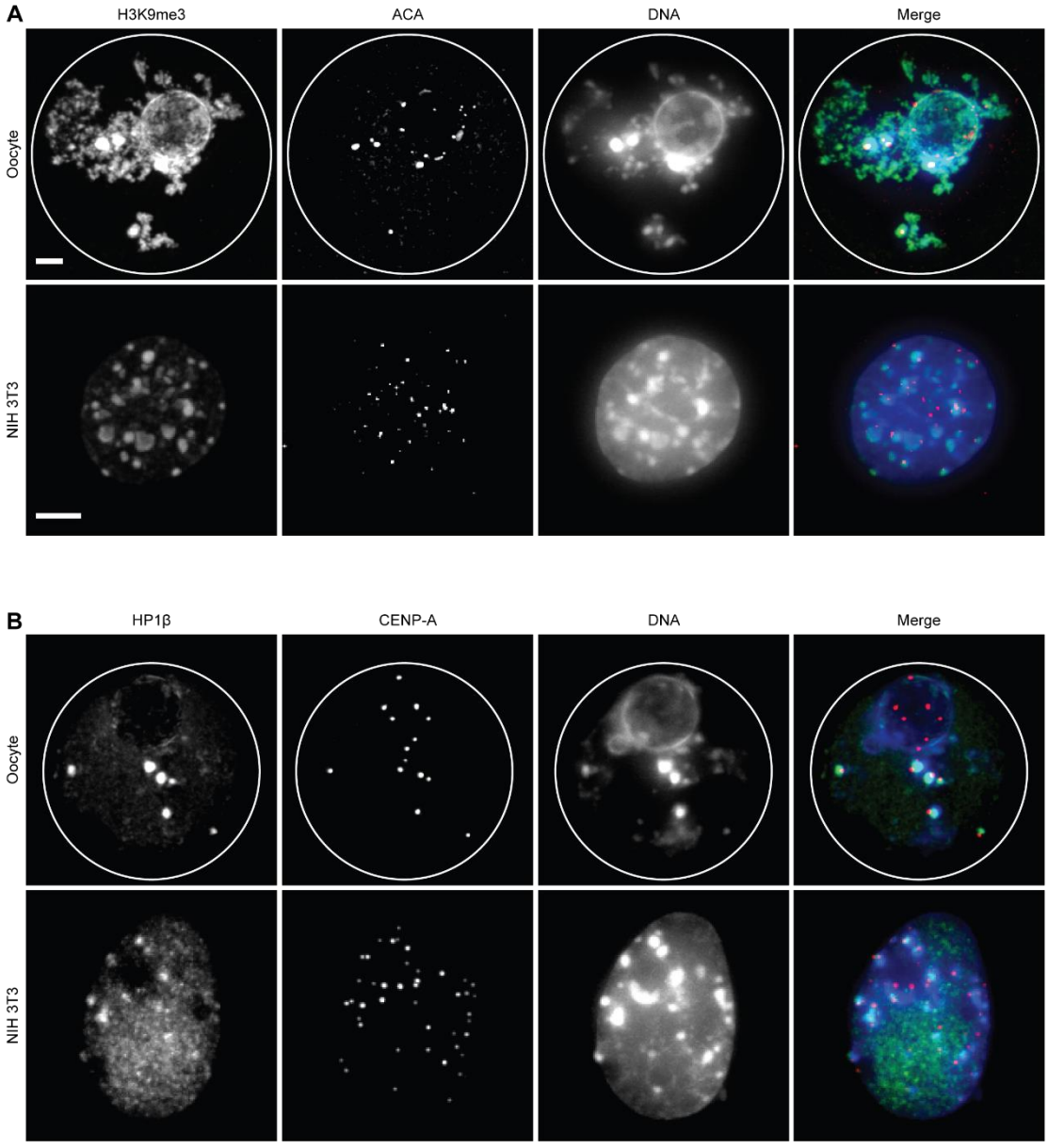

Figure 3.8 Pericentromeric chromatin marks localize similarly in NIH 3T3 cells and GV oocytes.

(**A**) H3K9me3 and (**B**) HP1β staining in GV oocytes and NIH 3T3 cells shows foci which colocalize with heterochromatin and centromeres. White circle represents nuclear envelope. Scale bar 5 μm. In (A), merged images: H3K9me3 is in green, ACA is in red, and DNA is in blue. In (B), merged images: HP1β is in green, CENP-A is in red, and DNA is in blue. Thus, there is no evidence that differences between oocytes and somatic cells in heterochromatin at pericentromeres explains any aspect of CENP-A retention. There could certainly be a role for centromere components binding to CENP-A nucleosomes or the intrinsic properties of CENP-A nucleosomes themselves. Scale bar 5 μm.

Cenpa Genotyping
Fwd Primer: 5'-GCAGAGCCACAGCTCCAGAGCA-3'
Rev Primer 1: 5'-CAGACTGCAGTTCCATCCCTACAGA-3'
Rev Primer 2: 5'-TGAACTGATGGCGAGCTCAGACC-3'

Band Sizes:

Cenpa Floxed Allele: 490 bp
Cenpa Wildtype Allele: 382 bp
Cenpa Recombined Allele: 285 bp

Initial Denaturation: 95ºC for 5 min
Denaturation: 95ºC for 30 sec
Annealing: 55ºC for 30 sec
Elongation: 72ºC for 2 min
30 cycles
Final Elongation: 72ºC for 5 min

Gdf9-Cre Genotyping
Fwd Primer: 5'-TCTGATGAAGTCAGGAAGAACC-3'
Rev Primer: 5'-GAGATGTCCTTCACTCTGATTC-3'

Band Sizes:

Gdf9-Cre: 499 bp

Initial Denaturation: 94ºC for 3 min
Denaturation: 94ºC for 30 sec
Annealing: 58ºC for 2 min
Elongation: 72ºC for 2 min
30 cycles
Final Elongation: 72ºC for 5 min

Flp Genotyping
Fwd Primer: 5'-CACTGATATTGTAAGTAGTTTGC-3'
Rev Primer: 5'-CTAGTGCGAAGTAGTGATCAGG-3'

Band Sizes:

Act-Flpe: 725 bp

Initial Denaturation: 94ºC for 3 min
Denaturation: 94ºC for 30 sec
Annealing: 58ºC for 1 min
Elongation: 72ºC for 1 min
35 cycles
Final Elongation: 72ºC for 2 min

Ddx4-Cre Genotyping
Fwd Primer: 5'-CACGTGCAGCCGTTTAAGCCGCGT-3'
Rev Primer: 5'-TTCCCATTCTAAACAACACCCTGAA-3'

Band Sizes:

Ddx4-Cre: 240 bp

Initial Denaturation: 94ºC for 3 min
Denaturation: 94ºC for 30 sec
Annealing: 67ºC for 1 min
Elongation: 72ºC for 1 min
35 cycles
Final Elongation: 72ºC for 2 min

Table 3.1 Genotyping primers and thermocycler programs.

3.5 Methods

3.5.1 Oocyte/Embryo collection, meiotic maturation, and culture

Mice were primed by intraperitoneal injection of 5 IU of equine chorionic gonadotropin (eCG) 48 h before oocyte collection. Full-grown, germinal vesicle (GV)-intact cumulus-enclosed oocytes were collected as previously described (Schultz et al., 1983) and denuded. The collection medium was bicarbonate-free minimal essential medium (Earle's salt) supplemented with polyvinylpyrrolidone (3 mg/mL) and 25 mM HEPES, pH 7.3 (MEM/PVP). Germinal vesicle breakdown was inhibited by including 2.5 μM milrinone (Wiersma et al., 1998). For microinjection experiments, oocytes were transferred to CZB medium (Chatot et al., 1989) containing 2.5 μM milrinone and cultured in an atmosphere of 5% CO_2 in air at 37°C. To assess oocyte maturation in vitro, oocytes were transferred to milrinone-free CZB medium and cultured for 16 h in 5% CO_2 in air at 37°C. For microinjection of 1-cell stage embryos, mice were consecutively injected with 5 IU of equine chorionic gonadotropic (eCG) and 5 IU of human chorionic gonadotropin (hCG) 48 h apart, then mated with B6D2F1/J males. 20 h after mating, 1-cell stage embryos were collected from oviducts in MEM/PVP with 3 mg/mL hyaluronidase, denuded, and cultured in KSOM (Erbach et al., 1994; Ho et al., 1995) in an atmosphere of 5% CO_2 in air at 37°C before and after microinjection.

3.5.2 Microinjection

GV oocytes were microinjected with ~5 pL of cRNAs in MEM/PVP containing 2.5 μM milrinone as previously described (Kurasawa et al., 1989). 1-cell stage embryos were injected with ~5 pL of cRNAs in MEM/PVP. cRNAs used for oocyte injections were CENP-A-GFP (600 ng/μl), CENP-A-Flag-HA (60ng/ul), H3.3-mCherry (300 ng/μL), 2xGFP-CENP-C (480 ng/μl) with two tandem copies of GFP. cRNAs used for embryo injections were CENP-A-GFP (600 ng/μl),

CENP-A-Flag-HA (60ng/ul), and 3xmCherry-CENP-C cRNA (500 ng/ul) with three tandem copies of mCherry.

3.5.3 Tissue Culture

NIH 3T3 cells were cultured in growth medium (Dulbecco's Modified Eagle's Medium supplemented with 10% Fetal Calf Serum and penicillin-streptomycin) at 37ºC in a humidified atmosphere with 5% CO_2.

3.5.4 Generation of Cenpa Conditional KO Mice

ES cells with exons 2-5 of *Cenpa* flanked by loxP sites and an FRT-flanked neomycin selection cassette between the 5' and 3'arms (Figure 3A) were purchased from the European Mouse Mutant Cell Repository (EuMMCR), (Cenpa$^{tm1a(EUCOMM)Wtsi}$, Clone ID: EPD0445_6_E07, Cell Type: C57BL/6M). Cells were injected into BALB/c blastocysts and transferred to pseudopregnant mothers to generate two chimeric founders (90% and 1-5% chimerism), which were germline transmitters of the mutant allele. The neomycin selection marker was removed with the FLP recombinase, by crossing the Neo::*Cenpa*$^{fl/+}$ mice with ACTB::Flpe mice (Stock #: 005703, The Jackson Laboratory). The resulting *Cenpa*$^{fl/fl}$ mice were mated with *Gdf9-Cre/+* (Stock #: 011062, The Jackson Laboratory) males, and the resulting *Cenpa*$^{fl/+}$*;Gdf9-Cre/+* males were mated with *Cenpa*$^{fl/fl}$ females to obtain *Cenpa*$^{fl/fl}$*;Gdf9-Cre/+* females. To obtain *Cenpa*$^{fl/+}$*;Ddx4-Cre/+* males, *Cenpa*$^{fl/fl}$ females were crossed to *Ddx4-Cre/+* males (Stock # 006954, The Jackson Laboratory). Mice were genotyped by PCR analysis of tail DNA extracted using the REDExtract-N-Amp Red Tissue PCR kit (Sigma-Aldrich) using primers and PCR programs listed in Table 3.1. We note that in a small fraction of animals generated from *Cenpa*$^{fl/fl}$*;Gdf9-Cre+* (♂) x *Cenpa*$^{fl/fl}$ (♀) were negative for *Gdf9-Cre* by our genotyping assay, but also genotyped as *Cenpa*$^{fl/-}$, indicating potentially aberrant Cre activity in the male. We avoided including any females with the *Cenpa*$^{fl/-}$ genotype in our analysis by genotyping with primers that

detect *Cenpa*^{fl}, *Cenpa*$^{+}$, and *Cenpa*$^{-}$ alleles. All animal experiments were approved by the Institutional Animal Use and Care Committee of the University of Pennsylvania and were consistent with National Institutes of Health guidelines.

3.5.5 Indirect Immunofluorescence

Mouse oocytes were fixed in freshly prepared 2% paraformaldehyde in PBS (pH 7.4) for 20 min at room temperature, washed through 3 drops of blocking solution (PBS containing 0.1% BSA and 0.01% Tween-20), permeabilized in PBS with 0.1% Triton X-100 for 15 min, washed in blocking solution for 15 min, incubated 1 h with primary antibodies, washed three times in blocking solution for 15 min, incubated 1 h with secondary antibodies, washed three times for 15 min in blocking buffer, and mounted in Vectashield with DAPI (1.5 µg/mL, Sigma-Aldrich) to visualize DNA. In experiments where CENP-A staining was perfomed on metaphase oocytes, we incubated oocytes with λ-phosphatase (New England Biolabs, #P0753S) prepared according to manufacturer's instructions for 2 hours at 30ºC immediately after permeabilization/blocking before proceeding with antibody incubation. Primary antibodies were human ACA autoimmune serum (1:50, PerkinElmer), rabbit anti-CENP-A (1:200, Cell Signaling #2048S), and rabbit anti-β-tubulin (9F3) monoclonal conjugated to Alexa Fluor 488 (1:75; Cell Signaling #3623), H3K9me3 (1:500, Abcam ab8898) and HP1β (1:200, Millipore MAB3448), anti-HA.11 (1:200, Covance MMS-101p). Secondary antibodies were Alexa Fluor 594–conjugated goat anti–human, Alexa Fluor 488-donkey anti-rabbit, Alexa Fluor 488-donkey anti-mouse, and Alexa Fluor 594 donkey anti-rabbit (1:100), Invitrogen).

3.5.6 Image Acquisition

Confocal images were collected as z-stacks with 0.3 µm (microinjection and meiotic maturation) or 0.5 µm (GV oocyte immunofluorescence) intervals to visualize all chromatin (25-30 µm range) using a microscope (DMI4000 B; Leica) equipped with a 20x 0.7 NA dry-objective lens

(meiotic maturation), a 63x 1.3 NA glycerol-immersion objective lens (microinjection), a 100x 1.4 NA oil-immersion lens (GV oocyte immunofluorescence and meiotic maturation), an xy piezo Z stage (Applied Scientific Instrumentation), a spinning disk confocal scanner (Yokogawa Corporation of America), an electron multiplier charge-coupled device camera (ImageEM C9100-13; Hamamatsu Photonics), and an LMM5 laser merge module with 488- and 593-nm diode lasers (Spectral Applied Research) controlled by MetaMorph software (Molecular Devices). For live imaging, oocytes and embryos were cultured in drops of either CZB or KSOM in FluoroDish (FD35-100, World Precision Instruments, Inc.) covered by mineral oil to prevent evaporation. Temperature was maintained at 37ºC with 5% CO_2 using an environmental chamber (Incubator BL; PeCon GmbH).

3.5.7 Image Analysis

Image analysis was done in ImageJ. The total amount of centromeric CENP-A in each GV oocyte was quantified by first defining the z-slices containing centromeres, based on CENP-A and ACA staining. A threshold CENP-A intensity and minimum particle size were determined manually for each oocyte, using the Object Counter3D macro. The threshold intensity varied between oocytes, depending usually on how clustered the centromeres were. The volume and average intensity of each particle was recorded. Background fluorescence, estimated from ROIs adjacent to but not including centromeres, was subtracted, and the integrated intensity of each particle was calculated as average intensity × volume. The total centromeric CENP-A intensity in each oocyte is the sum of all of the particles. Co-localization of ACA and CENP-A staining was used to ensure that all particles were actually centromeres. Total centromeric CENP-A intensity was averaged over all oocytes from each mouse. In each experiment, age-matched WT and KO mice were analyzed in parallel with young (7-12 week) C57BL/6J controls. To compare mice from difference experiments, results were normalized to the young C57BL/6J controls within each

experiment. These normalized values were then averaged together for WT and KO mice. To compare centromeres of homologous chromosomes at metaphase (Fig. 4E), the integrated intensity was calculated for each centromere as above and then a ratio was calculated as the brighter/dimmer centromere within each bivalent in all cases where homologous chromosomes could be unambiguously identified.

The GFP intensity in Fig. S1A was calculated by averaging 5 different nuclear GFP measurements of equivalent area and then subtracting the average of 5 different cytoplasmic GFP measurements for each oocyte.

3.5.8 Mating Assays

Females used in the fertility trials were housed with one male for 4 months, and the number of pups in each litter was recorded. Females that were mated to *Cenpa*$^{fl/+}$*;Ddx4-Cre/+* males were housed with one male for 6 months, and the number and *Cenpa* genotype of the pups in each litter were recorded.

3.5.9 Immunoblot

Samples derived from whole cell lysates were separated by SDS-PAGE and transferred to a nitrocellulose membrane for immunoblotting. Blots were probed using a rabbit anti-CENP-A antibody (1:200, Cell Signaling #2047S). Antibodies were detected using an ECL anti-rabbit IgG, horseradish peroxidase-conjugated secondary antibody (GE Healthcare, NA934V) at 1:2000 and Amersham ECL Select Western Blotting Detection Reagent (GE Healthcare, RPN2235).

3.5.10 mRNA quantitative RT-PCR

Total RNA was extracted from at least 21 full-grown oocytes using Trizol (Life Technologies), according to the manufacturer's protocol, except that 2 ng of *Egfp* RNA was

added to the Trizol at the beginning of RNA isolation to serve as an exogenous normalization gene. cDNA was prepared by reverse transcription of total RNA with Superscript II and random hexamer primers. One oocyte equivalent of the resulting cDNA was amplified using TaqMan probes and the ABI Prism Sequence Detection System 7000 (Applied Biosystems). Two replicates were run for each real-time PCR reaction; a minus template served as control. Quantification was normalized to Egfp and endogenous Ubf within the log-linear phase of the amplification curve obtained for each probe/ primer using the comparative Ct method (ABI PRISM 7700 Sequence Detection System, User Bulletin 2, Applied Biosystems, 1997). The TaqMan gene expression assays used were: Mm00483252_m1 (Cenpa), Mm00456972_m1 (Ubf). The TaqMan gene expression assay for Egfp was a custom order from ThermoFisher Scientific using the following primers: Forward: 5'- GCTACCCCGACCACATGAAG-3', Reverse: 5'-CGGGCATGGCGGACTT-3', Reporter Dye: FAM.

CHAPTER 4:

CENP-A Nucleosome Transmission through the Male Germline: A Story “In Progress”

4.1 Introduction

The haploid products of meiosis, round spermatids, begin to differentiate into mature spermtazoon through the process of spermiogenesis. During spermiogenesis, most of the cytoplasm is shed, a flagellum is formed, and nuclear compaction is achieved by dramatic chromatin reorganization (Rathke et al., 2014). The compaction of the nucleus is made possible by the replacement of nucleosomes, first with transition proteins, then with small, basic proteins called protamines (Balhorn, 2007; Hud et al., 1993). Chromatin assembled protamines allow the DNA to adopt a toroidal structure, (Balhorn et al., 2000) compacting it enough to fit inside the sperm head. The percentage of histone retention during this chromatin-to-nucleoprotamine transition is small (in humans an estimated ~4% of histones are retained (Brykczynska et al., 2010; Hammoud et al., 2009), but common among mammalian species is that CENP-A nucleosomes are retained (Palmer et al., 1990; Palmer et al., 1991). CENP-A was originally purified from mature bull sperm nuclei (Palmer et al., 1991), and immunoblot data comparing CENP-A protein levels between cells isolated from calf thymus and mature bull sperm demonstrate that CENP-A nucleosomes are completely retained through spermiogenesis (Palmer et al., 1990). Practically, this retention is likely because of CENP-A's critical role in demarcating the centromere and is the mechanism by which paternal centromeres are inherited by offspring. This biological phenomenon raises several questions related to centromere inheritance. How are CENP-A nucleosomes preferentially retained while most other histones are removed? Is it important for sperm to exert quantitative control of how many CENP-A nucleosomes are inherited by offspring? If the amount of CENP-A nucleosomes present in mature sperm is altered prior to fertilization, does this have an impact on the centromeres inherited by offspring? Does CENP-A have a function in chromatin organization during spermiogenesis? To answer any of these questions in mammals, it is necessary to devise a system that allows for control over the amount of CENP-A present in mature sperm. This chapter will focus on my efforts to develop a mouse

model that would allow for decreasing the amount of CENP-A present in mature sperm, as well as thoughts for exciting follow-up experiments utilizing this model system.

4.2 Approaches to Control CENP-A Levels in Mature Sperm

Previous work done to control CENP-A levels in mature sperm has used Drosophila as a model organism (Raychaudhuri et al., 2012), likely because of the relative ease of genetic manipulation compared to mouse. In one system, the endogenous *Cenpa* gene locus was replaced by *Cenpa-EGFP*, so that the *Cenpa-EGFP* expression was controlled by the endogenous *Cenpa* regulatory program (Raychaudhuri et al., 2012). The mutant *Cenpa-EGFP* flies allowed for use of the deGradFP system during spermatogenesis. In short, deGradFP allows for the depletion of GFP fusion proteins through expression of a recombinant ubiquitin ligase which specifically targets GFP (Caussinus et al., 2011). Using this system, CENP-A-EGFP was reduced such that centromeric CENP-A-EGFP signals in mature sperm could not be distinguished from background fluorescence. While this technique efficiently reduces the amount of CENP-A-EGFP present at the centromere, the magnitude of CENP-A loss greatly impairs paternal centromere function. Sperm from *Cenpa-EGFP* flies in which deGradFP is active contain paternal chromosomes that are unable to make correct kinetochore-microtubule attachments during mitosis. Obviously, a system which produces viable embryos is preferable for asking fundamental questions about centromere inheritance to offspring.

Drosophila has also been used to generate flies in which CENP-A can be either “over-loaded” at or partially depleted from centromeres (Raychaudhuri et al., 2012). In order to “over-load” CENP-A at centromeres, *Cenpa-EGFP* flies were engineered to simultaneously express exogenous CENP-A-EFGP using the UAS/GAL4 expression system (Brand and Perriman, 1993). In this case, the UAS promoter was used to drive expression of exogenous *Cenpa-EGFP* as well as exogenous *Cal1* expression (Raychaudhuri et al., 2012). Cal1 is the Drosophila CENP-A

specific histone chaperone in Drosophila (Chen et al., 2014). Using the *bag of marbles* (*bam)*, a gonad-specific gene required to initiate male and female gametogenesis (McKearin and Spradling, 1990), to drive GAL4-VP16 expression, this model system is reported to increase centromeric CENP-A levels by 7-fold, over controls lacking the UAS driven transgenes. In order to generate flies with partially depleted CENP-A, the UAS/Gal4 system was used again in *Cenpa-EGFP* flies with *UAS-Cenpa-RNAi* and *bam-GAL4-VP16*. In this system, CENP-A-EGFP levels were reduced between 2-3-fold in mature sperm when compared to flies that lacked *UAS-Cenpa-RNAi* (Raychaudhuri et al., 2012).

Interestingly, when sperm with either an elevated or reduced amount of CENP-A-EGFP is used to fertilize eggs from *Cenpa-EGFP* females, the amount of CENP-A-EGFP present at sperm centromeres seems to exert some control over how much CENP-A is loaded at centromeres of paternal origin in the embryo. When males that produced sperm with overloaded CENP-A-EFGP or reduced CENP-A-EGFP, respectively, were mated to females carrying *Cenpa-EGFP* and *Cenpc-Tomato* transgenes, the total centromeric CENP-A-EGFP intensity per nucleus was found to be 1.7x higher in embryos generated from males whose sperm had artificially higher levels of centromeric CENP-A-EGFP and reduced to ~70% in embryos created by sperm from males expressing *UAS-Cenpa-RNAi*, compared to embryos generated by *Cenpa-EGFP* males x *Cenpa-EFGP* females (Raychaudhuri et al., 2012). In both cases, the amount of CENP-A-EGFP present at sperm centromeres at the time of fertilization seemed to have some effect on the total amount of CENP-A that could ever be loaded at the centromere, though perhaps not entirely quantitative control.

Though the systems used in Drosophila would be quite suitable for studying centromere inheritance in mammals, the complexities of generating and validating transgenic mouse models make it challenging to translate the work done in Drosophila to a mammalian system. Generating

a similar mouse, that would overexpress tagged CENP-A specifically in the testis, would require engineering and validating expression of transgenes for minimally both exogenous CENP-A and HJURP. Since we had already generated *Cenpa* conditional knockout mice, as described in Chapter 3 (Smoak et al., 2016), it seemed feasible that by using commercially available mice expressing cre-recombinase under gonad specific promoters, we might be able to generate mice with a reduced amount of centromeric CENP-A. As discussed in previous chapters, in the absence of any nascent CENP-A protein, 50% of existing CENP-A protein is lost each cell cycle through dilution during S-phase (Jansen et al., 2007), eventually passing a threshold after which centromere function is impaired to disastrous effect (Black et al., 2007). Since spermatagonia proceed through some mitotic divisions prior to meiosis, this experimental approach exploits cell-cycle coupled CENP-A depletion through carefully timed deletion of *Cenpa,* with respect to spermatogenesis, to control the amount of CENP-A present in mature sperm. The timing of *Cenpa* excision is essential: if *Cenpa* is deleted too early, loss of CENP-A from centromeres prior to meiosis will likely cause meiotic arrest and/or cell death, with no mature sperm to use for experiments; if *Cenpa* is deleted too late, there will likely be no centromeric CENP-A loss. In the following sections, I will outline the rationale behind the available cre-drivers we selected, the preliminary results obtained from these experiments, and my thoughts on future directions to address interesting questions related to centromere inheritance through the male germline.

4.3 Preliminary Results

In order to measure whether we successfully depleted CENP-A in the testis with any of our mouse models, we established two key assays: 1) an immunofluorescence assay in which we stain for CENP-A in whole mouse testis tissue sections to determine the amount of CENP-A present in various spermatogenic cell types and 2) an immunoblotting assay that measures the total amount of CENP-A present in spermatogenic cells throughout spermatogenesis. This work

was done with material from the lab of Dr. Shelley L. Berger and the guidance of her post-doctoral fellow, Dr. Lacey J. Luense. To optimize the conditions for CENP-A staining in testis tissue section IF, I began by sectioning a frozen, unfixed mouse testis isolated from an SV129 mouse, at a thickness of 8μm per slice. Upon imaging, I was able to see centromeric CENP-A signals easily in various spermatogenic cell-types (Fig. 4.1A,B). However, there was a noticeable decrease in CENP-A signal from the round spermatid stage to the elongating/condensing spermatid stage, and in highly compacted spermatids CENP-A staining was almost undetectable (Fig. 4.1B). From these data, we concluded that our CENP-A staining protocol worked in the testis sections prepared from frozen, unfixed testes. However, we could not determine from this assay alone whether CENP-A was truly lost from the centromere in mature sperm, or if the CENP-A epitope recognized by our antibody was occluded due to increasing degrees of chromatin compaction. To answer this question, and learn more about total CENP-A levels throughout spermatogenesis, we decided to analyze total CENP-A levels from whole cell lysate isolated from various spermatogenic cell-types by immunoblot.

Total CENP-A levels in sperm have been measured by immunoblotting and the presence of CENP-A in mature sperm has been demonstrated by immunofluorescence assays (Palmer et al., 1990). Through collaboration with the Berger lab and Dr. Luense, we were able to obtain cell fractions enriched for various spermatogenic cell-types, affording us the opportunity to track total CENP-A protein through spermatogenesis. Utilizing a technique known as STA-PUT, the Berger lab used a BSA gravity gradient to isolate spermatogenic cells from meiotic, round spermatid, and elongating/condensing stages of spermatogenesis from a cell suspension prepared from 22 whole mouse testes isolated from SV129 mice (Bryant et al., 2013). The BSA gradient allows for collection of cell fractions, first collecting meiotic cells, which are the largest of the cell types isolated, followed by round spermatids, and finally elongating/condensing spermatids. Transition fractions were also collected (i.e. a mix of meiotic/round spermatids or round

spermatids/elongating/condensing spermatids). Mature sperm was collected directly from the cauda epididymis. Once I generated whole cell lysates prepared from carefully counted numbers of spermatogenic cells, I compared the total amount of CENP-A present in each spermatogenic cell fraction by loading 50,000 cell equivalents of each lysate in its respective lane. NIH 3T3 cell lysate was also used in order to make a comparison between the total amount of CENP-A protein through spermatogenesis to the amount of CENP-A ordinarily present in cycling somatic cells. Preliminary immunoblot data shows that total CENP-A protein stay essentially constant in spermatogenic cells from the meiotic through the round spermatid stages of spermatogenesis (Fig. 4.1C). A reduction of total CENP-A protein is observed once spermatids begin the elongating/condensing stage of spermatogenesis, with protein levels remaining essentially constant between the round/elongating/condensing spermatid fraction and the mature sperm isolated from the cauda epididymis. This analysis shows that the failure to detect CENP-A by immunofluorescence in highly compacted sperm chromatin in tissue sections is likely an artifact of epitope occlusion. However, these preliminary immunoblotting data do indicate that there is some CENP-A loss between the round spermatid stage and the elongating/condensing spermatid stage. Without a method to fractionate nuclear CENP-A from cytoplasmic CENP-A, it is difficult to conclude whether this difference is due to loss of chromatin bound CENP-A or loss of cytoplasmic CENP-A from naturally occurring cytoplasmic shedding during the transition from round spermatids to elongating spermatids. This analysis should be repeated on STA-PUT samples retrieved from another set of mice in order to have more biological replicates to validate the trend.

Though immunoblotting results left us with unresolved questions regarding the reduction in total CENP-A protein levels between the round spermatid and elongating/condensing spermatid stages, these data were helpful in determining which spermatogenic cell types in our immunofluorescence assay have robust CENP-A staining, and would be suitable for quantifying a reduction in chromatin bound CENP-A. Since any CENP-A depletion via conditional knockout of

Cenpa would hinge on enough mitotic divisions to lose CENP-A through dilution at S-phase, any CENP-A loss should be apparent in meiotic spermatocytes and at the latest in round spermatids, both of which have robust CENP-A signal in our immunofluorescence assay (Fig. 4.2A). As such, the general approach to our assay was to generate mice in which *Cenpa* was conditionally inactivated only in the testis and only prior to meiosis. After surveying the available Cre mice with developmentally appropriate promoters from the Jackson lab, we selected three Cre lines that might prove useful: the Ddx4-Cre (Gallardo et al., 2007), Stra8-Cre (Anderson et al., 2008; Sadate-Ngatchou, et al., 2008), and Ddx4-Cre(ER^{T2}) (John et al., 2008) lines (Fig. 4.2B). Endogenous *Ddx4* expression turns on in primordial germ cells before they commit to differentiate into oogonia or spermatogonia and remains on in spermatogenic cells (Toyooka et al., 2000), while the *Stra8* promoter turns on just prior to meiotic entry (Anderson et al., 2008). The Ddx4-Cre(ER^{T2}) line works identically to the Ddx4-Cre line, except that excision by cre-recombinase is induced by administering tamoxifen to the animal (John et al., 2008). This is because the cre-recombinase is fused with an ER^{T2} domain, which causes the Cre-ER^{T2} to be sequestered in the cytoplasm (Feil et al., 2009). Tamoxifen binding to the ER^{T2} domain causes the Cre-ER^{T2} to localize to the nucleus.

We began by generating *Cenpa$^{fl/fl}$;Ddx4-Cre/*+ and *Cenpa$^{fl/fl}$;Stra8-Cre/*+ animals according to the breeding schemes in Fig. 4.3A,B, as *Cenpa* deletions via these strains were the most straightforward way to deplete CENP-A in spermatogenic cells. Once the males reached sexual maturity, we isolated testis from *Cenpa$^{fl/fl}$;Ddx4-Cre/*+ and *Cenpa$^{fl/fl}$;Stra8-Cre/*+ males, using littermates that were *Cenpa$^{fl/fl}$;*+/+ as a control. These testes were then sectioned and stained for both CENP-A as well as SYCP2 (Fig. 4.3C). SYCP2 is a synaptonemal complex protein present in meiotic cells, and was used as a marker to identify meiotic cells. Due to the organization of seminiferous tubules, identifying where the meiotic spermatocytes are aids in finding round and elongating/condensing spermatids (Fig 4.2A). The stark size difference in

testes dissected from *Cenpa$^{fl/fl}$;Ddx4-Cre/+* males (4.3D) compared to *Cenpa$^{fl/fl}$;+/+* controls made it evident that the knockout of *Cenpa* in the primordial germ cells was likely too early. Analysis of testes sections from *Cenpa$^{fl/fl}$;Ddx4-Cre/+* males confirmed that the seminiferous tubules were completely devoid of any spermatogenic cells (Fig. 4.3C). As such, this line is not capable of producing any sperm with altered CENP-A levels. Testes isolated from *Cenpa$^{fl/fl}$;Stra8-Cre/+* males were smaller than *Cenpa$^{fl/fl}$;+/+* controls, though the size differential was not as dramatic as we previously observed with *Cenpa$^{fl/fl}$;Ddx4-Cre/+* males (Fig. 4.3D). While we did see spermatogenic cells in *Cenpa$^{fl/fl}$;Stra8-Cre/+* testes, the phenotype was variable between seminiferous tubules and even within seminiferous tubules. In many seminiferous tubules, meiotic spermatocytes cells appeared to be arrested in meiosis, with no detectable CENP-A signal and decreased SYCP2. The number of round spermatids seen in *Cenpa$^{fl/fl}$;Stra8-Cre/+* seminiferous tubules analyzed was noticeably less than found in *Cenpa$^{fl/fl}$;+/+* and virtually no elongating/condensing spermatids were found in these tubules (Fig. 4.3C). Other seminiferous tubules were capable of producing a small number of elongating/condensing spermatids, though no mature sperm were found in the epididymis isolated from the *Cenpa$^{fl/fl}$;Stra8-Cre/+* male. Since *Stra8-Cre* expression begins in early-stage spermatogonia and continues to increase through pre-leptotene-stage spermatocytes (Anderson et al., 2008), it is possible that the variable phenotypes seen in *Cenpa$^{fl/fl}$;Stra8-Cre/+* seminiferous tubules are a consequence of differential timing and efficiency of *Cenpa* deletion, leading to an ultimate phenotype that is difficult to interpret. As such, we concluded that *Cenpa$^{fl/fl}$;Stra8-Cre/+* males are unsuitable for reliably generating mature sperm with a reduced amount of CENP-A.

After concluding that neither *Cenpa$^{fl/fl}$;Ddx4-Cre/+* nor *Cenpa$^{fl/fl}$;Stra8-Cre/+* males would generate mature sperm with reduced CENP-A, we decided the best alternative route was to use an inducible system to control the timing of *Cenpa* excision more precisely. Thus, we generated *Cenpa$^{fl/fl}$;Ddx4-Cre(ER^{T2})/+* males according to the breeding scheme in Fig. 4.4A. While cre-

excision in *Cenpa$^{fl/fl}$;Ddx4-Cre(ER^{T2})/+* animals should be tamoxifen-inducible in both males and females, successful excision using this Cre line has only been reported in female gametes. Thus, I first needed to optimize the induction protocol. In order to get a baseline on the efficiency of tamoxifen-mediated Cre excision, I followed the protocol established for female gametes (John et al., 2008) and injected *Cenpa$^{fl/fl}$;Ddx4-Cre(ER^{T2})/+* and control *Cenpa$^{fl/fl}$;+/+* mice with tamoxifen dissolved in corn oil (See Appendix A), then dissected testes from both mice ~6 weeks later. At the same time, I also dissected testes from an uninjected littermate that was *Cenpa$^{fl/fl}$;Ddx4-Cre(ER^{T2})/+* as a control to ensure that the Cre(ER^{T2}) was not active in the absence of tamoxifen. Since spermatogenesis from spermatogonial stem cell to condensed spermatid takes ~5 weeks in the mouse, my hypothesis was that spermatogonial stem cells expressing Cre(ER^{T2}) in tamoxifen-injected mice would die in just a few cell divisions after *Cenpa* excision and thus after 6 weeks, there would be large-scale loss of spermatogenic cells in the testes of tamoxifen-injected *Cenpa$^{fl/fl}$;Ddx4-Cre(ER^{T2})/+* males. Therefore, if the tamoxifen induction protocol worked, then injected *Cenpa$^{fl/fl}$;Ddx4-Cre(ER^{T2})/+* males should have much smaller testes and immunostaining of testis sections from their testes should reveal decreased numbers of spermatogenic cells when compared to injected *Cenpa$^{fl/fl}$;+/+* and uninjected *Cenpa$^{fl/fl}$;Ddx4-Cre(ER^{T2})/+* controls. Upon dissection, there was no discernable difference between testes isolated from injected *Cenpa$^{fl/fl}$;Ddx4-Cre(ER^{T2})/+*, *Cenpa$^{fl/fl}$;+/+*, and uninjected *Cenpa$^{fl/fl}$;Ddx4-Cre(ER^{T2})/+* mice (Fig. 4.4C). Further, immunofluorescence of testes sections taken from each animal confirm that there is no obvious difference in the number or type of spermatogenic cells present in seminiferous tubules from the animals tested (Fig. 4.4B). I concluded from these data that the tamoxifen-induction protocol that I used was ineffective, though happily I also conclude that there is no Cre(ER^{T2}) activity in the absence of tamoxifen.

There are several variables that can be changed that may yield successful tamoxifen-induced *Cenpa* excision. First, it may be that more time is needed to see an obvious effect of the

Cenpa excision on spermatogenesis. Simply following the same injection protocol, but allowing more time for spermatogenic cells to lose CENP-A protein, may reveal that the protocol works. Second, it is possible that the tamoxifen-dose is either too low (in that more injections, a higher concentration of tamoxifen, or both are needed) or that the tamoxifen is not reaching the testes uniformly through intraperitoneal injection. Finally, administration of high doses of tamoxifen via oral gavage is an alternative route for induction, though the absorbance of drugs in mice via oral gavage is typically lower than when administered by intraperitoneal injection. Still, it is worthwhile to continue to optimize the induction protocol, as the *Cenpa*$^{fl/fl}$*;Ddx4-Cre(ER*^{T2}*)/+* males currently represent our best chance to generate a mouse model in which we can reduce the amount of centromeric CENP-A protein in mature sperm.

4.4 Future Directions

The preliminary results described in this section lay the groundwork for a mouse model system that could be used to generate mature sperm with reduced CENP-A protein. As outlined at the conclusion of Section 4.3, further experiments should be done to determine whether tamoxifen-induced *Cenpa* excision that leads to depleted CENP-A in sperm is possible with *Cenpa*$^{fl/fl}$*;Ddx4-Cre(ER*^{T2}*)/+* males. If it is possible to optimize the protocol in adult males such that *Cenpa* excision can be temporally controlled, the next step would be to optimize the excision timing so that one could easily collect a population of mature sperm in which centromeric CENP-A protein has been reliably depleted in all sperm. This is a tricky problem, since robust *Cenpa* excision in Cre(ER^{T2}) containing cells will eventually render males infertile as spermatogonial stem cells lose CENP-A through cell division. This leaves a finite window to collect CENP-A depleted sperm or have the males mate naturally to analyze the effects of CENP-A depleted sperm on centromere inheritance in early embryogenesis or the next generation. Further, even if induced *Cenpa* excision in adult males is very robust, adult males will always have

spermatogenic cells that are either in meiosis or further along in spermatogenesis, which will make it difficult, if not impossible to tell which mature sperm in a population have pre-excision levels of CENP-A and which have lost CENP-A protein.

In an effort avoid these complications, once the tamoxifen induction protocol is worked out in adult males, *Cenpa* excision could be induced in male pups shortly after birth, right at the beginning of spermatogenesis. In this way, all of the sperm the mouse will ever produce will have undergone *Cenpa* excision and thus all of the mature sperm available in the epididymis for either downstream biophysical or biochemical assays, *in vitro* fertilization, or natural mating should have reduced levels of CENP-A, relative to animals with an intact *Cenpa* locus. Since we can detect CENP-A protein in mature sperm by immunoblotting, the level of chromatin bound CENP-A protein present in sperm isolated from induced males can easily be compared to that isolated from uninduced control males as an initial validation that the two populations have different CENP-A levels. Additional information about how different the CENP-A protein levels are between mature sperm from both groups, as well as the uniformity of CENP-A knockdown in the induced males, should be easily quantified by comparing the amount of CENP-A signal in round spermatids between the two groups. Round spermatids are already haploid and will not undergo any further mitotic divisions as they develop into mature sperm, so no further CENP-A loss should occur between the two stages. As such, analyzing the amount of CENP-A protein in round spermatids, which have robust CENP-A staining compared to elongating/condensing spermatids, should be sufficient to determine the extent of CENP-A knockdown in the induced mice compared to, as well as the uniformity of CENP-A levels in the reduced sperm.

Building a mouse model system in which the amount of CENP-A nucleosomes can be decreased in pre-meiotic spermatogenic cells opens avenues to probe centromere function in late spermatogenesis. In round spermatids, centromeric and pericentromeric chromatin cluster

together so form the so-called chromocenter (Gurevitch et al., 2001). Reduction of CENP-A nucleosomes in spermatogenic cells may help determine whether retention of CENP-A nucleosomes contribute to chromatin organization around the chromocenter, by analyzing the nuclear morphology of CENP-A depleted round spermatids (Meistrich et al., 2013). Alternatively, CENP-A depleted sperm can be used to answer interesting questions related to centromere inheritance. As discussed in Section 4.2, fly eggs fertilized with CENP-A depleted sperm give rise to offspring whose cells maintain the reduced amount of centromeric CENP-A (Raychaudhuri et al., 2012). These data suggest that the number of centromeric CENP-A nucleosomes inherited by the embryo at fertilization may determine the amount of CENP-A nucleosomes that can ever be at the centromere. Using CENP-A depleted sperm to create mouse embryos and measuring the amount of centromeric CENP-A during early embryogenesis could reveal whether the same phenomenon is true in mammals. Are reduced CENP-A levels problematic, particularly in meiosis where homologous chromosomes are paired? Previous work demonstrates that in the meiotic context, differences in centromere proteins can bias chromosome segregation (Chmátal et al., 2014). Reduced CENP-A levels may have a direct effect on chromosome inheritance. Alternatively, if reduced CENP-A levels on paternal chromatin are restored to wildtype levels, are there boundary elements that set the size of the centromere? Existing evidence suggests that pericentromeric chromatin may serve as a boundary element (Blower and Karpen, 2001; Maggert and Karpen, 2001; Partridge et al., 2000; Volpe et al., 2002), and may be a good place to begin inquiry. When considering these questions, it becomes clear that much about centromere inheritance and function through the male germline remains unknown. Generating mouse models to answer them will greatly aid in our understanding of centromere inheritance through the male germline.

4.5 Conclusions and Outlook

The vital role of CENP-A nucleosomes in centromere inheritance and chromosome segregation during early embryogenesis are clear. However, the fundamental mechanisms that facilitate CENP-A nucleosome inheritance through the male germline remain mysterious. In this chapter, I have highlighted my efforts to generate a suitable mouse model to pursue these questions, as well as assays that I established in order to validate the system. Though the ideal mouse model remains elusive, the *Cenpa$^{fl/fl}$;Ddx4-Cre(ER^{T2})/+* may yet yield the desired phenotype and greatly enhance our understanding of the mechanisms behind centromere inheritance through the male germline. Additionally, the advent of CRISPR technology has opened the door to easier mouse transgenesis and will likely augment efforts to develop new methods for protein manipulation in all sorts of mouse tissues. Harnessing these tools to alter CENP-A levels in the germline will deepen our understanding of the molecular mechanisms governing transgenerational centromere inheritance.

4.6 Methods

4.6.1 Generation of Cenpa Conditional KO Mice

Cenpa$^{fl/fl}$ mice were mated with *Ddx4-Cre/+* (Stock #: 006954, The Jackson Laboratory) males, and the resulting *Cenpa$^{fl/+}$;Ddx4-Cre/+* males were mated with *Cenpa$^{fl/fl}$* females to obtain *Cenpa$^{fl/fl}$;Ddx4-Cre/+* males. *Cenpa$^{fl/fl}$* mice were mated with *Stra8-Cre/+* (Stock #: 017490, The Jackson Laboratory) males, and the resulting *Cenpa$^{fl/+}$;Stra8-Cre/+* males were mated with *Cenpa$^{fl/fl}$* females to obtain *Cenpa$^{fl/fl}$;Stra8-Cre/+* males. *Cenpa$^{fl/fl}$* mice were mated with *Ddx4-Cre(ER^{T2})/+* (Stock #: 024760, The Jackson Laboratory) males, and the resulting *Cenpa$^{fl/+}$;Ddx4-Cre(ER^{T2})/+* males were mated with *Cenpa$^{fl/fl}$* females to obtain *Cenpa$^{fl/fl}$; Ddx4-Cre(ER^{T2})/+* males. Because Cre-excision is tamoxifen inducible in this line, *Cenpa$^{fl/fl}$; Ddx4-Cre(ER^{T2})/+* animals are fertile and can be bred to *Cenpa$^{fl/fl}$* animals to yield desired experimental and control

mice. Mice were genotyped by PCR analysis of tail DNA extracted using the REDExtract-N-Amp Red Tissue PCR kit (Sigma-Aldrich) using primers and PCR programs listed in Table 4.1. All animal experiments were approved by the Institutional Animal Use and Care Committee of the University of Pennsylvania and were consistent with National Institutes of Health guidelines.

4.6.2 Immunoblot

Samples derived from whole cell lysates were separated by SDS-PAGE and transferred to a nitrocellulose membrane for immunoblotting. Blots were probed using a rabbit anti-CENP-A antibody (1:200, Cell Signaling #2047S). Antibodies were detected using an ECL anti-rabbit IgG, horseradish peroxidase-conjugated secondary antibody (GE Healthcare, NA934V) at 1:2000 and Amersham ECL Select Western Blotting Detection Reagent (GE Healthcare, RPN2235).

4.6.3 Indirect Immunofluorescence

Testes were dissected out of mice, placed in tubes, flash-frozen with liquid N_2 and placed at -80°C until mounted for cryosectioning. See Appendix for detailed protocol. Testes were sectioned at a thickness of 8µm and were fixed with freshly prepared 4% paraformaldehyde in PBS (pH 7.4) for 15 min at room temperature, quenched in 100mM Glycine, then washed with PBS before being permeabilized with PBS+0.1% Triton X-100 for 2 min. Sections were blocked with 3% donkey serum for 1 hour at 37°C, incubated 1 h with primary antibodies at 37°C, washed three times in blocking solution for 5 min, incubated 1 h with secondary antibodies at 37°C, washed three times for 5 min in blocking buffer, and mounted in Vectashield with DAPI (5 µg/mL, Sigma-Aldrich) to visualize DNA. Primary antibodies were rabbit anti-CENP-A (1:200, Cell Signaling #2048S), and anti-SYCP2 (Gift from Jeremy Wang, UPenn). Secondary antibodies were Alexa Fluor 594–conjugated donkey anti–rabbit, Alexa Fluor 488-donkey anti-rabbit, and Alexa Fluor 594 goat anti-guinea pig (1:100), (Invitrogen) and FITC-anti-guinea pig (Gift from Jeremy Wang, UPenn).

4.6.4 Image Acquisition

Confocal images were collected as z-stacks with 0.5 µm intervals to visualize tissue sections using a microscope (DMI4000 B; Leica) equipped with a 20x 0.7 NA dry-objective lens, a 63x 1.3 NA glycerol-immersion objective lens, a 100x 1.4 NA oil-immersion lens, an xy piezo Z stage (Applied Scientific Instrumentation), a spinning disk confocal scanner (Yokogawa Corporation of America), an electron multiplier charge-coupled device camera (ImageEM C9100-13; Hamamatsu Photonics), and an LMM5 laser merge module with 488- and 593-nm diode lasers (Spectral Applied Research) controlled by MetaMorph software (Molecular Devices).

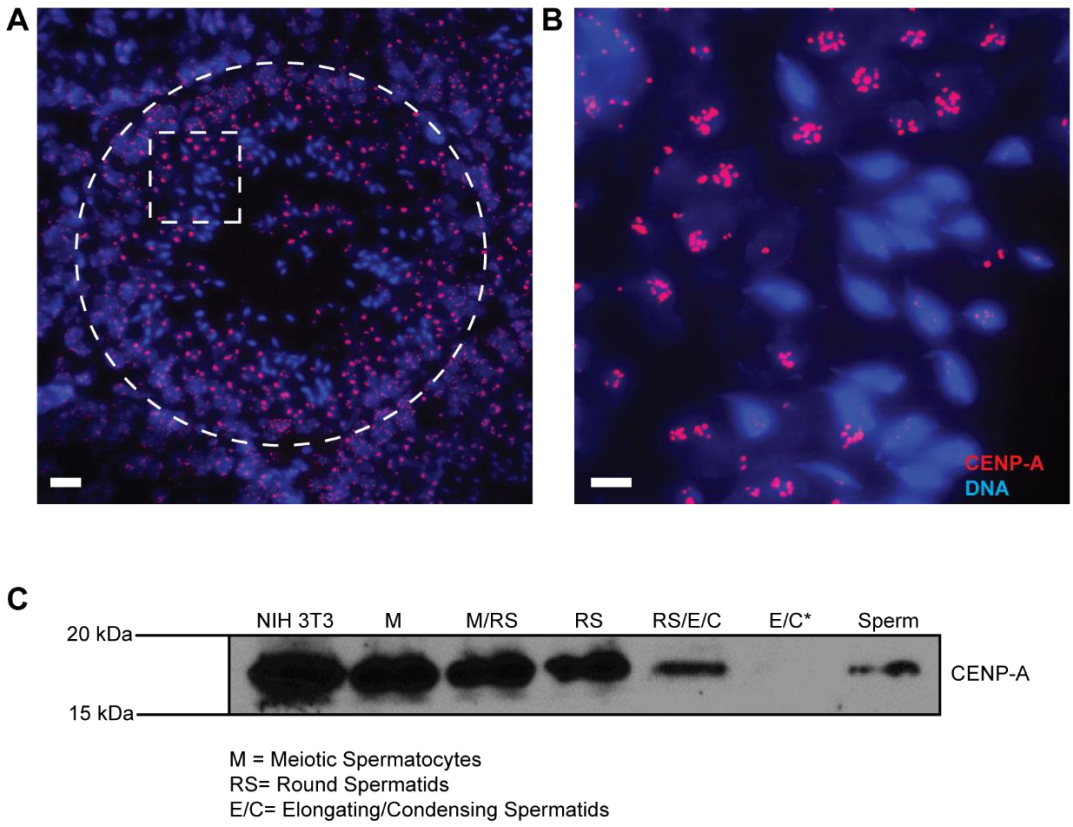

Figure 4.1 Evaluating CENP-A protein levels in testes by immunofluorescence and immunoblot.

(**A**) Cryosection of a seminiferous tubule from an SV129 mouse (20x). Scale bar= 20µm White dashed circle represent boundaries of seminiferous tubule; white box represents regions shown at 100x in (B). (**B**) 100X magnification of selected region of seminiferous tubule from (A). Scale bar = 5µm White dashed circles represent boundaries of seminiferous tubule; white box represents regions shown at 100x (**C**) CENP-A levels decrease in sperm development in the transition between round spermatids and elongating/condensing spermatids, though CENP-A is still present in mature sperm. E/C*, during STA-PUT the E/C spermtids co-elute with red blood cells, skewing the cell count of E/C spermatids. As such, much fewer than 50,000 cells were loaded in that lane.

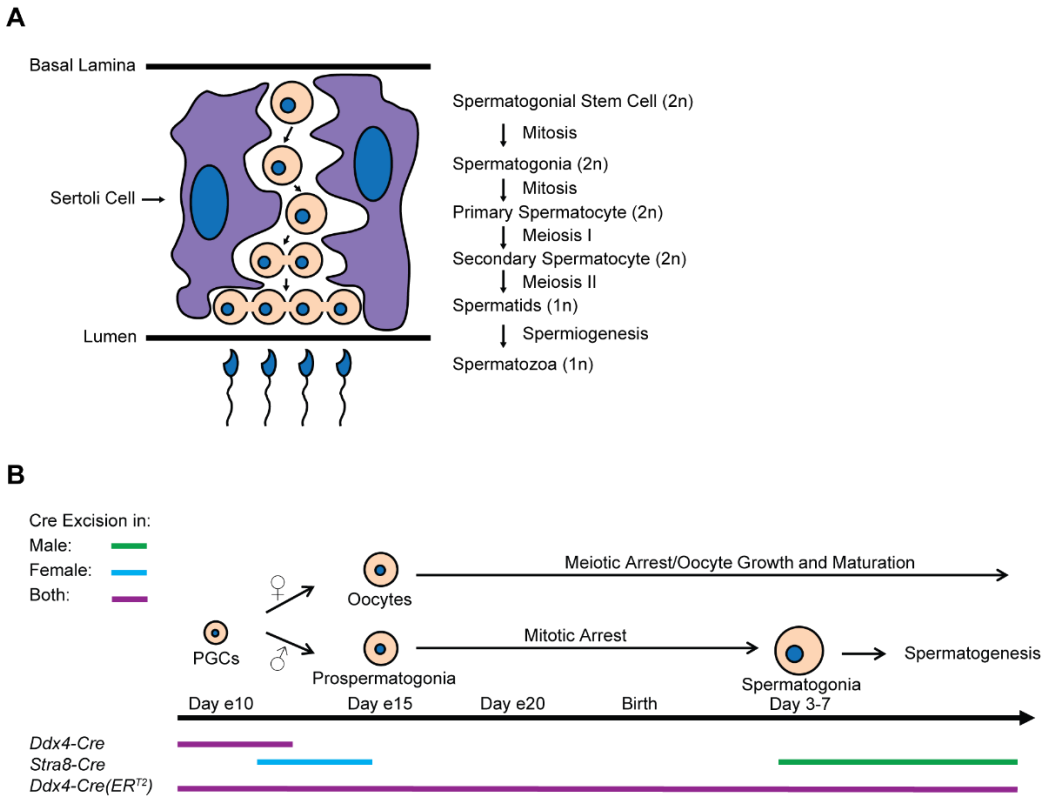

Figure 4.2 Schematic of spermatogenesis and germline specific Cre excision.

(**A**) Schematic of spermatogenesis indicating mitotic activity. For ideal CENP-A depletion, *Cenpa* excision should occur during the mitotic stages (**B**) Schematic of Cre expression using different germline specific Cre drivers.

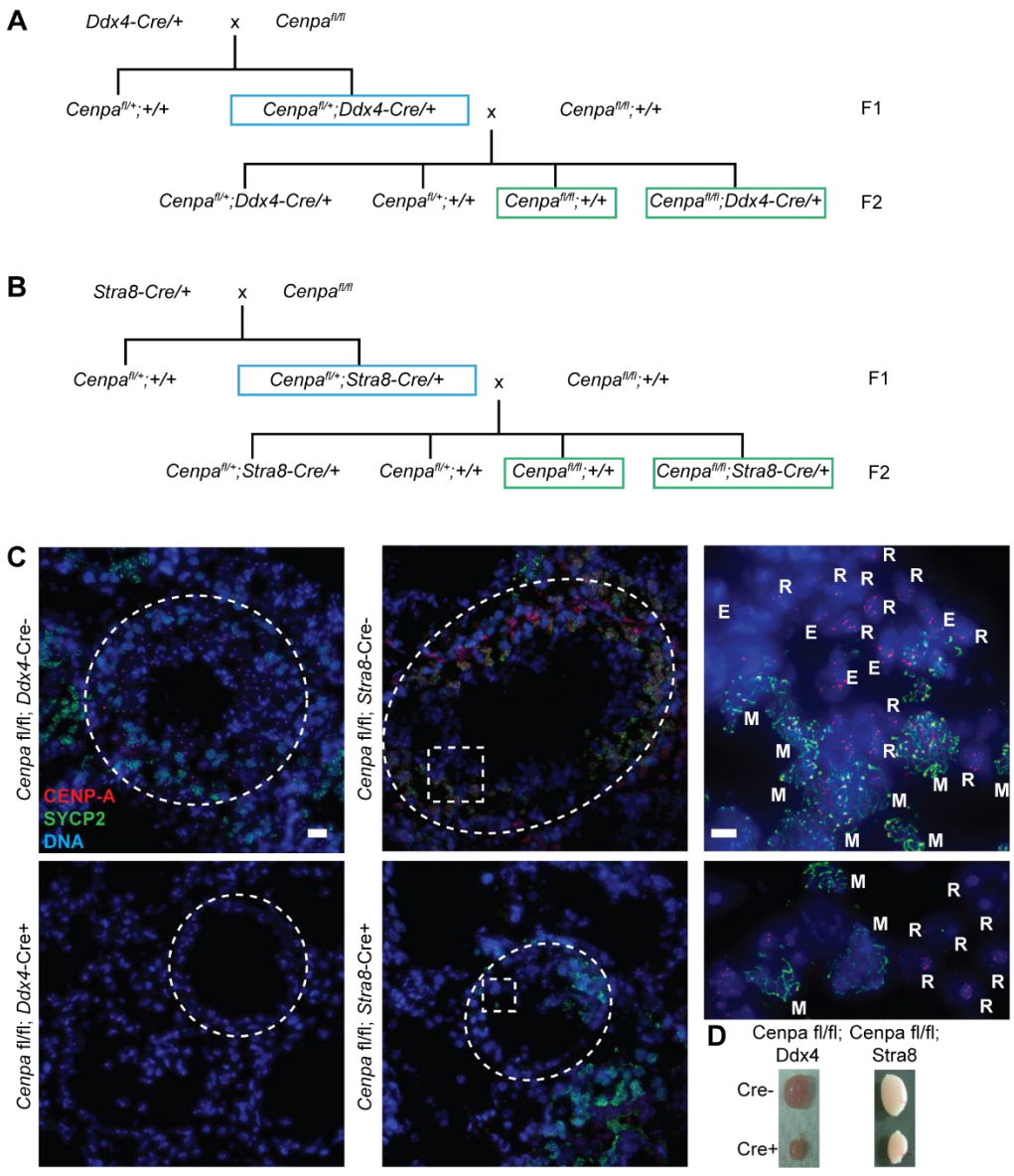

Figure 4.3 Cenpa excision by Ddx4-Cre or Stra8-Cre does not yield viable sperm.

(**A, B**) Breeding schemes used to generate *Cenpa$^{fl.fl}$;Ddx4-Cre*/+ and *Cenpa$^{fl.fl}$;Stra8-Cre*/+ mice. (**C**) Cryosections of testes isolated from either *Cenpa$^{fl.fl}$;Ddx4-Cre*/+ and *Cenpa$^{fl.fl}$;Stra8-Cre*/+ mice, stained for CENP-A, SYCP2, and DNA. Scale bars = 20µm (20x)

images and 5µm (100x). White dashed circles represent boundaries of seminiferous tubule; white box represents regions shown at 100x on right side of figure. The letters M, R, and E denote one meiotic, round, and elongating spermatogenic cell respectively, illustrating that there are fewer of these spermatogenic cell types in testes of *Cenpa*$^{fl.fl}$*;Stra8-Cre/+* males compared to controls.. (**D**) Photographs of whole testes isolated from mice used in (C).

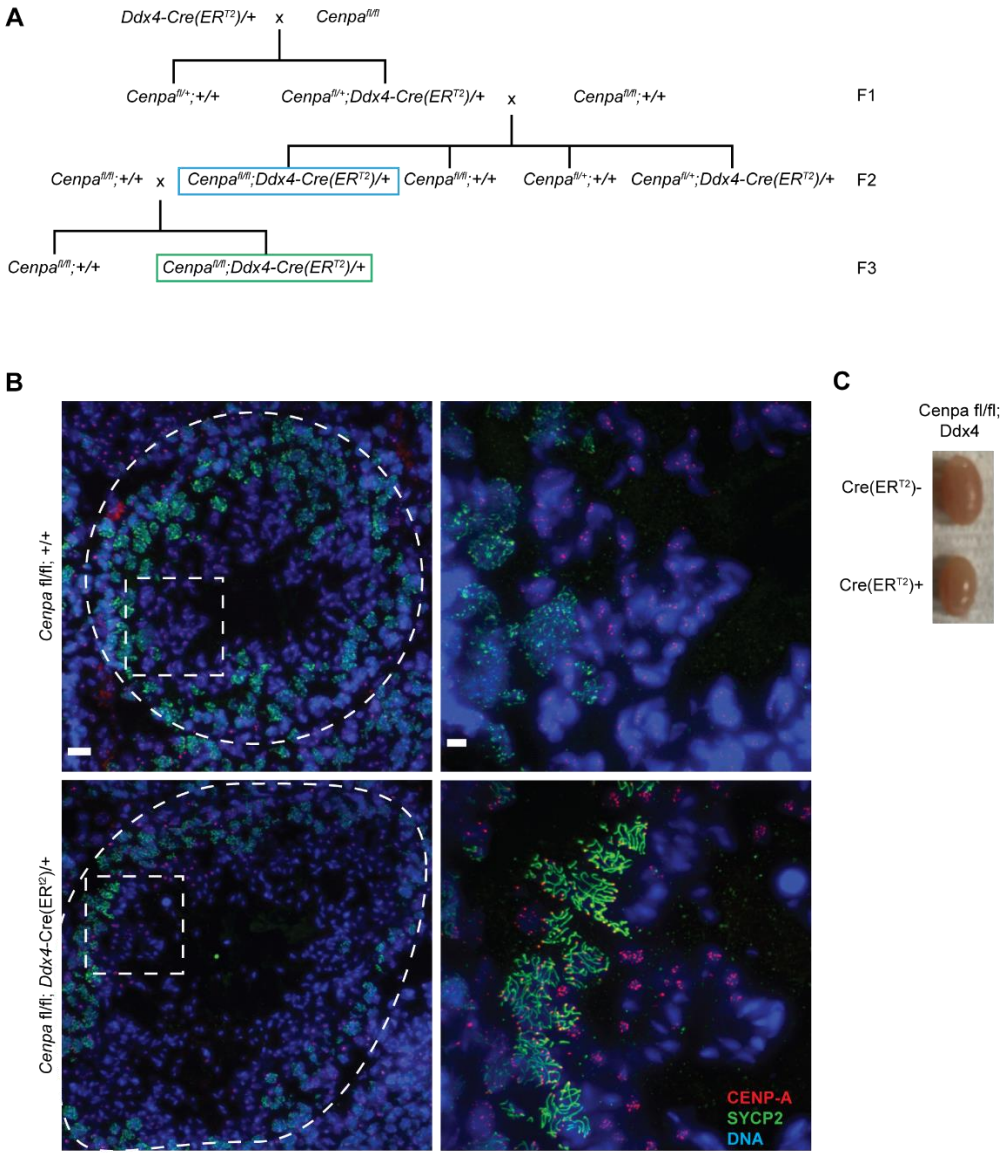

Figure 4.4 Generation of Cenpa$^{fl/fl}$;Ddx4-Cre(ER^{T2})/+ mice and initial tamoxifen induction response.

(**A**) Breeding schemes used to generate *Cenpa$^{fl.fl}$;Ddx4-Cre(ER^{T2})/+* mice. (**B**) Cryosections of testes isolated from *Cenpa$^{fl.fl}$;Ddx4-Cre(ER^{T2})/+*, stained for CENP-A, SYCP2, and DNA. Scale bars = 20µm (20x) images and 5µm (63x). White dashed circles represent

boundaries of seminiferous tubule; white box represents regions shown at 63x on right side of page

Cenpa Genotyping
Fwd Primer: 5'-GCAGAGCCACAGCTCCAGAGCA-3'
Rev Primer 1: 5'-CAGACTGCAGTTCCATCCCTACAGA-3'
Rev Primer 2: 5'-TGAACTGATGGCGAGCTCAGACC-3'

Band Sizes:

Cenpa Floxed Allele: 490 bp
Cenpa Wildtype Allele: 382 bp
Cenpa Recombined Allele: 285 bp

Initial Denaturation: 95ºC for 5 min
Denaturation: 95ºC for 30 sec
Annealing: 55ºC for 30 sec
Elongation: 72ºC for 2 min
Final Elongation: 72ºC for 5 min
30 cycles

Ddx4-Cre & *Ddx4-Cre(ER^{T2})* Genotyping
Fwd Primer: 5'-CACGTGCAGCCGTTTAAGCCGCGT-3'
Rev Primer: 5'-TTCCCATTCTAAACAACACCCTGAA-3'

Band Sizes:

Ddx4-Cre & *Ddx4-Cre(ER^{T2})*: 240 bp

Initial Denaturation: 94ºC for 3 min
Denaturation: 94ºC for 30 sec
Annealing: 67ºC for 1 min
Elongation: 72ºC for 1 min
Final Elongation: 72ºC for 2 min
35 cycles

Stra8-Cre Genotyping
Fwd Primer: 5'-GTGCAAGCTGAACAACAGGA-3'
Rev Primer: 5'-AGGGACACAGCATTGGAGTC-3'

Band Sizes:

Stra8-Cre: 179 bp

Initial Denaturation: 94ºC for 3 min
Denaturation: 94ºC for 30 sec
Annealing: 60ºC for 1 min
Elongation: 72ºC for 1 min
Final Elongation: 72ºC for 2 min
30 cycles

Table 4.1 Genotyping primers and thermocycler programs.

Chapter 5:

Conclusions

5.1 Summary

The work presented in this dissertation has deepened our understanding of transgenerational centromere inheritance, both broadly and in the specialized case of centromere inheritance through the germline. In collaboration with others, I demonstrated that CENP-A nucleosomes are strongly retained at their centromere of origin, while CENP-A nucleosomes that are ectopically localized to chromatin are lost over time. Further, through experiments in which I knocked down the CENP-A nucleosome binding protein CENP-C, I found that loss of CENP-C leads to dramatic loss of CENP-A nucleosomes at the centromere within one cell cycle. These findings show that CENP-C plays an important role in the stable retention of CENP-A nucleosomes at the centromere, which allows CENP-A nucleosomes to be transmitted to daughter cells. Additionally, I determined that stable retention of CENP-A nucleosomes is the mechanism by which centromeres are inherited through the female mammalian germline. Finally, I detailed my efforts to generate a mouse model to study CENP-A retention and transmission in the male germline. Though a suitable mouse model remains elusive, I was successful in creating assays to validate suitable mice, and have high hopes for the *Cenpa*$^{fl/fl}$*;Ddx4-Cre(ER*^{T2}*)*/+ males.

While my dissertation work has answered some fundamental questions regarding centromere inheritance, much remains unknown. In the following sections, I briefly summarize the conclusions from the research presented in Chapters 2-4, and highlight opportunities to extend this work further into the mammalian germline.

5.2 Future Directions for Chapters 2 and 3

Though the experiments presented in Chapter 2 and 3 were done in different systems, my work on both chapters addressed the same fundamental question: by what mechanisms are centromeres inherited by offspring, be they daughter cells or mouse pups. In Chapter 2, I

describe a collaborative effort in which we determined that CENP-C binding to CENP-A nucleosomes physically changes the shape of CENP-A nucleosomes. Using elegant FRET experiments, we demonstrated that on their own in solution, CENP-A nucleosomes adopt a conformation such that the H2A/H2B dimers are ~5 Å further away from each other than they are in conventional histone H3.1 containing nucleosomes. However, when the same assay is performed with the addition of the central domain of CENP-C (CENP-C^{CD}), CENP-A nucleosomes adopt a conformation similar to H3.1 nucleosomes, suggesting that CENP-C^{CD} was physically altering the shape of CENP-A nucleosomes. Hydrogen-deuterium exchange coupled with mass spectrometry further confirmed that CENP-C^{CD} binding to CENP-A nucleosomes changed the physical shape of CENP-A nucleosomes. Not only did CENP-C^{CD} stabilize portions of CENP-A nucleosomes that directly interact with CENP-C^{CD}, but also stabilized regions within the CENP-A nucleosome that it did not directly interact with.

To understand the functional effects of CENP-C mediated stabilization of CENP-A nucleosomes, I developed several cell culture assays. First, I established a live-cell photoactivation assay utilizing a photoconvertible form of GFP fused to CENP-A (CENP-A-PAGFG) and overexpressed CENP-A-PAGFP such that CENP-A-PAGFP was enriched at centromeres but was also present on chromosome arms. We sought to discover whether CENP-A-PAGFP was stably retained both at centromeres and chromosome arms. The assay revealed that CENP-A-PAGFP that ectopically localized to chromosome arms had a half-life similar to H3.1-PAGFP, while the CENP-A-PAGFP at the centromere remained constant. This data caused us to look at centromere proteins that could be responsible for enhanced stability of CENP-A nucleosomes, and since the biophysical data we had collected showed that CENP-C^{CD} was able to stabilize features of the CENP-A nucleosome, we wondered whether CENP-C played a role in CENP-A nucleosome retention. Using a fluorescent pulse-chase approach, we determined that depletion of CENP-C drastically reduces the amount of CENP-A at the centromere. Together, our

results show that as a result of the physical changes CENP-C makes by binding to CENP-A nucleosomes, it plays a direct role in stabile retention of CENP-A nucleosomes at the centromere, which is vital for centromere inheritance.

In Chapter 3, I asked how centromeres are inherited through the female mammalian germline. My hypothesis was that centromere inheritance was either CENP-A independent, dependent on a meiotic loading pathway, or dependent on the stability of CENP-A nucleosomes. Utilizing a sophisticated genetic approach, in which I generated and validated an oocyte-specific *Cenpa* conditional knockout mouse, I demonstrated that the amount of CENP-A present at centromeres from both wildtype and knockout oocytes was equivalent in oocytes from animals >12 months old. Further, oocytes from knockout animals had no trouble maturing into MII eggs and females were totally fertile. These data show that stable retention of CENP-A nucleosomes is the mechanism by which centromere identity is inherited through the female mammalian germline.

Though the work presented in these chapters fills a large gap in our understanding of transgenerational centromere inheritance by virtue of CENP-A nucleosome stability, the molecular basis of that stability, particularly in oocytes, remains poorly understood. As such, future work could focus on determining whether CENP-C plays a similar role in stabilizing CENP-A nucleosomes during prophase I arrest, as it does in cycling somatic cells. Deleting *Cenpc* in mice is embryonic lethal, so an oocyte-specific genetic conditional knockout approach targeting the *Cenpc1* gene in mouse and then aging the mice to study the effect of CENP-C loss at the centromere would be the most elegant way to determine if CENP-C is playing a role. However, embryonic stem cells (ESCs) with a floxed *Cenpc1* mutant allele are not commercially available, leaving two routes to generate the animal. The first possibility is to generate a targeted ESC line that is heterozygous for the floxed *Cenpc1* allele and contains a neomycin selection cassette.

Once the cell line has been validated and karyotyped, the ESCs could be injected blastocysts and transferred to recipient surrogate mothers. The second possibility is to utilize CRISPR/Cas9 to introduce *loxP* sites at the *Cenpc1* allele. CRISPR/Cas9 reagents would be injected into 1-cell embryos prior to pronuclear fusion (Yang et al., 2013; Yang et al., 2014), develop the embryos *in vitro* to the blastocyst stage, and transfer any embryos to recipient surrogate mothers. Any pups born could then be genotyped for the floxed *Cenpc1* allele.

Since CENP-C does exhibit protein turnover (Hemmerich et al., 2008), it is possible to try and perturb the protein on a shorter timescale and yield interesting data without the difficulty and expense of generating a conditional knockout mouse. Currently, the success of morpholino and/or siRNA knockdown in full-grown GV oocytes is completely dependent on the turnover rate of the target protein, and is limited by the fact that you cannot culture the cells for longer than ~36 hours without compromising their ability to mature to metaphase II or their overall survival. A workaround to this problem is to inject morpholinos and/or siRNA targeting CENP-C into follicle-enclosed oocytes when they are secondary follicles (Jaffe and Terasaki, 2004; Jaffe et al., 2009). This method allows more time for protein turnover, because oocytes within intact secondary follicles can be injected and then cultured for 5-7 days within the follicle to the pre-antral stage. At this point, the oocytes will still be arrested at prophase I, but can be taken out of the follicle and should mature normally to metaphase II. Injecting a morpholino/siRNA combination into follicle-enclosed oocytes that targets *Cenpc1* mRNA, may allow enough time for CENP-C protein to be knocked down and assay whether CENP-C depletion at centromeres in oocytes destabilizes CENP-A. Another potential target protein with this approach is CENP-N, which remains the only other known protein that binds CENP-A nucleosomes directly (Carroll et al., 2009; Guse et al., 2011; McKinley et al., 2015). Depletion of either of these proteins may disrupt CENP-A nucleosome stability and negatively impact centromere function during meiosis and ultimately, centromere inheritance.

Another avenue is to test whether CENP-A nucleosome stability is dependent on intrinsic features of CENP-A nucleosomes, in particular the hydrophobic stitch residues within the CATD which were discussed in Chapter 1. Since mutation of all 6 hydrophobic stitch residues abrogates the ability of CENP-A nucleosomes to remain chromatin bound, it is possible that a single mutation or a combination of residues might lead to a less severe CENP-A phenotype. Generating a CENP-A protein with a hydrophobic stitch mutation that subtly destabilizes CENP-A nucleosome retention could help uncover whether these residues are essential for centromere inheritance on the order of months to years in a biologically relevant system. Prior to making a mouse, suitable hydrophobic stitch mutants could be evaluated in tissue culture cells by using a fluorescent pulse-chase assay to monitor mutant CENP-A loss over the course of a few cell cycles, so only the most promising candidates are used. Since there is no way to know *a priori* whether certain mutations will be severely deleterious to centromere function, a sophisticated cell culture system could be designed where cells live off of two distinct copies of *Cenpa*. One *Cenpa* allele would express CENP-A-GFP-AID, modeled off of the auxin inducible degradation system used in other studies (Holland et al., 2012; Fachinetti et al., 2015). The other allele would express the mutant CENP-A fused to the SNAP-tag, to allow for pulse-chase labeling of mutant CENP-A turnover. At the time of the experiment, the wildtype CENP-A-GFP-AID could be inducibly degraded, allowing for clear phenotype analysis of each mutant made. Determining the molecular basis of CENP-A nucleosome stability in the oocyte will only serve to expand our knowledge of the requirements for centromere inheritance both in the germline and beyond.

5.3 Future Directions for Chapter 4

Understanding how centromeres are inherited by the 1-cell stage embryo requires a deeper understanding of how centromeres are transmitted through both types of gametes. In Chapter 4, I discussed my efforts to perturb the amount of CENP-A nucleosomes in mammalian

sperm, in order to answer fundamental questions about centromere inheritance during spermatogenesis. Though this work is not fully completed, it sets the stage for the future directions that I outline in Section 4.4. In the absence of *in vitro* spermatogenic culture systems, manipulating protein levels through timed genetic knockout remains the best pathway for altering protein levels during mammalian spermatogenesis.

5.4 Concluding Remarks

Our comprehension of centromere biology has grown by leaps and bounds in the last 30+ years. Though we understand a lot about the nature of centromeres and the epigenetic way they are inherited, the role of many molecular players is not fully defined yet, and we are only now scratching the surface of the molecular pathways that ensure centromere transmission to offspring through gametes. Understanding the molecular workings of the locus that directs chromosome segregation, affords us the opportunity to understand the links between centromere inheritance and genetic inheritance; continuing to connect and extend the work of Mendel and Flemming nearly a century and a half later.

BIBLIOGRAPHY

Adhikari, D., Zheng, W., Shen, Y., Gorre, N., Hämäläinen, T., Cooney, A. J., … Liu, K. (2010). Tsc/mTORC1 signaling in oocytes governs the quiescence and activation of primordial follicles. *Human Molecular Genetics*, *19*(3), 397–410. http://doi.org/10.1093/hmg/ddp483

Akiyama, T., Suzuki, O., Matsuda, J., & Aoki, F. (2011). Dynamic replacement of histone H3 variants reprograms epigenetic marks in early mouse embryos. *PLoS Genetics*, *7*(10), 1–12. http://doi.org/10.1371/journal.pgen.1002279

Amor, D. J., Bentley, K., Ryan, J., Perry, J., Wong, L., Slater, H., & Choo, K. H. A. (2004). Human centromere repositioning “in progress”. *Proceedings of the National Academy of Sciences of the United States of America*, *101*(17), 6542–7. http://doi.org/10.1073/pnas.0308637101

Anderson, E. L., Baltus, A. E., Roepers-Gajadien, H. L., Hassold, T. J., de Rooij, D. G., van Pelt, A. M. M., & Page, D. C. (2008). Stra8 and its inducer, retinoic acid, regulate meiotic initiation in both spermatogenesis and oogenesis in mice. *Proceedings of the National Academy of Sciences of the United States of America*, *105*(39), 14976–80. http://doi.org/10.1073/pnas.0807297105

Armache, K.-J., Garlick, J. D., Canzio, D., Narlikar, G. J., & Kingston, R. E. (2011). Structural basis of silencing: Sir3 BAH domain in complex with a nucleosome at 3.0 Å resolution. *Science (New York, N.Y.)*, *334*(6058), 977–982. http://doi.org/10.1126/science.1210915

Balhorn, R. (2007). The protamine family of sperm nuclear proteins. *Genome Biology*, *8*(9), 227. http://doi.org/10.1186/gb-2007-8-9-227

Balhorn, R., Brewer, L., & Corzett, M. (2000). DNA condensation by protamine and arginine-rich peptides: analysis of toroid stability using single DNA molecules. *Molecular Reproduction and Development*, *56*(2 Suppl), 230–234. http://doi.org/10.1002/(SICI)1098-2795(200006)56:2+<230::AID-MRD3>3.0.CO;2-V

Barnhart, M. C., Kuich, P. H. J. L., Stellfox, M. E., Ward, J. A., Bassett, E. A., Black, B. E., & Foltz, D. R. (2011). HJURP is a CENP-A chromatin assembly factor sufficient to form a functional de novo kinetochore. *Journal of Cell Biology*, *194*(2), 229–243. http://doi.org/10.1083/jcb.201012017

Barry, A. E., Howman, E. V., Cancilla, M. R., Saffery, R., & Choo, K. H. A. (1999). Sequence analysis of an 80 kb human neocentromere. *Human Molecular Genetics*, *8*(2), 217–227. http://doi.org/10.1093/hmg/8.2.217

Bassett, E. A., DeNizio, J., Barnhart-Dailey, M. C., Panchenko, T., Sekulic, N., Rogers, D. J., … Black, B. E. (2012). HJURP uses distinct CENP-A surfaces to recognize and to stabilize CENP-A/histone H4 for centromere assembly. *Developmental Cell*, *22*(4), 749–762. http://doi.org/10.1016/j.devcel.2012.02.001

Bassett, E. A., Wood, S., Salimian, K. J., Ajith, S., Foltz, D. R., & Black, B. E. (2010). Epigenetic centromere specification directs aurora B accumulation but is insufficient to efficiently correct mitotic errors. *The Journal of Cell Biology*, *190*(2), 177–185. http://doi.org/10.1083/jcb.201001035

Black, B. E., & Cleveland, D. W. (2011). Epigenetic centromere propagation and the nature of CENP-A nucleosomes. *Cell*, *144*(4), 471–479. http://doi.org/10.1016/j.cell.2011.02.002

Black, B. E., Foltz, D. R., Chakravarthy, S., Luger, K., Woods, V. L., & Cleveland, D. W. (2004). Structural determinants for generating centromeric chromatin. *Nature*, *430*(6999), 578–82. http://doi.org/10.1038/nature02766

Black, B. E., Jansen, L. E. T., Maddox, P. S., Foltz, D. R., Desai, A. B., Shah, J. V, & Cleveland, D. W. (2007). Centromere identity maintained by nucleosomes assembled with histone H3 containing the CENP-A targeting domain. *Molecular Cell*, *25*(2), 309–22. http://doi.org/10.1016/j.molcel.2006.12.018

Bloom Carbon,J., K. S. (1982). Yeast centromere DNA isin a unique and highly ordered structure in chromosomes andsmall circularminichromosomes. *Cell*, *29*(June), 305–317.

Blower, M. D., & Karpen, G. H. (2001). The role of Drosophila CID in kinetochore formation, cell-cycle progression and heterochromatin interactions. *Nature Cell Biology*, *3*(8), 730–739. http://doi.org/10.1038/35087045

Bodor, D. L., Rodríguez, M. G., Moreno, N., & Jansen, L. E. T. (2012). Analysis of protein turnover by quantitative SNAP-based pulse-chase imaging. *Current Protocols in Cell Biology / Editorial Board, Juan S. Bonifacino ... [et Al.]*, *Chapter 8*, Unit8.8. http://doi.org/10.1002/0471143030.cb0808s55

Bodor, D. L., Valente, L. P., Mata, J. F., Black, B. E., & Jansen, L. E. T. (2013). Assembly in G1 phase and long-term stability are unique intrinsic features of CENP-A nucleosomes. *Molecular Biology of the Cell*, *24*, 923–932. http://doi.org/10.1091/mbc.E13-01-0034

Boveri, T. (1902). *Uber mehrpolige Mitosen als Mittel zur Analyse des Zellkerns*. Wurzburg: Stuber.

Brand, A. H., & Perrimon, N. (1993). Targeted gene expression as a means of altering cell fates and generating dominant phenotypes. *Development (Cambridge, England)*, *118*(2), 401–15. http://doi.org/10.1101/lm.1331809

Bryant, J. M., Meyer-Ficca, M. L., Dang, V. M., Berger, S. L., & Meyer, R. G. (2013). Separation of spermatogenic cell types using STA-PUT velocity sedimentation. *Journal of Visualized Experiments : JoVE*, (80), 1–9. http://doi.org/10.3791/50648

Brykczynska, U., Hisano, M., Erkek, S., Ramos, L., Oakeley, E. J., Roloff, T. C., … Peters, A. H. F. M. (2010). Repressive and active histone methylation mark distinct promoters in human and mouse spermatozoa. *Nature Structural & Molecular Biology*, *17*(6), 679–87. http://doi.org/10.1038/nsmb.1821

Buchwitz, B. J., Ahmad, K., Moore, L. L., Roth, M. B., & Henikoff, S. (1999). A histone-H3-like protein in C . elegans. *Nature*, *401*(October), 547–548. http://doi.org/10.1038/44062

Bui, M., Dimitriadis, E. K., Hoischen, C., An, E., Quénet, D., Giebe, S., … Dalal, Y. (2012). Cell-cycle-dependent structural transitions in the human CENP-A nucleosome in vivo. *Cell*, *150*(2), 317–326. http://doi.org/10.1016/j.cell.2012.05.035

Burkhardt, S., Borsos, M., Szydlowska, A., Godwin, J., Williams, S. A., Cohen, P. E., … Tachibana-Konwalski, K. (2016). Chromosome Cohesion Established by Rec8- Cohesin in Fetal Oocytes Is Maintained without Detectable Turnover in Oocytes Arrested for Months in Mice Report Chromosome Cohesion Established by Rec8-Cohesin in Fetal Oocytes Is Maintained without Detectable Tur. *Current Biology*, 1–8. http://doi.org/10.1016/j.cub.2015.12.073

Carroll, C. W., Milks, K. J., & Straight, A. F. (2010). Dual recognition of CENP-A nucleosomes is required for centromere assembly. *The Journal of Cell Biology*, *189*(7), 1143–1155. http://doi.org/10.1083/jcb.201001013

Carroll, C. W., Silva, M. C. C., Godek, K. M., Jansen, L. E. T., & Straight, A. F. (2009). Centromere assembly requires the direct recognition of CENP-A nucleosomes by CENP-N. *Nature Cell Biology*, *11*(7), 896–902. http://doi.org/10.1038/ncb1899

Caussinus, E., Kanca, O., & Affolter, M. (2011). Fluorescent fusion protein knockout mediated by anti-GFP nanobody. *Nature Structural & Molecular Biology*, *19*(1), 117–121. http://doi.org/10.1038/nsmb.2180

Chatot, C. L., Ziomek, C. A., Bavister, B. D., Lewis, J. L., & Torres, I. (1989). An improved culture medium supports development of random-bred 1-cell mouse embryos in vitro. *Journal of Reproduction and Fertility*, *86*(2), 679–688. http://doi.org/10.1530/jrf.0.0860679

Cheeseman, I. M., & Desai, A. (2008). Molecular architecture of the kinetochore–microtubule interface. *Nature Reviews Molecular Cell Biology*, *9*(1), 33–46. http://doi.org/10.1038/nrm2310

Chen, C. C., Dechassa, M. L., Bettini, E., Ledoux, M. B., Belisario, C., Heun, P., … Mellone, B. G. (2014). CAL1 is the Drosophila CENP-A assembly factor. *Journal of Cell Biology*, *204*(3), 313–329. http://doi.org/10.1083/jcb.201305036

Chen, Y., Baker, R. E., Keith, K. C., Harris, K., Stoler, S., & Fitzgerald-Hayes, M. (2000). The N terminus of the centromere H3-like protein Cse4p performs an essential function distinct from that of the histone fold domain. *Molecular and Cellular Biology*, *20*(18), 7037–7048. http://doi.org/10.1128/MCB.20.18.7037-7048.2000

Chiang, T., Duncan, F. E., Schindler, K., Schultz, R. M., & Lampson, M. A. (2010). Evidence that weakened centromere cohesion is a leading cause of age-related aneuploidy in oocytes. *Current Biology*, *20*(17), 1522–1528. http://doi.org/10.1016/j.cub.2010.06.069

Chmátal, L., Gabriel, S. I., Mitsainas, G. P., Martínez-Vargas, J., Ventura, J., Searle, J. B., … Lampson, M. A. (2014). Centromere Strength Provides the Cell Biological Basis for Meiotic

Drive and Karyotype Evolution in Mice. *Current Biology*, *24*(19), 2295–2300. http://doi.org/10.1016/j.cub.2014.08.017

Choo, K. H. (1997). Centromere DNA dynamics: latent centromeres and neocentromere formation. *American Journal of Human Genetics*, *61*, 1225–1233. http://doi.org/10.1086/301657

Clarke, L., & Carbon, J. (1980). Isolation of a yeast centromere and construction of functional small circular chromosomes. *Nature*, *287*(5782), 504–509. http://doi.org/10.1038/287504a0

Commerford, S. L., Carsten, A. L., & Cronkite, E. P. (1982). Histone turnover within nonproliferating cells. *Proceedings of the National Academy of Sciences of the United States of America*, *79*(4), 1163–1165. http://doi.org/10.1073/pnas.79.4.1163

Crosby, G. A., & Demas, J. N. (1971). Measurement of photoluminescence quantum yields. Review. *The Journal of Physical Chemistry*, *75*(8), 991–1024. http://doi.org/10.1021/j100678a001

Depinet, T. W., Zackowski, J. L., Earnshaw, W. C., Kaffe, S., Sekhon, G. S., Stallard, R., … Schwartz, S. (1997). Characterization of neo-centromeres in marker chromosomes lacking detectable alpha-satellite DNA. *Human Molecular Genetics*, *6*(8), 1195–1204. http://doi.org/10.1093/hmg/6.8.1195

Dunleavy, E. M., Almouzni, G., & Karpen, G. H. (2011). H3.3 is deposited at centromeres in S phase as a placeholder for newly assembled CENP-A in G_1 phase. *Nucleus (Austin, Tex.)*, *2*(2), 146–157. http://doi.org/10.4161/nucl.2.2.15211

Dunleavy, E. M., Beier, N. L., Gorgescu, W., Tang, J., Costes, S. V, & Karpen, G. H. (2012). The cell cycle timing of centromeric chromatin assembly in Drosophila meiosis is distinct from mitosis yet requires CAL1 and CENP-C. *PLoS Biology*, *10*(12), 1–16. http://doi.org/10.1371/journal.pbio.1001460

Dunleavy, E. M., Roche, D., Tagami, H., Lacoste, N., Ray-Gallet, D., Nakamura, Y., … Almouzni-Pettinotti, G. (2009). HJURP Is a Cell-Cycle-Dependent Maintenance and Deposition Factor of CENP-A at Centromeres. *Cell*, *137*(3), 485–497. http://doi.org/10.1016/j.cell.2009.02.040

Dyer, P. N., Edayathumangalam, R. S., White, C. L., Bao, Y., Chakravarthy, S., Muthurajan, U. M., & Luger, K. (2004). Reconstitution of nucleosome core particles from recombinant histones and DNA. *Methods in Enzymology*, *375*, 23–44.

Earnshaw, W. C. (2015). Discovering centromere proteins: from cold white hands to the A, B, C of CENPs. *Nature Reviews Molecular Cell Biology*, *16*(7), 443–449. http://doi.org/10.1038/nrm4001

Erbach, G. T., Lawitts, J. A., Papaioannou, V. E., & Biggers, J. D. (1994). Differential growth of the mouse preimplantation embryo in chemically defined media. *Biology of Reproduction*, *50*(5), 1027–1033. http://doi.org/doi: 10.1095/biolreprod50.5.1027

Erhardt, S., Mellone, B. G., Betts, C. M., Zhang, W., Karpen, G. H., & Straight, A. F. (2008).

Genome-wide analysis reveals a cell cycle-dependent mechanism controlling centromere propagation. *The Journal of Cell Biology*, *183*(5), 805–18. http://doi.org/10.1083/jcb.200806038

Erkek, S., Hisano, M., Liang, C.-Y., Gill, M., Murr, R., Dieker, J., … Peters, A. H. F. M. (2013). Molecular determinants of nucleosome retention at CpG-rich sequences in mouse spermatozoa. *Nature Structural & Molecular Biology*, *20*(7), 868–75. http://doi.org/10.1038/nsmb.2599

Fachinetti, D., Han, J. S., McMahon, M. A., Ly, P., Abdullah, A., Wong, A. J., & Cleveland, D. W. (2015). DNA Sequence-Specific Binding of CENP-B Enhances the Fidelity of Human Centromere Function. *Developmental Cell*, *33*(3), 314–327. http://doi.org/10.1016/j.devcel.2015.03.020

Falk, S. J., Guo, L. Y., Sekulic, N., Smoak, E. M., Mani, T., Logsdon, G. A., … Black, B. E. (2015). CENP-C reshapes and stabilizes CENP-A nucleosomes at the centromere. *Science (New York, N.Y.)*, *348*(6235), 699–704. http://doi.org/10.1126/science.1259308

Falk, S. J., Lee, J., Sekulic, N., Sennett, M. A., Lee, T.-H., & Black, B. E. (2016). CENP-C directs a structural transition of CENP-A nucleosomes mainly through sliding of DNA gyres. *Nature Structural & Molecular Biology*, *2*(February), 1–6. http://doi.org/10.1038/nsmb.3175

Fitzgerald-Hayes, M., Clarke, L., & Carbon, J. (1982). Nucleotide sequence comparisons and functional analysis of yeast centromere DNAs. *Cell*, *29*(1), 235–44. http://doi.org/10.1016/0092-8674(82)90108-8

Flemming, W. (1882). *Zellsubstanz, kern und zelltheilung*. Leipzig: F.C.W. Vogel.

Foltz, D. R., Jansen, L. E. T., Bailey, A. O., Yates, J. R., Bassett, E. A., Wood, S., … Cleveland, D. W. (2009). Centromere-Specific Assembly of CENP-A Nucleosomes Is Mediated by HJURP. *Cell*, *137*(3), 472–484. http://doi.org/10.1016/j.cell.2009.02.039

Foltz, D. R., Jansen, L. E. T., Black, B. E., Bailey, A. O., Yates, J. R., & Cleveland, D. W. (2006). The human CENP-A centromeric nucleosome-associated complex. *Nature Cell Biology*, *8*(5), 458–69. http://doi.org/10.1038/ncb1397

Forster, T. (1946). Energiewanderung und Fluoreszenz. *Naturwissenschaften*, *33*(6), 166–175. http://doi.org/10.1007/BF00585226

Fujita, Y., Hayashi, T., Kiyomitsu, T., Toyoda, Y., Kokubu, A., Obuse, C., & Yanagida, M. (2007). Priming of Centromere for CENP-A Recruitment by Human hMis18-alpha, hMis18-beta, and M18BP1. *Developmental Cell*, *12*(1), 17–30. http://doi.org/10.1016/j.devcel.2006.11.002

Fukagawa, T., & Brown, W. R. (1997). Efficient conditional mutation of the vertebrate CENP-C gene. *Human Molecular Genetics*, *6*(13), 2301–2308.

Furuyama, T., Codomo, C. A., & Henikoff, S. (2013). Reconstitution of hemisomes on budding yeast centromeric DNA. *Nucleic Acids Research*, *41*(11), 5769–5783. http://doi.org/10.1093/nar/gkt314

Gallardo, T., Shirley, L., John, G. B., & Castrillon, D. H. (2007). Generation of a germ cell-specific mouse transgenic cre line, Vasa-Cre. *Genesis*, *417*, 413–417. http://doi.org/10.1002/dvg

Gassmann, R., Rechtsteiner, A., Yuen, K. W., Muroyama, A., Egelhofer, T., Gaydos, L., … Desai, A. (2012). An inverse relationship to germline transcription defines centromeric chromatin in C. elegans. *Nature*, *484*(7395), 534–537. http://doi.org/10.1038/nature10973

Goshima, G., Kiyomitsu, T., Yoda, K., & Yanagida, M. (2003). Human centromere chromatin protein hMis12, essential for equal segregation, is independent of CENP-A loading pathway. *Journal of Cell Biology*, *160*(1), 25–39. http://doi.org/10.1083/jcb.200210005

Gurevitch, M., Amiel, A., Ben-Zion, M., Fejgin, M., & Bartoov, B. (2001). Acrocentric centromere organization within the chromocenter of the human sperm nucleus. *Molecular Reproduction and Development*, *60*(4), 507–516. http://doi.org/10.1002/mrd.1116

Guse, A., Carroll, C. W., Moree, B., Fuller, C. J., & Straight, A. F. (2011). In vitro centromere and kinetochore assembly on defined chromatin templates. *Nature*, *477*(7364), 354–358. http://doi.org/10.1038/nature10379

Hall, M., Frank, E., Holmes, G., Pfahringer, B., Reutemann, P., & Witten, I. H. (2009). The WEKA Data Mining Software: An Update. *SIGKDD Explor. Newsl.*, *11*(1), 10–18. http://doi.org/10.1145/1656274.1656278

Hammoud, S. S., Nix, D. A., Zhang, H., Purwar, J., Carrell, D. T., & Cairns, B. R. (2009). Distinctive chromatin in human sperm packages genes for embryo development. *Nature*, *460*(7254), 473–8. http://doi.org/10.1038/nature08162

Harp, J. M., Uberbacher, E. C., Roberson, A. E., Palmer, E. L., Gewiess, A., & Bunick, G. J. (1996). X-ray Diffraction Analysis of Crystals Containing Twofold Symmetric Nucleosome Core Particles. *Acta Crystallographica Section D Biological Crystallography*, *52*(2), 283–288. http://doi.org/10.1107/S0907444995009139

Hassold, T., & Hunt, P. (2001). To err (meiotically) is human: the genesis of human aneuploidy. *Nature Reviews. Genetics*, *2*(4), 280–291. http://doi.org/10.1038/35066065

Hasson, D., Panchenko, T., Salimian, K. J., Salman, M. U., Sekulic, N., Alonso, A., … Black, B. E. (2013). The octamer is the major form of CENP-A nucleosomes at human centromeres. *Nature Structural & Molecular Biology*, *20*(6), 687–695. http://doi.org/10.1038/nsmb.2562

Hayashi, T., Fujita, Y., Iwasaki, O., Adachi, Y., Takahashi, K., & Yanagida, M. (2004). Mis16 and Mis18 are required for CENP-A loading and histone deacetylation at centromeres. *Cell*, *118*(6), 715–729. http://doi.org/10.1016/j.cell.2004.09.002

Hemmerich, P., Weidtkamp-Peters, S., Hoischen, C., Schmiedeberg, L., Erliandri, I., & Diekmann, S. (2008). Dynamics of inner kinetochore assembly and maintenance in living cells. *Journal of Cell Biology*, *180*(6), 1101–1114. http://doi.org/10.1083/jcb.200710052

Henikoff, S., Ramachandran, S., Krassovsky, K., Bryson, T. D., Codomo, C. A., Brogaard, K., … Henikoff, J. G. (2014). The budding yeast Centromere DNA Element II wraps a stable Cse4

hemisome in either orientation in vivo. *eLife*, *3*(0), e01861–e01861. http://doi.org/10.7554/eLife.01861

Heun, P., Erhardt, S., Blower, M. D., Weiss, S., Skora, A. D., & Karpen, G. H. (2006). Mislocalization of the Drosophila centromere-specific histone CID promotes formation of functional ectopic kinetochores. *Developmental Cell*, *10*(3), 303–315. http://doi.org/10.1016/j.devcel.2006.01.014

Ho, Y., Wigglesworth, K., Eppig, J. J., & Schultz, R. M. (1995). Preimplantation development of mouse embryos in KSOM: augmentation by amino acids and analysis of gene expression. *Molecular Reproduction and Development*, *41*(2), 232–8. http://doi.org/10.1002/mrd.1080410214

Holland, A. J., Fachinetti, D., Han, J. S., & Cleveland, D. W. (2012). Inducible, reversible system for the rapid and complete degradation of proteins in mammalian cells. *Proceedings of the National Academy of Sciences of the United States of America*, *109*(49), E3350–7. http://doi.org/10.1073/pnas.1216880109

Horz, W., & Altenburger, W. (1981). Nucleotide sequence of mouse satellite DNA. *Nucleic*, *9*(3), 683–696.

Howman, E. V, Fowler, K. J., Newson, A. J., Redward, S., MacDonald, A. C., Kalitsis, P., & Choo, K. H. (2000). Early disruption of centromeric chromatin organization in centromere protein A (Cenpa) null mice. *Proceedings of the National Academy of Sciences of the United States of America*, *97*(3), 1148–53. Retrieved from http://www.pubmedcentral.nih.gov/articlerender.fcgi?artid=15551&tool=pmcentrez&rendertype=abstract

Hud, N. V., Allen, M. J., Downing, K. H., Lee, J., & Balhorn, R. (1993). Identification of the Elemental Packing Unit of DNA in Mammalian Sperm Cells by Atomic Force Microscopy. *Biochemical and Biophysical Research Communications*. http://doi.org/10.1006/bbrc.1993.1773

Jaffe, L. A., Norris, R. P., Freudzon, M., Ratzan, W. J., & Lisa, M. (2009). Microinjection of follicle-enclosed mouse oocytes. *Methods in Molecular Biology*, *518*, 1–15. http://doi.org/10.1007/978-1-59745-202-1

Jaffe, L. A., & Terasaki, M. (2004). Quantitative Microinjection of Oocytes, Eggs, and Embryos. *Methods Cell Biol*, *74*, 219–242. http://doi.org/10.1016/j.surg.2006.10.010.Use

Jansen, L. E. T., Black, B. E., Foltz, D. R., & Cleveland, D. W. (2007). Propagation of centromeric chromatin requires exit from mitosis. *The Journal of Cell Biology*, *176*(6), 795–805. http://doi.org/10.1083/jcb.200701066

John, G. B., Gallardo, T. D., Shirley, L. J., & Castrillon, D. H. (2008). Foxo3 is a PI3K-dependent molecular switch controlling the initiation of oocyte growth. *Developmental Biology*, *321*(1), 197–204. http://doi.org/10.1016/j.ydbio.2008.06.017

Kan, Z.-Y., Mayne, L., Chetty, P. S., & Englander, S. W. (2011). ExMS: data analysis for HX-MS

experiments. *Journal of the American Society for Mass Spectrometry*, *22*(11), 1906–1915. http://doi.org/10.1007/s13361-011-0236-3

Kassianidis, E., Pearson, R. J., & Philp, D. (2006). Probing structural effects on replication efficiency through comparative analyses of families of potential self-replicators. *Chemistry (Weinheim an Der Bergstrasse, Germany)*, *12*(34), 8798–8812. http://doi.org/10.1002/chem.200600460

Kato, H., Jiang, J., Zhou, B.-R., Rozendaal, M., Feng, H., Ghirlando, R., … Bai, Y. (2013). A conserved mechanism for centromeric nucleosome recognition by centromere protein CENP-C. *Science (New York, N.Y.)*, *340*(6136), 1110–3. http://doi.org/10.1126/science.1235532

Khandelia, P., Yap, K., & Makeyev, E. V. (2011). Streamlined platform for short hairpin RNA interference and transgenesis in cultured mammalian cells. *Proceedings of the National Academy of Sciences of the United States of America*, *108*(31), 12799–12804. http://doi.org/10.1073/pnas.1103532108

Kim, I. S., Lee, M., Park, K. C., Jeon, Y., Park, J. H., Hwang, E. J., … Kim, K. Il. (2012). Roles of Mis18α in Epigenetic Regulation of Centromeric Chromatin and CENP-A Loading. *Molecular Cell*, *46*(3), 260–273. http://doi.org/10.1016/j.molcel.2012.03.021

Kline, S. R. (2006). Reduction and analysis of SANS and USANS data using IGOR Pro. *Journal of Applied Crystallography*, *39*(6), 895–900. http://doi.org/10.1107/S0021889806035059

Kops, G. J. P. L., Weaver, B. a a, & Cleveland, D. W. (2005). On the road to cancer: aneuploidy and the mitotic checkpoint. *Nature Reviews. Cancer*, *5*(10), 773–785. http://doi.org/10.1038/nrc1714

Kornberg, R. D. (1977). Structure of chromatin. *Annual Review of Biochemistry*, *46*, 931–954. http://doi.org/10.1146/annurev.bi.46.070177.004435

Kubin, R. F., & Fletcher, A. N. (1982). Fluorescence quantum yields of some rhodamine dyes. *Journal of Luminescence*, *27*(4), 455–462. http://doi.org/10.1016/0022-2313(82)90045-X

Kurasawa, S., Schultz, R. M., & Kopf, G. S. (1989). Egg-induced modifications of the zona pellucida of mouse eggs: effects of microinjected inositol 1,4,5-trisphosphate. *Developmental Biology*, *133*(1), 295–304. http://doi.org/10.1016/0012-1606(89)90320-5

Lacoste, N., Woolfe, A., Tachiwana, H., Garea, A. V., Barth, T., Cantaloube, S., … Almouzni, G. (2014). Mislocalization of the centromeric histone variant CenH3/CENP-A in human cells depends on the chaperone DAXX. *Molecular Cell*, *53*(4), 631–44. http://doi.org/10.1016/j.molcel.2014.01.018

Lakowicz, J. R. (2007). *Principles of Fluorescence Spectroscopy*. Springer.

Lan, Z.-J., Xu, X., & Cooney, A. J. (2004). Differential oocyte-specific expression of Cre recombinase activity in GDF-9-iCre, Zp3cre, and Msx2Cre transgenic mice. *Biology of Reproduction*, *71*(5), 1469–1474. http://doi.org/10.1095/biolreprod.104.031757

Lermontova, I., Koroleva, O., Rutten, T., Fuchs, J., Schubert, V., Moraes, I., … Schubert, I. (2011). Knockdown of CENH3 in Arabidopsis reduces mitotic divisions and causes sterility by disturbed meiotic chromosome segregation. *Plant Journal*, *68*(1), 40–50. http://doi.org/10.1111/j.1365-313X.2011.04664.x

Lermontova, I., Schubert, V., Fuchs, J., Klatte, S., Macas, J., & Schubert, I. (2006). Loading of Arabidopsis centromeric histone CENH3 occurs mainly during G2 and requires the presence of the histone fold domain. *The Plant Cell*, *18*(10), 2443–51. http://doi.org/10.1105/tpc.106.043174

Lister, L. M., Kouznetsova, A., Hyslop, L. A., Kalleas, D., Pace, S. L., Barel, J. C., … Herbert, M. (2010). Age-related meiotic segregation errors in mammalian oocytes are preceded by depletion of cohesin and Sgo2. *Current Biology*, *20*(17), 1511–1521. http://doi.org/10.1016/j.cub.2010.08.023

Liu, D., Vleugel, M., Backer, C. B., Hori, T., Fukagawa, T., Cheeseman, I. M., & Lampson, M. A. (2010). Regulated targeting of protein phosphatase 1 to the outer kinetochore by KNL1 opposes Aurora B kinase. *Journal of Cell Biology*, *188*(6), 809–820. http://doi.org/10.1083/jcb.201001006

Lorenz, M., Hillisch, A., Goodman, S. D., & Diekmann, S. (1999). Global structure similarities of intact and nicked DNA complexed with IHF measured in solution by fluorescence resonance energy transfer. *Nucleic Acids Research*, *27*(23), 4619–4625.

Lowary, P. T., & Widom, J. (1998). New DNA sequence rules for high affinity binding to histone octamer and sequence-directed nucleosome positioning. *Journal of Molecular Biology*, *276*(1), 19–42. http://doi.org/10.1006/jmbi.1997.1494

Maddox, P. S., Hyndman, F., Monen, J., Oegema, K., & Desai, A. (2007). Functional genomics identifies a Myb domain-containing protein family required for assembly of CENP-A chromatin. *Journal of Cell Biology*, *176*(6), 757–763. http://doi.org/10.1083/jcb.200701065

Maehara, K., Takahashi, K., & Saitoh, S. (2010). CENP-A reduction induces a p53-dependent cellular senescence response to protect cells from executing defective mitoses. *Molecular and Cellular Biology*, *30*(9), 2090–2104. http://doi.org/10.1128/MCB.01318-09

Maggert, K. A., & Karpen, G. H. (2001). The activation of a neocentromere in Drosophila requires proximity to an endogenous centromere. *Genetics*, *158*(4), 1615–1628.

Makde, R. D., England, J. R., Yennawar, H. P., & Tan, S. (2010). Structure of RCC1 chromatin factor bound to the nucleosome core particle. *Nature*, *467*(7315), 562–566. http://doi.org/10.1038/nature09321

Manuelidis. (1978). Chromosomal localization of complex and simple repeated human DNAs. *Chromosoma*, *66*, 23–32.

Manuelidis, L. (1976). Repeating restriction fragments of human DNA. *Nucleic*, *3*(11), 3063–3076.

Manuelidis, L. (1981). CONSENSUS SEQUENCE OF MOUSE SATELLITE DNA INDICATES

TANDEM 116 BASEPAIR REPEATS IT IS DERIVED cut the 240 or 480 basepairs fragments to any visible degree and AvaII cut satellite could not be further cleaved by EcoRII (not shown). Sequencing also con- f. *Federation of European Biochemical Societies*, *129*(1), 25–28.

Masters, P. M., Bada, J. L., & Zigler Jr., J. S. (1977). Aspartic acid racemisation in the human lens during ageing and in cataract formation. *Nature*, *268*, 71–73. http://doi.org/doi:10.1038/268071a0

McKearin, D. M., & Spradling, a C. (1990). *bag-of-marbles*: a *Drosophila* gene required to initiate both male and female gametogenesis. *Genes & Development*, *4*(12b), 2242–2251. http://doi.org/10.1101/gad.4.12b.2242

McKinley, K. L., & Cheeseman, I. M. (2014). Polo-like kinase 1 licenses CENP-a deposition at centromeres. *Cell*, *158*(2), 397–411. http://doi.org/10.1016/j.cell.2014.06.016

McKinley, K. L., Sekulic, N., Guo, L. Y., Tsinman, T., Black, B. E., & Cheeseman, I. M. (2015). The CENP-L-N Complex Forms a Critical Node in an Integrated Meshwork of Interactions at the Centromere-Kinetochore Interface. *Molecular Cell*, *60*(6), 886–898. http://doi.org/10.1016/j.molcel.2015.10.027

Meistrich, M. L., & Hess, R. A. (2013). Assessment of Spermatogenesis Through Staging of Seminiferous Tubules. In *Spermatogenesis Methods and Protocols* (pp. 299–308). http://doi.org/10.1007/978-1-62703-038-0

Mendel, G. (1865). Experiments in Plant Hybridization. *Journal of the Royal Horticultural Society*, *IV*(1865), 3–47. Retrieved from http://www.esp.org/foundations/genetics/classical/gm-65.pdf

Mendiburo, M. J., Padeken, J., Fulop, S., Schepers, A., & Heun, P. (2011). Drosophila CENH3 Is Sufficient for Centromere Formation. *Science*, *334*(November), 686–690. http://doi.org/10.1126/science.1206880

Meyer-Ficca, M. L., Lonchar, J. D., Ihara, M., Bader, J. J., & Meyer, R. G. (2013). Alteration of poly(ADP-ribose) metabolism affects murine sperm nuclear architecture by impairing pericentric heterochromatin condensation. *Chromosoma*, *122*(4), 319–335. http://doi.org/10.1007/s00412-013-0416-y

Milks, K. J., Moree, B., & Straight, A. F. (2009). Dissection of CENP-C-directed centromere and kinetochore assembly. *Molecular Biology of the Cell*, *20*(19), 4246–55. http://doi.org/10.1091/mbc.E09-05-0378

Monen, J., Maddox, P. S., Hyndman, F., Oegema, K., & Desai, A. (2005). Differential role of CENP-A in the segregation of holocentric C. elegans chromosomes during meiosis and mitosis. *Nature Cell Biology*, *7*(12), 1248–1255. http://doi.org/10.1038/ncb1331

Moree, B., Meyer, C. B., Fuller, C. J., & Straight, A. F. (2011). CENP-C recruits M18BP1 to centromeres to promote CENP-A chromatin assembly. *The Journal of Cell Biology*, *194*(6), 855–71. http://doi.org/10.1083/jcb.201106079

Morgan, T. H. (1910). Sex Limited Inheritance in Drosophila. *Science (New York, N.Y.)*, *32*(812), 120–122. http://doi.org/10.1126/science.32.812.120

Nashun, B., Hill, P. W. S., Smallwood, S. A., Dharmalingam, G., Amouroux, R., Clark, S. J., … Hajkova, P. (2015). Continuous histone replacement by Hira is essential for normal transcriptional regulation and de novo DNA methylation during mouse oogenesis. *Molecular Cell*, *60*, 611–625. http://doi.org/10.1016/j.molcel.2015.10.010

Nguyen, T., & Francis, M. B. (2003). Practical synthetic route to functionalized rhodamine dyes. *Organic Letters*, *5*(18), 3245–3248. http://doi.org/10.1021/ol035135z

Oegema, K., Desai, A., Rybina, S., Kirkham, M., & Hyman, A. A. (2001). Functional analysis of kinetochore assembly in Caenorhabditis elegans. *Journal of Cell Biology*, *153*(6), 1209–1225. http://doi.org/10.1083/jcb.153.6.1209

Okada, M., Cheeseman, I. M., Hori, T., Okawa, K., McLeod, I. X., Yates, J. R., … Fukagawa, T. (2006). The CENP-H-I complex is required for the efficient incorporation of newly synthesized CENP-A into centromeres. *Nature Cell Biology*, *8*(5), 446–457. http://doi.org/10.1038/ncb1396

Palmer, D. K., Day, K. O., Trongt, H. Le, Charbonneau, H., & Margolis, R. L. (1991). Purification of the centromere-specific protein CENP-A and demonstration that it is a distinctive histone. *Proceedings of the National Academy of Sciences of the United States of America*, *88*(May), 3734–3738.

Palmer, D. K., O'Day, K., & Margolis, R. L. (1990). The centromere specific histone CENP-A is selectively retained in discrete foci in mammalian sperm nuclei. *Chromosoma*, *100*(1), 32–6. Retrieved from http://www.ncbi.nlm.nih.gov/pubmed/2101350

Palmer, D. K., Palmer, D. K., O'Day, K., O'Day, K., Wener, M. H., Wener, M. H., … Margolis, R. L. (1987). A 17-kD centromere protein (CENP-A) copurifies with nucleosome core particles and with histones. *The Journal of Cell Biology*, *104*(4), 805–815. http://doi.org/10.1083/jcb.104.4.805

Pan, H., O'Brien, M. J., Wigglesworth, K., Eppig, J. J., & Schultz, R. M. (2005). Transcript profiling during mouse oocyte development and the effect of gonadotropin priming and development in vitro. *Developmental Biology*, *286*(2), 493–506. http://doi.org/10.1016/j.ydbio.2005.08.023

Panzeri, L., & Philippsen, P. (1982). Centromeric DNA from chromosome VI in Saccharomyces cerevisiae strains. *The EMBO Journal*, *1*(12), 1605–11. Retrieved from http://www.ncbi.nlm.nih.gov/pubmed/9169873

Partridge, J. F., Borgstrøm, B., & Allshire, R. C. (2000). Distinct protein interaction domains and protein spreading in a complex centromere. *Genes and Development*, *14*(7), 783–791. http://doi.org/10.1101/gad.14.7.783

Pelleg, D., & Moore, A. (2000). X-means: Extending K-means with Efficient Estimation of the Number of Clusters. In *In Proceedings of the 17th International Conf. on Machine Learning* (pp. 727–734). Morgan Kaufmann.

Perpelescu, M., & Fukagawa, T. (2011). The ABCs of CENPs. *Chromosoma*, *120*, 425–446. http://doi.org/10.1007/s00412-011-0330-0

Pietras, D. F., Bennett, K. L., Siracusa, L. D., Woodworth-gutai, M., Chapman, V. M., Gross, K. W., … Hastie, N. D. (1983). Construction of a small Mus musculus repetitive DNA library: Identification of a new satedllite sequence in mus musculus. *Nucleic Acids Research*, *11*(20), 6965–6983. http://doi.org/10.1093/nar/11.20.6965

Przewloka, M. R., Venkei, Z., Bolanos-Garcia, V. M., Debski, J., Dadlez, M., & Glover, D. M. (2011). CENP-C is a structural platform for kinetochore assembly. *Current Biology: CB*, *21*(5), 399–405. http://doi.org/10.1016/j.cub.2011.02.005

Rathke, C., Baarends, W. M., Awe, S., & Renkawitz-Pohl, R. (2014). Chromatin dynamics during spermiogenesis. *Biochimica et Biophysica Acta - Gene Regulatory Mechanisms*, *1839*(3), 155–168. http://doi.org/10.1016/j.bbagrm.2013.08.004

Ravi, M., & Chan, S. W. L. (2010). Haploid plants produced by centromere-mediated genome elimination. *Nature*, *464*(7288), 615–618. http://doi.org/10.1038/nature08842

Raychaudhuri, N., Dubruille, R., Orsi, G. a, Bagheri, H. C., Loppin, B., & Lehner, C. F. (2012). Transgenerational propagation and quantitative maintenance of paternal centromeres depends on Cid/Cenp-A presence in Drosophila sperm. *PLoS Biology*, *10*(12), e1001434. http://doi.org/10.1371/journal.pbio.1001434

Ray-Gallet, D., Woolfe, A., Vassias, I., Pellentz, C., Lacoste, N., Puri, A., … Almouzni, G. (2011). Dynamics of histone H3 deposition in vivo reveal a nucleosome gap-filling mechanism for H3.3 to maintain chromatin integrity. *Molecular Cell*, *44*(6), 928–941. http://doi.org/10.1016/j.molcel.2011.12.006

Reddy, P., Liu, L., Adhikari, D., Jagarlamudi, K., Rajareddy, S., Shen, Y., … Liu, K. (2008). Oocyte-specific deletion of Pten causes premature activation of the primordial follicle pool. *Science (New York, N.Y.)*, *319*(5863), 611–613. http://doi.org/10.1126/science.1152257

Régnier, V., Vagnarelli, P., Fukagawa, T., Zerjal, T., Burns, E., Trouche, D., … Brown, W. (2005). CENP-A is required for accurate chromosome segregation and sustained kinetochore association of BubR1. *Molecular and Cellular Biology*, *25*(10), 3967–3981. http://doi.org/10.1128/MCB.25.10.3967-3981.2005

Richter, M., Chakrabarti, A., Ruttekolk, I. R., Wiesner, B., Beyermann, M., Brock, R., & Rademann, J. (2012). Multivalent design of apoptosis-inducing bid-BH3 peptide-oligosaccharides boosts the intracellular activity at identical overall peptide concentrations. *Chemistry (Weinheim an Der Bergstrasse, Germany)*, *18*(52), 16708–16715. http://doi.org/10.1002/chem.201202276

Sadate-Ngatchou, P. I., Payne, C. J., Dearth, A. T., & Braun, R. E. (2008). Cre recombinase activity specific to postnatal, premeiotic male germ cells in transgenic mice. *Genesis (New York, N.Y. : 2000)*, *46*(12), 738–42. http://doi.org/10.1002/dvg.20437

Samans, B., Yang, Y., Krebs, S., Sarode, G. V., Blum, H., Reichenbach, M., …

Schagdarsurengin, U. (2014). Uniformity of nucleosome preservation pattern in mammalian sperm and Its connection to repetitive DNA elements. *Developmental Cell*, *30*(1), 23–35. http://doi.org/10.1016/j.devcel.2014.05.023

Sanyal, K., & Carbon, J. (2002). The CENP-A homolog CaCse4p in the pathogenic yeast Candida albicans is a centromere protein essential for chromosome transmission. *Proc. Nat. Acad. Sci. USA*, *99*(20), 12969–12974. http://doi.org/10.1073/pnas.162488299

Saunders, M., Fitzgerald-Hayes, M., & Bloom, K. (1988). Chromatin structure of altered yeast centromeres. *Proceedings of the National Academy of Sciences of the United States of America*, *85*(1), 175–9. Retrieved from http://www.pubmedcentral.nih.gov/articlerender.fcgi?artid=279506&tool=pmcentrez&rendertype=abstract

Savas, J. N., Toyama, B. H., Xu, T., Yates, J. R., & Hetzer, M. W. (2012). Extremely long-lived nuclear pore proteins in the rat brain. *Science (New York, N.Y.)*, *335*(6071), 942. http://doi.org/10.1126/science.1217421

Schneider, C. A., Rasband, W. S., & Eliceiri, K. W. (2012). NIH Image to ImageJ: 25 years of image analysis. *Nature Methods*, *9*(7), 671–675. http://doi.org/10.1038/nmeth.2089

Schultz, R. M., Montgomery, R. R., & Belanoff, J. R. (1983). Regulation of mouse oocyte meiotic maturation: implication of a decrease in oocyte cAMP and protein dephosphorylation in commitment to resume meiosis. *Developmental Biology*, *97*(2), 264–273. http://doi.org/10.1016/0012-1606(83)90085-4

Scott, K. C., & Sullivan, B. A. (2014). Neocentromeres: A place for everything and everything in its place. *Trends in Genetics*, *30*(2), 66–74. http://doi.org/10.1016/j.tig.2013.11.003

Screpanti, E., De Antoni, A., Alushin, G. M., Petrovic, A., Melis, T., Nogales, E., & Musacchio, A. (2011). Direct binding of Cenp-C to the Mis12 complex joins the inner and outer kinetochore. *Current Biology: CB*, *21*(5), 391–398. http://doi.org/10.1016/j.cub.2010.12.039

Sekulic, N., Bassett, E. a, Rogers, D. J., & Black, B. E. (2010). The structure of (CENP-A-H4)(2) reveals physical features that mark centromeres. *Nature*, *467*(7313), 347–51. http://doi.org/10.1038/nature09323

Shelby, R. D., Monier, K., & Sullivan, K. F. (2000). Chromatin assembly at kinetochores is uncoupled from DNA replication. *Journal of Cell Biology*, *151*(5), 1113–1118. http://doi.org/10.1083/jcb.151.5.1113

Shelby, R. D., Vafa, O., & Sullivan, K. F. (1997). Assembly of CENP-A into centromeric chromatin requires a cooperative array of nucleosomal DNA contact sites. *Journal of Cell Biology*, *136*(3), 501–513. http://doi.org/10.1083/jcb.136.3.501

Silva, M. C. C., Bodor, D. L., Stellfox, M. E., Martins, N. M. C., Hochegger, H., Foltz, D. R., & Jansen, L. E. T. (2012). Cdk Activity Couples Epigenetic Centromere Inheritance to Cell Cycle Progression. *Developmental Cell*, *22*(1), 52–63. http://doi.org/10.1016/j.devcel.2011.10.014

Smoak, E. M., Stein, P., Schultz, R. M., Lampson, M. A., & Black, B. E. (2016). Long-term retention of CENP-A nucleosomes in mammalian oocytes underpins transgenerational inheritance of centromere indentity. *Current Biology*, *In Press*, 1–7. http://doi.org/10.1016/j.cub.2016.02.061

Stoler, S., Keith, K. C., Curnick, K. E., & Fitzgerald-Hayes, M. (1995). A mutation in CSE4, an essential gene encoding a novel chromatin-associated protein in yeast, causes chromosome nondisjunction and cell cycle arrest at mitosis. *Genes & Development*, *9*(5), 573–586. http://doi.org/10.1101/gad.9.5.573

Stryer, L., & Haugland, R. P. (1967). Energy transfer: a spectroscopic ruler. *Proceedings of the National Academy of Sciences of the United States of America*, *58*(2), 719–726.

Subramanian, V. V., & Bickel, S. E. (2008). Aging predisposes oocytes to meiotic nondisjunction when the cohesin subunit SMC1 is reduced. *PLoS Genetics*, *4*(11), 1–12. http://doi.org/10.1371/journal.pgen.1000263

Sullivan, B., & Karpen, G. (2001). Centromere identity in Drosophila is not determined in vivo by replication timing. *Journal of Cell Biology*, *154*(4), 683–690. http://doi.org/10.1083/jcb.200103001

Sullivan, K. F., Hechenberger, M., & Masri, K. (1994). Human CENP-A contains a histone H3 related histone fold domain that is required for targeting to the centromere. *The Journal of Cell Biology*, *127*(3), 581–592. http://doi.org/10.1083/jcb.127.3.581

Susanne, F., Valtcheva, N., & Feil, R. (2009). Inducible Cre Mice. In *Gene Knockout Protocols* (Vol. 530, pp. 343–363). http://doi.org/10.1007/978-1-59745-471-1_18

Sutton, W. S. (1903). The Chromosomes in Heredity. *Biology Bulletin*, *4*, 231–250.

Tachiwana, H., Kagawa, W., Shiga, T., Osakabe, A., Miya, Y., Saito, K., … Kurumizaka, H. (2011). Crystal structure of the human centromeric nucleosome containing CENP-A. *Nature*, *476*(7359), 232–235. http://doi.org/10.1038/nature10258

Takayama, Y., Sato, H., Saitoh, S., Ogiyama, Y., Masuda, F., & Takahashi, K. (2008). Biphasic Incorporation of Centromeric Histone CENP-A in Fission Yeast. *Molecular Biology of the Cell*, *19*, 682–690. http://doi.org/10.1091/mbc.E07

Tang, M. C. W., Jacobs, S. A., Mattiske, D. M., Soh, Y. M., Graham, A. N., Tran, A., … Mann, J. R. (2015). Contribution of the two genes encoding histone variant H3.3 to viability and fertility in mice. *PLOS Genetics*, *11*(2), e1004964. http://doi.org/10.1371/journal.pgen.1004964

Tomkiel, J., Cooke, C. A., Saitoh, H., Bernat, R. L., & Earnshaw, W. C. (1994). CENP-C is required for maintaining proper kinetochore size and for a timely transition to anaphase. *The Journal of Cell Biology*, *125*(3), 531–545.

Toyama, B. H., Savas, J. N., Park, S. K., Harris, M. S., Ingolia, N. T., Yates, J. R., & Hetzer, M. W. (2013). Identification of long-lived proteins reveals exceptional stability of essential

cellular structures. *Cell*, *154*(5), 971–982. http://doi.org/10.1016/j.cell.2013.07.037

Toyooka, Y., Tsunekawa, N., Takahashi, Y., Matsui, Y., Satoh, M., & Noce, T. (2000). Expression and intracellular localization of mouse Vasa-homologue protein during germ cell development. *Mechanisms of Development*, *93*(1-2), 139–149. http://doi.org/10.1016/S0925-4773(00)00283-5

Uhlenhaut, N. H., Jakob, S., Anlag, K., Eisenberger, T., Sekido, R., Kress, J., … Treier, M. (2009). Somatic sex reprogramming of adult ovaries to testes by FOXL2 ablation. *Cell*, *139*(6), 1130–1142. http://doi.org/10.1016/j.cell.2009.11.021

van de Werken, C., van de Werken, C., van der Heijden, G. W., van der Heijden, G. W., Eleveld, C., Eleveld, C., … Baart, E. B. (2014). Paternal heterochromatin formation in human embryos is H3K9/HP1 directed and primed by sperm-derived histone modifications. *Nature Communications*, *5*(May), 5868. http://doi.org/10.1038/ncomms6868

Verzijl, N., DeGroot, J., Thorpe, S. R., Bank, R. A., Shaw, J. N., Lyons, T. J., … TeKoppele, J. M. (2000). Effect of collagen turnover on the accumulation of advanced glycation end products. *Journal of Biological Chemistry*, *275*(50), 39027–39031. http://doi.org/10.1074/jbc.M006700200

Volpe, T. a, Kidner, C., Hall, I. M., Teng, G., Grewal, S. I. S., & Martienssen, R. a. (2002). Regulation of heterochromatic silencing and histone H3 lysine-9 methylation by RNAi. *Science (New York, N.Y.)*, *297*(5588), 1833–1837. http://doi.org/10.1126/science.1074973

Von Stetina, J. R., & Orr-Weaver, T. L. (2011). Developmental control of oocyte maturation and egg activation in metazoan models. *Cold Spring Harbor Perspectives in Biology*, *3*(10), 1–19. http://doi.org/10.1101/cshperspect.a005553

Waye, J. S., & Willard, H. F. (1987). Nucleotide sequence heterogeneity of alpha satellite repetitive DNA: A survey of alphoid sequences from different human chromosomes. *Nucleic Acids Research*, *15*(18), 7549–7569. http://doi.org/10.1093/nar/15.18.7549

Whitten, A. E., Cai, S., & Trewhella, J. (2008). *MULCh* : modules for the analysis of small-angle neutron contrast variation data from biomolecular assemblies. *Journal of Applied Crystallography*, *41*(1), 222–226. http://doi.org/10.1107/S0021889807055136

Wiersma, A., Hirsch, B., Tsafriri, A., Hanssen, R. G. J. M., Van De Kant, M., Kloosterboer, H. J., … Hsueh, a. J. W. (1998). Phosphodiesterase 3 inhibitors suppress oocyte maturation and consequent pregnancy without affecting ovulation and cyclicity in rodents. *Journal of Clinical Investigation*, *102*(3), 532–537. http://doi.org/10.1172/JCI2566

Willard, H. F., & Waye, J. S. (1987). Chromosome-specific subsets of human alpha satellite DNA: analysis of sequence divergence within and between chromosomal subsets and evidence for an ancestral pentameric repeat. *Journal of Molecular Evolution*, *25*, 207–214.

Yang, H., Wang, H., & Jaenisch, R. (2014). Generating genetically modified mice using CRISPR/Cas-mediated genome engineering. *Nature Protocols*, *9*(8), 1956–1968. http://doi.org/10.1038/nprot.2014.134

Yang, H., Wang, H., Shivalila, C. S., Cheng, A. W., Shi, L., & Jaenisch, R. (2013). One-step generation of mice carrying reporter and conditional alleles by CRISPR/Cas-mediated genome engineering. *Cell*, *154*(6), 1370–9. http://doi.org/10.1016/j.cell.2013.08.022

Appendix A: Protocols for Chapter 2

Notes on PAGFP Assays

For an inducible cell line, determine what concentration of drug (in this case doxycycline) you need to add to media and how long you need to wait in order to see your desired effect. Then, the typical experimental schedule is as follows:

Day 1: Set up 6-well plate of cells. Plate on 18mm diameter circular coverslips or 22mm x 22mm square coverslips, depending on the chamber you will use for live imaging. The coverslip thickness should be 1.5.

From a 5mL cell suspension made from a 95% confluent parental 10cm plate, spilt 100-600ul cells in each well (i.e. 100µl of cell suspension into first well, 200µl in second well, etc.). This setup ensures there are a range of cell densities to choose from for imaging on Day 3. Each well should have a final volume of 2 mL of media (this includes any induction agent if you need to add any).

Day 2: Replace media and add fresh induction agent again.

Day 3: Pre-warm the microscope stage (both the stage insert and the live imaging chamber) to 37°C. The stage is usually set higher than 37°C (~43°C) in order to offset the room temperature, and keep the media/cell chamber at 37degC. You should calibrate the correct temperature settings for the stage at least twice a year, usually in summer and winter (when the seasonal building temperatures are most likely to change).

Prepare media with induction drug if you want cells to remain induced during live imaging. After selecting the coverslip with ideal confluency (usually the coverslips you plated with either 200µl or 300µl of cells on Day 1), assemble your live imaging chamber. Since you will be imaging the cells for a long time on a heated stage, media will evaporate. To prevent this, add 100-150ul will be mineral oil layered on top to prevent evaporation of the media. It should be just enough oil to form a nice seal all around the media.

For live imaging media, I have found that cells are happier for the long time courses in DMEM+10% FBS+1% Pen/Strep, rather than L15. Make sure you order DMEM without phenol red, to avoid any false fluorescence. Since you are using DMEM, which is a bicarbonate buffered media, you will want to use CO_2 during your live imaging. CO_2 will be able to exchange through the mineral oil.

To begin, I first located all of the cells I wanted to image and save their positions on the stage. Look for cells with smaller nuclei, as these are usually G1 or early S-phase cells. Avoid cells with large nuclei if your assay will be compromised by cells going through mitosis. Cells with large nuclei are likely in G2 and will undergo mitosis before the final timepoint. Once you find all of your cells (usually, tracking ~20 cells per experiment is reasonable), take a “before” image. Once all of the before images are acquired, photoactivate each cell one by one. The laser power and number of repetitions will be dependent on your particular protein (localization, expression level, etc).

Once all cells have been activated, make any corrections in x-,y-, or z-planes by DIC to avoid photobleaching. Then, take a T=0 image (after photoactivation).

Set-up a timelapse to image cells in DIC every 15-20 minutes for however many hours you wish to track them. To minimize photobleaching, only image in DIC during this time. You need only acquire a single z-plane to accurately track the fate of each cell. Once the time course is finished, you can assemble each DIC image for each cell by Importing Sequence into ImageJ to determine if your activated cell is still near its original position.

Appendix B: Protocols for Chapter 4

Immunofluorescence on Cryosections of Mouse Testis

Protocol for Sectioning Pre-Fixed Testes:

Dissection and Fixation of Testes

NB: If you choose to fix the testes before sectioning, beware that prolonged fixation can lead to blocked epitopes and you may have to try antigen recovery (Incubating tissue sections in 10mM Sodium Citrate at 80°) in order to get any signal at all. For this reason, I normally section unfixed testes, even though they can be more difficult to section.

1) Prepare 4% PFA in PBS. Perform in fume hood.

2) (Optional): If interested in collecting fully mature sperm, remove cauda epididymedes and vas deferens and place in 1 mL PBS at 37°C for 15 min after making several incisions in the epididymedes. After sperm have swum out, spin down liquid (700g 5min) and remove supernatant. Resuspend in 1mL PBS. If you want to make sperm smear slides for immunofluorescence, pipette some of this sperm suspension onto a glass slide and proceed with the protocol below. Spin down and resuspend in somatic cell lysis buffer (0.1% SDS, 0.5% Triton X-100 in DEPC H_2O) on ice for 20min, to ensure a pure population of mature sperm. Spin down at 10,000g for 3min and remove supernatant. Resuspend in 1mL PBS and use 25uL for counting (mix this 25uL with 8% formaldehyde in PBS and count sperm) via hemocytometer. Spin down the rest of the sperm, remove supernatant, and flash-freeze by dipping the tube into liquid N_2. Store samples at -80°C. To use sample for immunoblotting, resuspend in appropriate amount of sample buffer to allow for 10^6 sperm/15uL/lane.

3) Place one testis in 10mL 4% PFA overnight at 4°C on shaker. Over the next several days, follow this protocol. The next day, wash 3x6mL PBS. Place the testis in 15% sucrose in PBS. Leave at 4°C until it sinks (~6 hours). Place the testis in 30% sucrose in PBS. Leave at 4°C until it sinks (over night). Use a KimWipe to remove excess sucrose solution and mount for cryosectioning.

4) Fill a 35mm petri dish with a enough OCT so that when tilted at an angle, enough OCT pools at an edge so that the testis can be thoroughly coated. Place fixed testis in the OCT and coat the testis with OCT by using a pair of tweezers to rotate the testis. Fill a tissue mold (Tissue-TEK Cryomold 4566) half-way with OCT and place the testis in the mold. Try to get the testis to stand up perpendicular to the bottom of the tissue mold and place the bottom of the mold directly on a piece of dry ice. As the OCT freezes it will turn an opaque white. Once you are sure the testis has been frozen in place, you can fill the rest of the mold with OCT to cover the testis and wait until all of the OCT is white. Some testis are bigger than others and will require larger tissue molds or more OCT. Once done, place on dry ice while you prepare other samples, or place at -80°C until you are ready to crysection.

5) Cryosection at 8um keep slides at -80°C until ready for immunofluorescence. You should bring a laboratory marker that cannot be erased with ethanol, SUPERFROST-Plus slides, a box of dry ice to hold your slidebox/samples, and your samples. Cryosectioning protocol will be specific to the device used. Place between 5-6 sections/slide, evenly spaced apart. The tissue sections adhere better to slides that are at room temperature, so do not store your slides within the -20°C chamber while cryosectioning.

Immunofluorescence of Fixed Testes Sections

1) I draw a small circle with a PAP Pen to limit the volume of reagents necessary for immunofluorescence. The exact volume will vary depending on the size of the circle drawn, but remember it is important to keep the samples from drying out during the procedure. The PAP Pen will form a hydrophobic barrier that will keep all of your aqueous reagents inside the circle. The only time the PAP Pen barrier may fail is when during permeabilization, because the Triton-100X may break up the barrier. If this happens, simply draw another circle with the PAP Pen to reinforce the original circle and proceed.

2) Wash PFA-fixed cryosections with PBS at room temperature (RT) for 10 min.

3) Incubate in 0.1% Triton X100 2min at 4°C or RT.

4) Wash 3x5min PBS.

5) Incubate in 3% donkey serum in PBS 1hr at 37°C.

   NB: For incubation at 37degC, create a humidified chamber by repurposing an empty P1000 or P100 box. Turn it upside down and line the lid with wet paper towels and cover these with parafilm. Then you can place the slides on the parafilm, close the box and carefully move the box into a 37degC incubator for the incubations. Since the box is opaque, is serves the added purpose of blocking light when you incubate with secondary antibodies, though you can also cover the clearer plastic with aluminum foil if you prefer.

6) Incubate in primary antibody 1hr at 37°C in 3% donkey serum in PBS.

7) Wash 3x5min PBS.

8) Incubate in secondary antibody (in 3% donkey serum in PBS).

9) Wash 3x5min PBS.

10) Incubate in DAPI (5ug/mL PBS) for 5 minutes. Wash once in PBS for 5 minutes.

11) Embed tissues in Prolong Gold or Vectashield. As an alternative to incubating with DAPI in Step 10, you can add DAPI right to the Vectashield stock (5ug/mL Vectashield). Cover with

coverslip, I usually find that three 11mm x 22mm coverslips will suffice to seal 6 evenly spaced tissue sections. Use clear nail polish on the coverslip edges to lock them in place.

Protocol for Sectioning Unfixed Testes:

The protocol for staining unfixed testes is virtually identical to the protocol for handling fixed testes.

1) (Optional): If interested in collecting fully mature sperm, remove cauda epididymedes and vas deferens and place in 1 mL PBS at 37°C for 15 min after making several incisions in the epididymedes. After sperm have swum out, spin down liquid (700g 5min) and remove supernatant. Resuspend in 1mL PBS. If you want to make sperm smear slides for immunofluorescence, pipette some of this sperm suspension onto a glass slide and proceed with the protocol below. Spin down and resuspend in somatic cell lysis buffer (0.1% SDS, 0.5% Triton X-100 in DEPC H_2O) on ice for 20min, to ensure a pure population of mature sperm. Spin down at 10,000g for 3min and remove supernatant. Resuspend in 1mL PBS and use 25uL for counting (mix this 25uL with 8% formaldehyde in PBS and count sperm) via hemocytometer. Spin down the rest of the sperm, remove supernatant, and flash-freeze by dipping the tube into liquid N_2. Store samples at -80°C. To use sample for immunoblotting, resuspend in appropriate amount of sample buffer to allow for 10^6 sperm/15uL/lane.

2) Remove testes and place each testes into a carefully labeled tube. Flash freeze samples in liquid N_2 and store at -80°C until ready to mount for cryosectioning, or mount after immediately after flash-freezing.

3) When ready to mount frozen testes, keep them on dry ice the entire time so they do not thaw. Fill a 35mm petri dish with a enough OCT so that when tilted at an angle, enough OCT pools at an edge so that the testis can be thoroughly coated. Place fixed testis in the OCT and coat the testis with OCT by using a pair of tweezers to rotate the testis. Fill a tissue mold (Tissue-TEK Cryomold 4566) half-way with OCT and place the testis in the mold. Try to get the testis to stand up perpendicular to the bottom of the tissue mold and place the bottom of the mold directly on a piece of dry ice. As the OCT freezes it will turn an opaque white. Once you are sure the testis has been frozen in place, you can fill the rest of the mold with OCT to cover the testis and wait until all of the OCT is white. Some testis are bigger than others and will require larger tissue molds or more OCT. Once done, place on dry ice while you prepare other samples, or place at -80°C until you are ready to crysection.

4) Cryosection at 8um keep slides at -80°C until ready for immunofluorescence. You should bring a laboratory marker that cannot be erased with ethanol, SUPERFROST-Plus slides, a box of dry ice to hold your slidebox/samples, and your samples. Cryosectioning protocol will be specific to the device used. Place between 5-6 sections/slide, evenly spaced apart. The tissue sections adhere better to slides that are at room temperature, so do not store your slides within the -20°C chamber while cryosectioning.

Immunofluorescence of Unfixed Testes Sections

1) Prepare 4% formaldehyde in PBS. Use the safety hood.

2) I draw a small circle with a PAP Pen to limit the volume of reagents necessary for immunofluorescence. The exact volume will vary depending on the size of the circle drawn, but remember it is important to keep the samples from drying out during the procedure. The PAP Pen will form a hydrophobic barrier that will keep all of your aqueous reagents inside the circle. The only time the PAP Pen barrier may fail is when during permeabilization, because the Triton-100X may break up the barrier. If this happens, simply draw another circle with the PAP Pen to reinforce the original circle and proceed.

3) Fix cryosections with 4% formaldehyde for 15min.

4) Wash 2x5min PBS.

5) Incubate in 100mM Glycine (375mg/50mL) in PBS 1min at room temperature. This will quench the formaldehyde reaction.

6) Wash 2x5min PBS.

7) Incubate in 0.1% Triton X100 2min at 4°C or RT.

8) Wash 3x5min PBS.

9) Incubate in 3% donkey serum in PBS 1hr at 37°C.

   NB: For incubation at 37degC, create a humidified chamber by repurposing an empty P1000 or P100 box. Turn it upside down and line the lid with wet paper towels and cover these with parafilm. Then you can place the slides on the parafilm, close the box and carefully move the box into a 37degC incubator for the incubations. Since the box is opaque, is serves the added purpose of blocking light when you incubate with secondary antibodies, though you can also cover the clearer plastic with aluminum foil if you prefer.

10) Incubate in primary antibody 1hr at 37°C in 3% donkey serum in PBS.

11) Wash 3x5min PBS.

12) Incubate in secondary antibody (in 3% donkey serum in PBS).

13) Wash 3x5min PBS.

14) Incubate in DAPI (5ug/mL PBS) for 5 minutes. Wash once in PBS for 5 minutes.

15) Embed tissues in Prolong Gold or Vectashield. As an alternative to incubating with DAPI in Step 12, you can add DAPI right to the Vectashield stock (5ug/mL Vectashield). Cover with coverslip, I usually find that three 11mm x 22mm coverslips will suffice to seal 6 evenly spaced tissue sections. Use clear nail polish on the coverslip edges to lock them in place.

Tamoxifen Preparation

Procedure:

1) Place 2 mL of corn oil (Sigma: C-8267) in a 15 mL Falcon Tube
2) Heat corn oil to 42°C for 30 minutes. Use this time to take Tamoxifen (Sigma: T-5648) out and equilibrate to RT prior to weighing.
3) Add 40 mg Tamoxifen into the pre-heated corn oil (Final Concentration of Tamoxifen is 20mg/mL)
4) Wrap vial with aluminum foil.
5) Place in a shaker at 37°C for several hours.
6) Tamoxifen can be difficult to dissolve. Vortex frequently to break up clumps.
7) Once tamoxifen is dissolved, the solution can be stored at 4°C for up to 1 month.
8) Administer 100µl of 20 mg/mL tamoxifen solution by intraperitoneal injection once a day for 3 days.

Notes:

- The concentration of tamoxifen or number of injections may need to be increased dependent, on the efficiency of induction in the targeted tissue.
- Some protocols suspend tamoxifen in 100% ethanol at a concentration of 100 mg/mL and then dilute this solution in corn oil to a final concentration of 20 mg/mL. I have also tried this method of tamoxifen preparation, but the ethanol and corn oil did not mix well together, which would make it difficult to ensure consistent injections. As such, I dissolved the tamoxifen directly in corn oil.